U.PORTO
FEUP FACULDADE DE ENGENHARIA
UNIVERSIDADE DO PORTO

ANALYSIS OF A TYPICAL OFFSHORE TUBULAR KT-JOINT TO EVALUATE THE SCF AND SIF VALUES

João Nuno da Silva Pedro Castanheira da Costa

Dissertation submitted to
Faculdade de Engenharia da Universidadedo Porto
For the degree of:
Mestre em Engenharia Mecânica

Supervisor:
Prof. José A.F.O. Correia
(University of Porto, Portugal)

Supervisors:
Prof. Abilio M.P. De Jesus
(University of Porto, Portugal)
Prof. Dimitrios G. Pavlou
(University of Stavanger, Norway)

Mestrado integrado em Engenharia Mecânica
Especialização em Projeto e Construção Mecânica

Porto, September 2019

Á minha família...

Acknowledgments

The realization of this thesis could never have been conceivable without the help, support and motivation of a few people to whom I leave my much-appreciated gratitude.

First of all, I would like to express my sincere thankfulness to my thesis supervisor Doctor José António Correia for all the assistance and valuable lessons and advices given during the time of the realization of this thesis.

Secondly, to Professor Dimitios G. Pavlou I leave a special thanks for the extraordinary welcoming and all the help and accessibility showed in the explanation and sharing of information. Furthermore, I would like to express my acknowledgements to all my co-supervisors, Prof. Abílio De Jesus and Prof. Dimitrios Pavlou, who also gave crucial contributes to this master thesis.

The last but not the least, a debt of gratitude to the engineers Paulo Jorge Carmona Mendes and António Mourão for all the time and help made available as well as wise councils for the most entangled issues that may have had risen in the realization of this thesis.

I would like to express my acknowledgements to FCT - Fundação para a Ciência e Tecnologia which supported this work through national funds; UID/ECI/047 08/2019 – CONSTRUCT – Instituto de I&D em Estruturas e Construções funded by national funds through the FCT/MCTES (PIDDAC); and ERASMUS+ program.

I additionally thank the Faculty of Engineering of the University of Porto (FEUP) and the University of Stavanger (Norway) for their support and facilities that were made available to me.

At long last, a major thanks to my friends, family and girlfriend, for the incredible quality and bolster they have constantly given me along my scholarly course.

João Costa

September 04, 2019



Agradecimentos

A realização desta tese nunca poderia ter sido concebível sem a ajuda, apoio e motivação de algumas pessoas a quem quero expressar a minha sincera gratidão.

Em primeiro lugar, eu gostaria de exprimir a minha gratidão sincera ao meu supervisor de tese doutor José António Correia por toda a toda a ajuda, valiosas lições e conselhos dados durante a realização desta tese.

Em segundo lugar, ao professor Dimitios G. Pavlou deixo um especial obrigado pelas extraordinárias boas-vindas e toda a ajuda e a acessibilidade mostradas na explicação e compartilha de informação. Além disso, gostaria de expressar meus agradecimentos a todos os meus co-orientadores, Prof. Abílio De Jesus e Prof. Dimitrios Pavlou, que também deram contribuições cruciais para esta tese de mestrado.

Por último mas não menos importante, a minha total gratidão aos Engenheiros Paulo Jorge Carmona Mendes e António Mourão por todo o tempo e ajuda postos à disposição bem como sábios concelhos para as questões mais complexas que poderiam surgir na realização da tese.

Eu gostaria de expressar os meus agradecimentos à FCT - Fundação para a Ciência e Tecnologia que suportou este trabalho através de fundos nacionais; UID/ECI/047 08/2019 – CONSTRUCT – Instituto de I&D em Estruturas e Construções financiado por fundos nacionais através do FCT/MCTES (PIDDAC); e ao programa ERASMUS+.

Agradeço ainda à Faculdade da Engenharia da Universidade do Porto (FEUP) e à Universidade de Stavanger (Noruega) pela ajuda e por facultar as instalações para a realização deste trabalho.

Finalmente, os meus sinceros agradecimentos aos meus amigos, família e namorada, pela grande força e pelo apoio incondicional que constantemente me deram ao longo do meu percurso académico.

João Costa

04 de Setembro de 2019

Abstract

The organization of increasingly sustainable power source all around the globe is bringing about huge vitality security, environmental change relief and loads of monetary advantages. Support structures are thought to be one of the main drivers for reducing costs in order to make the wind industry more economically efficient. Foundations and towers should be fit for purpose, extending their effective service life but avoiding costs of oversizing. Most of the offshore platforms are normally fixed to seabed and constructed as a truss framework with tubular members as structural elements. The area around the tubular joint has been highly considered among engineers. The stress concentration and stress intensity are the primordial factors in the study of fatigue design. This work was developed with the purpose of studying both stress concentration factors (SCF) and stress intensity factors (SIF) for the typical offshore KT-joint based either on the parametric equations proposed by Lloyd and Efthymiou for the SCF, and IIW, BS7910 and SINTAP standards for SIF. To do a proper study on the matter, an exhaustive and extensive review and state was made. In this way, comparisons between the analytical and numerical solutions were done.

KEYWORDS: Offshore Engineering, Tubular Joint, Hot-Spot Stress, Stress Concentration Factor, Stress Intensity Factor, Parametric Equations

Resumo

A organização de uma fonte de energia cada vez mais sustentável em todo o mundo está a trazer uma enorme vitalidade de segurança, atenuação da mudança ambiental e balanços monetários favoráveis. As estruturas de apoio são pensadas para ser um dos principais impulsionadores para a redução de custos a fim de tornar a indústria eólica mais economicamente eficiente. As fundações e as estruturas devem ser adequadas ao propósito estendendo a sua vida de serviço duma forma eficaz evitando custos de sobredimensionamento. A maioria das plataformas offshore são fixadas ao fundo do mar e construídos como estrutura do tipo treliça com membros tubulares servindo de elementos da estrutura. A área em torno da junta tubular tem sido altamente considerada e investigada por engenheiros. O fator de concentração de tensões e o fator de intensidade de tensões são os fatores primordiais no estudo de vida à fadiga. Este trabalho foi desenvolvido com o objetivo de estudar tanto o fator de concentração de tensões (SCF) como o fator de intensidade de tensões (SIF) de uma ligação tubular KT, quer com base nas equações paramétricas propostas por Loyd e Efthymiou para o primeiro parâmetro, e nas normas IIW, BS7910 e SINTAP para o SIF. Para fazer um estudo adequado sobre o assunto, uma revisão exaustiva e extensa foi feita. Assim, comparações foram feitas entre as soluções analíticas e numéricas para os parâmetros em estudo.

PALAVRAS-CHAVE: Engenharia Offshore, Ligação Tubular, Tensões Hot-Spot, Fator de Concentração de Tensões, Fator de Intensidade de Tensões, Equações paramétricas

General Index

1. Introduction 1
1.1 Motivation 1
1.2 Objectives 1
1.3 Outline of thesis 2
2. Review on tubular offshore structures and fatigue assessment methods 3
2.1 Introduction 3
2.2 Offshore tubular joints 4
2.2.1 Introduction 4
2.3 Fatigue of offshore structures 6
2.3.1 Introduction 6
2.3.2 Damage accumulation method 9
2.3.3 Nominal stress approach 9
2.3.4 Hot-Spot stress approach 11
2.3.4.1 Type “a” hot-spots 12
2.3.4.2 Type “b” hot-spots 13
2.4 Definition of stress concentration factor (SCF) 14
2.5 Definition of stress intensity factor (SIF) 15
2.6 Estimation of SCF and SIF values based on design codes 17
2.6.1 Superposition of stresses in tubular joints 17
2.6.2 Parametric equations 19
2.6.2.1 Efthymiou equations 19
2.6.2.2 Lloyd’s Register equations 23
2.6.3 Calculation of SIF by IIW standards 23
2.6.4 Calculation of SIF by BS 7910 standards 24
2.7 Review on finite element analysis to evaluate the SCF and SIF values of tubular joints 26
3. Evaluation of SCF values of a typical tubular KT-joint based on numerical simulation 30
3.1. Introduction 30
3.2. Geometry of the Tubular KT-joint under consideration 30
3.3. SCF evaluation based on DNVGL code/Efthymiou parametric equations 32
3.4. SCF evaluation based on Lloyd’s register (LR) equations 35
3.5. SCF evaluation based on numerical analysis 40
3.6. Conclusions 58
4. Evaluation of SIF values of a typical tubular KT-joint 61
4.1. Introduction 61
4.2. SIF evaluation based on BS7910 standard 61

4.2.1 BS7910 standard rules 61
4.2.2 Results 64
4.2.2.1 Brace B1 64
4.2.2.2 Brace B2 69
4.2.2.3 Brace B3 71
4.3. SIF evaluation based on IIW recommendations 75
4.3.1 Rules from IIW recommendations 75
4.3.2 Results 78
4.3.3.1 Brace B1 78
4.3.3.2 Brace B2 79
4.3.3.3 Brace B3 81
4.4 SIF evaluation on SINTAP standard 82
4.4.1 SINTAP standard Rules 82
4.4.2 Results 85
4.4.2.1 Brace B1 85
4.4.2.2 Brace B2 89
4.4.2.3 Brace B3 90
4.5. Comparison and discussion 95
5. Conclusions and future works 99
5.1 Conclusions 99
5.2 Future works 99
Bibliographic References 100

List of figures

Figure 1 - Piled Structure and Gravity Structure of Brent [4]. 3
Figure 2 - Types of offshore structures [4]. 4
Figure 3 - Types of tubular joints along with their nomenclature [8]. 5
Figure 4 – Offshore tubular joints: (a) Example of offshore jacket structure; (b) Definition of the geometrical parameters of a joint; (c) Different types of IPB loadings [9]. 6
Figure 5 - S-N curves for offshore connections or details based on DNVGL standard [10]. 7
Figure 6 - Definition of nominal stress distribution in chord and brace side [1]. 7
Figure 7 - Definition of geometric stress distribution in chord and brace side [1]. 8
Figure 8 - Definition of notch stress distribution in chord and brace side [1]. 9
Figure 9 - Nominal stress approach for assessing the fatigue strength and service life of non-welded structural components [12]. 10
Figure 10 - Definition of hot-spot stress [15]. 11
Figure 11 - Stress distribution through the thickness of the weld toe and its components [17]. 11
Figure 12 - Reference points at different types of meshing [17]. 14
Figure 13 - Stress concentration in tubular joint [8]. 15
Figure 14 - Illustration of arbitrary KT-Joint with definition of saddle and crown points [1]. 17
Figure 15 - Superposition of stresses [24]. 18
Figure 16 - Stress intensity factor for surface cracks [17]. 24
Figure 17 - Examples of welded joints [28]. 25
Figure 18 - Stress intensity magnification factor Mb for surface flaws in bending [28]. 25
Figure 19 – Complete profile solid FE T-joint model [15]. 27
Figure 20 – Case study a) Jacket-type offshore structure and b) KT-type tubular joint [26]. 31
Figure 21 - Solid model with designation of the braces [26]. 42
Figure 22 - Solid model with the principal stress points [26]. 42
Figure 23 - Solid model with the details of the size of the 8-nodes cube solid elements and 6-nodes triangular solid elements in braces and chord, respectively in the blue zone, 0.15m (Exterior zone) [26]. 43
Figure 24 - Solid FE model with the details of the size of the 8-nodes solid elements in green with 5E-2 meters in size [26]. 43
Figure 25 - Solid FE model with the designed meshing refinement (Front view) [26]. 43
Figure 26 - Solid FE model with the designed meshing refinement (Side view) [26]. 43
Figure 27 - Solid FE model with the designed meshing refinement (Top view) [26]. 43
Figure 28 - 3D FE model of the KT-Joint under consideration [26]. 44
Figure 29 - Solid model with the representation of the axial forces [26]. 46
Figure 30 - Details about the support conditions used in the FE model: a) Fixed support; b) Displacement. [26]. 46
Figure 31 - Solid model with identification of fixed support [26]. 47
Figure 32 - Solid model with identification of restricted and free directions [26]. 47
Figure 33 - Stress fields for axial loading case in the KT-joint under consideration [26]. 48
Figure 34 - Stress fields for axial loading case in the KT-joint under consideration (Closer look) [26]. 48
Figure 35 - Stress distribution in brace B1 for axial loading case: Side 1 [26]. 49
Figure 36 - Stress distribution in brace B1 for axial loading case: Side 2 [26]. 49
Figure 37 - Stress distribution in brace B1 for axial loading case: Side 3 [26]. 50
Figure 38 - Stress distribution in brace B1 for axial loading case: Side 4 [26]. 50
Figure 39 - Stress distribution in brace B2 for axial loading case: Side 1 [26]. 51
Figure 40 - Stress distribution in brace B2 for axial loading case: Side 2 [26]. 51
Figure 41 - Stress distribution in brace B2 for axial loading case: Side 3 [26]. 52
Figure 42 - Stress distribution in brace B2 for axial loading case: Side 4 [26]. 52
Figure 43 - Stress distribution in brace B3 for axial loading case: Side 1 [26]. 53
Figure 44 - Stress distribution in brace B3 for axial loading case: Side 2 [26]. 53

Figure 45 - Stress distribution in brace B3 for axial loading case: Side 3 [26]. 54
Figure 47 - Stress distribution in chord for axial loading case [26]. 55
Figure 48 - Path stresses in chord crown for axial loading case [26] 56
Figure 49 - Path stress in brace crown B1 for axial loading case (Side 1 and 2) [26] 57
Figure 50 - Path stress in brace saddle B1 for axial loading case (Side 3 and 4) [26] 57
Figure 51 - Path stress in brace crown B2 for axial loading case (Side 1 and 2) [26]. 57
Figure 52 - Path stress in brace saddle B2 for axial loading case (Side 3 and 4) [26] 57
Figure 53 - Path stress in brace crown B3 for axial loading case (Side 1 and 2) [26] 58
Figure 54 - Path stress in brace saddle B3 for axial loading case (Side 3 and 4) [26] 58
Figure 55 - Surface flaw [27]. 62
Figure 56 - *SIF vs. a* curves for the Brace B1 using BS7910 standard based on Lloyd's Register, DNV standard, and FEA: $a/c = 0.1$. 65
Figure 57 - *SIF vs. a* curves for the Brace B1 using BS7910 standard based on Lloyd's Register, DNV standard, and FEA: $a/c = 0.2$. 66
Figure 58 - *SIF vs. a* curves for the Brace B1 using BS7910 standard based on Lloyd's Register, DNV standard, and FEA: $a/c = 0.3$. 66
Figure 59 - *SIF vs. a* curves for the Brace B1 using BS7910 standard based on Lloyd's Register, DNV standard, and FEA: $a/c = 0.4$. 67
Figure 60 - *SIF vs. a* curves for the Brace B1 using BS7910 standard based on Lloyd's Register, DNV standard, and FEA: $a/c = 0.5$. 67
Figure 61 - *SIF vs. a* curves for the Brace B1 using BS7910 standard based on DNV standard for $\sigma n = 12.5MPa$: $0.1 \leq a/c \leq 0.5$. 68
Figure 62 - *SIF vs. a* curves for the Brace B1 using BS7910 standard based on DNV standard for $\sigma n = 12.5MPa$: $0.6 \leq a/c \leq 1.0$. 68
Figure 63 - *SIF vs. a* curves for the Brace B1 using BS7910 standard based on DNV standard for $\sigma n = 12.5MPa$: $1.2 \leq a/c \leq 2$. 69
Figure 64 - *SIF vs. a* curves for the Brace B2 using BS7910 standard based on Lloyd's Register, DNV standard, and FEA: $a/c = 0.1$. 70
Figure 65 - *SIF vs. a* curves for the Brace B2 using BS7910 standard based on DNV standard for $\sigma n = 37.3MPa$: $0.6 \leq a/c \leq 1.0$. 70
Figure 66 - *SIF vs. a* curves for the Brace B1 using BS7910 standard based on DNV standard for $\sigma n = 37.3MPa$: $1.2 \leq a/c \leq 2.0$. 71
Figure 67 - *SIF vs. a* curves for the Brace B3 using BS7910 standard based on Lloyd's Register, DNV standard, and FEA: $a/c = 0.1$. 72
Figure 68 - *SIF vs. a* curves for the Brace B3 using BS7910 standard based on Lloyd's Register, DNV standard, and FEA: $a/c = 0.2$. 72
Figure 69 - *SIF vs. a* curves for the Brace B3 using BS7910 standard based on Lloyd's Register, DNV standard, and FEA: $a/c = 0.3$. 73
Figure 70 - *SIF vs. a* curves for the Brace B3 using BS7910 standard based on Lloyd's Register, DNV standard, and FEA: $a/c = 0.4$. 73
Figure 71 - *SIF vs. a* curves for the Brace B3 using BS7910 standard based on Lloyd's Register, DNV standard, and FEA: $a/c = 0.5$. 74
Figure 72 - *SIF vs. a* curves for the Brace B3 using BS7910 standard based on DNV standard for $\sigma n = 21.2MPa$: $0.6 \leq a/c \leq 1.0$. 74
Figure 73 - *SIF vs. a* curves for the Brace B3 using BS7910 standard based on DNV standard for $\sigma n = 21.2MPa$: $1.2 \leq a/c \leq 2$. 75
Figure 74 - *SIF vs. a* curves for the Brace B1 using IIW recommendations based on Lloyd's Register, DNV standard, and FEA: $a/c = 0.1$. 78
Figure 75 - *SIF vs. a* curves for the Brace B1 using IIW recommendations based on Lloyd's Register, DNV standard, and FEA: $a/c = 0.2$. 79
Figure 76 - *SIF vs. a* curves for the Brace B1 using IIW recommendations based on DNV standard for $\sigma n = 12.5MPa$: $0.6 \leq a/c \leq 0.9$ 79

Figure 77 - *SIF vs. a* curves for the Brace B2 using IIW recommendations based on Lloyd's Register, DNV standard, and FEA: $a/c = 0.1$. 80
Figure 78 - *SIF vs. a* curves for the Brace B2 using IIW recommendations based on DNV standard for $\sigma n = 37.3MPa$: $0.6 \leq a/c \leq 0.9$ 80
Figure 79 - *SIF vs. a* curves for the Brace B3 using IIW recommendations based on Lloyd's Register, DNV standard, and FEA: $a/c = 0.1$. 81
Figure 80 - *SIF vs. a* curves for the Brace B3 using IIW recommendations based on DNV standard for $\sigma n = 21.2MPa$: $0.6 \leq a/c \leq 0.9$ 82
Figure 81 - T-joint description. 83
Where the limits to the stress intensity factor solution are the following: 84
Figure 82 - Y-joint description 85
Figure 83 - *SIF vs. a* curves for the chord side (brace B1) using SINTAP standard based on the SCF values obtained using the Lloyd's Register, DNV standard, and FEA: $a/c = 0.1$. 86
Figure 84 - *SIF vs. a* curves for the chord side (brace B1) using SINTAP standard based on the SCF values obtained using the Lloyd's Register, DNV standard, and FEA: $a/c = 0.2$. 86
Figure 85 - *SIF vs. a* curves for the chord side (brace B1) using SINTAP standard based on the SCF values obtained using the Lloyd's Register, DNV standard, and FEA: $a/c = 0.3$. 87
Figure 86 - *SIF vs. a* curves for the chord side (brace B1) using SINTAP standard based on the SCF values obtained using the Lloyd's Register, DNV standard, and FEA: $a/c = 0.4$. 87
Figure 87 - *SIF vs. a* curves for the brace side (brace B1) using SINTAP standard based on the SCF values obtained using the Lloyd's Register, DNV standard, and FEA: $a/c = 0.1$. 88
Figure 88 - *SIF vs. a* curves for the brace side (brace B1) using SINTAP standard based on the SCF values obtained using the Lloyd's Register, DNV standard, and FEA: $a/c = 0.2$. 88
Figure 89 - *SIF vs. a* curves for the brace side (brace B1) using SINTAP standard based on the SCF values obtained using the Lloyd's Register, DNV standard, and FEA: $a/c = 0.3$. 89
Figure 90 - *SIF vs. a* curves for the brace side (brace B1) using SINTAP standard based on the SCF values obtained using the Lloyd's Register, DNV standard, and FEA: $a/c = 0.4$. 89
Figure 91 - Crack size and SIF values for different crack growth ratios (σ=10,9385 MPa) 90
Figure 92 - *SIF vs. a* curves for the chord side (brace B3) using SINTAP standard based on the SCF values obtained using the Lloyd's Register, DNV standard, and FEA: $a/c = 0.1$. 91
Figure 93 - *SIF vs. a* curves for the chord side (brace B3) using SINTAP standard based on the SCF values obtained using the Lloyd's Register, DNV standard, and FEA: $a/c = 0.2$. 91
Figure 94 - *SIF vs. a* curves for the chord side (brace B3) using SINTAP standard based on the SCF values obtained using the Lloyd's Register, DNV standard, and FEA: $a/c = 0.3$. 92
Figure 95 - *SIF vs. a* curves for the chord side (brace B3) using SINTAP standard based on the SCF values obtained using the Lloyd's Register, DNV standard, and FEA: $a/c = 0.4$. 92
Figure 96 - *SIF vs. a* curves for the brace side (brace B3) using SINTAP standard based on the SCF values obtained using the Lloyd's Register, DNV standard, and FEA: $a/c = 0.1$. 93
Figure 97 - *SIF vs. a* curves for the chord side (brace B3) using SINTAP standard based on the SCF values obtained using the Lloyd's Register, DNV standard, and FEA: $a/c = 0.2$. 93
Figure 98 - *SIF vs. a* curves for the chord side (brace B3) using SINTAP standard based on the SCF values obtained using the Lloyd's Register, DNV standard, and FEA: $a/c = 0.3$. 94
Figure 99 - *SIF vs. a* curves for the chord side (brace B3) using SINTAP standard based on the SCF values obtained using the Lloyd's Register, DNV standard, and FEA: $a/c = 0.4$. 94
Figure 100 - *SIF vs. a* curves for the Brace B1 using BS7910, IIW and SINTAP standards based on DNV standard for $\sigma n = 12.51MPa$: $a/c = 0.1$. 97
Figure 101 - SIF vs. a curves for the Brace B1 using BS7910 and IIW to compare M_{km} and M_{kb} values: a/c = 0.1. 98

List of tables

Table 1 - Types of hot-spots [17]. 12
Table 2 - Recommended meshing and extrapolation [17]. 14
Table 3 - Stress concentration factors for simple KT tubular joints and overlap KT joints [24]. 21
Table 4 - Stress concentration factors for simple KT tubular joints and overlap KT joints [24] (continued). 22
Table 5 - SCFs comparison [15]. 28
Table 6 - Cost of computation comparison [15]. 29
Table 7 - Comparative analysis of submodel accuracy [15]. 29
Table 8 - Geometric properties of the KT-type joint case study [26]. 31
Table 9 - Angles between joint elements according to Figure 20b, [26]. 34
Table 10 - Geometrical parameters and stress concentration factors calculation [26] 34
Table 11 - Lloyd's SCF calculation [26]. 39
Table 12 - Material properties 40
Table 13 - The variation of minimum yield strength (N/mm2) with thickness for S420 40
Table 14 - Chemical properties of S420 steel [33] 41
Table 15 - Loads used in numerical model of the KT-joint [26] 45
Table 16 - Nominal stresses and section properties [26]. 45
Table 17 - Stress concentration factors in chord crown (axial) [26] 56
Table 18 - Results of the hot-spot stress distribution and stress concentration factor for Brace B1 due to axial loading [26] 57
Table 19 - Results of the hot spot stress distribution and stress concentration factor for Brace B2 due to axial loading [26] 57
Table 20 - Results of the hot spot stress distribution and stress concentration factor for Brace B3 due to axial loading 58
Table 21 - Validity range of values for both parametric equations [26] 58
Table 22 - SCF comparison between DNV code and Lloyd [26] 59
Table 23 - Stress concentration factors for axial loading case from the Lloyd and DNVGL parametric equations and finite element analysis [26] 59
Table 24 - Deviation of stress concentration factors between DNV-FEA and between Lloyd-FEA for axial loading case [26] 60
Table 25 - Values of v and w for axial and bending loading [28] 64
Table 26 - constants A and B 85
Table 27 - Validity range of values according to standards 95
Table 28 - SIF comparison between BS7910, IIW and SINTAP standards 96

List of abbreviations

API	American petroleum institute
AWS	American welding society
CHS	Circular hollow section
Den	Department of energy
FEA	Finite element analysis
FEM	Finite element method
GoM	Gulf of Mexico
HSE	Health and safety executive
HSS	Hot-spot stress
IIW	International Institute of Welding
IPB	In plane bending
IWM	International welding machine
LDAR	Linear damage accumulation rule
OPB	Out of plane bending
SCF	Stress concentration factor
SCFAS	Stress concentration factor at the saddle for axial load
SCFAC	Stress concentration factor at the crown for axial load
SCFMIP	Stress concentration factor for in plane moment
SCFMOP	Stress concentration factor for out of plane moment
SIF	Stress intensity factor
UK	United Kingdom
UKOSRP	United Kingdom offshore steels research project

1. Introduction

1.1 Motivation

The majority of offshore platforms installed in shallow water, where drilling and extraction of oil and/or gas is under 300 meters, are fixed to the seabed and use tubular members as structural elements to build truss frameworks. The environment surrounding the offshore platforms implicates various cycles or repetitive loadings such as wind, waves, currents and earthquakes, which causes time-varying stresses resulting in global and/or local fatigue damage to the structure. This topic has become a great deal to engineers on previous and recent offshore platform installation design, especially the area around tubular joints [1].
The resistance against fatigue crack propagation has been investigated since the mid-1980s due to the increasing computing power in order to improve calculation accuracy and understand the behavior of the structures in marine environments so that their working lifetime expectancy is prolonged. All the major multinational companies that work in the oil and gas business are interested in offshore structures. These companies provide continuous support for research and development that will enhance the ability of their engineering firms and construction contractors to support their business needs [2].
In this way, the stress concentration factors (SCF) and stress intensity factors (SIF) for a typical KT-joint of offshore structures based on parametric solutions are calculated and discussed. These parameters are extremely important in the fatigue design and residual lifetime of offshore structures applications.

1.2 Objectives

Nowadays, we come across with the increasing usage of tubular structures in various constructions whether they are offshore installations, trusses, high rise buildings, road pole signals and so on. The reason goes through its excellent structural performance as well as its attractive appearance. However, the existing stress concentration, especially in the welded parts of these structures is an aspect of extreme relevance with regard to fatigue design in the context of tubular and non-tubular joints. Many detailed studies are needed to make a more consistent procedure to estimate the stress concentration factors (SCF). In this study, it is aimed to make a comparison between the obtained SCF values for an offshore tubular KT-joint from the analytical equations (Lloyd and Efthymiou) and finite element simulation in order to estimate more suitable and reliable the fatigue design.
Additionally, due to the environmental cycling loading that often lead to fatigue damage in the form of cracks emanating from the weld toes at the joints, becomes essential a proper understanding of the crack growth. Then, the stress intensity factors (SIF) need to be evaluated using analytical and numerical simulations with aims to contribute to the enhanced prediction of the residual lifetime of structural joints in

offshore structures. Hence, a comparison for the M_k factors and SIF solutions, using the assumptions proposed by IIW, BS7910 and SINTAP standards, are made.

1.3 Outline of thesis

This thesis is organized by an introduction (Chapter 1), a review on tubular offshore structures and fatigue design aspects (Chapter 2), a discussion of the collected SCF values for a typical tubular KT-joint based on numerical simulation and analytical formulations (Chapter 3), an evaluation of SIF values for a typical tubular KT-joint based on BS7910 standard, SINTAP and IIW recommendations, and finally, the conclusions and future works (Chapter 5).
In Chapter 1 (Introduction) is presented the motivation, the objectives, and the thesis organization.
In Chapter 2 is made a detailed review of offshore structures, tubular connections, fatigue, hot-spot and nominal stress approaches, stress concentration factors (SCF), stress intensity factors (SIF) and a review on finite element analysis used to evaluate the SCF and SIF values.
An evaluation of the stress concentration factor values for a typical KT tubular joints collected in literature is made (Chapter 3). A comparison and discussion between DNVGL code/Efthymiou and Lloyd's register (LR) parametric equations as well as numerical analysis to evaluate the SCF values for the joint under consideration are made. The hot-spot stresses and SCF values are determined with aims to be used in analytical calculations of the SIF values.
In Chapter 4, analytical calculations of the SIF factors and M_k values based on IIW, BS7910 and SINTAP standards were made and a comparison was made.
Conclusions and future works related to this study are presented in Chapter 5.

2. Review on tubular offshore structures and fatigue assessment methods

2.1 Introduction

Offshore platforms, also referred to oil platforms are large structural facilities used to drill well and extract oil and natural gas. It was the growing demand for exploration and production of these hydrocarbons that provided a continuous and thorough search for developments in this area. Over the past 40 years, two major types of fixed platforms have been developed (Fig. 1): the steel template, which was pioneered in the Gulf of Mexico (GoM); and the concrete gravity type, first developed in the North Sea. Recently, a third type, the tension-leg platform, has been used to drill wells and develop gas projects in deep water [3]. The different types of offshore structures are shown in Figure 2.

Fatigue is the weakening of a certain material, steel structure or mechanical component, caused by the appliance of loads. In other words, the progressive and localized structural damage which occurs when submitted to cyclic loading. One of the main reasons for damage to steel structures, especially welded components, is fatigue cracking that if not controlled can grow into failure or collapse which can bring severe consequences. Fatigue failure in offshore structures is quite different from ordinary mechanical machines as the number of cyclic loading is much more pronounced and the wave forces applied to the structure are inconsistent, corresponding to stochastic and nonlinear loading.

Therefore, period inspections and monitoring have to be carried out to improve the safety of personnel and resources, so the sustainability of floating structures increases.

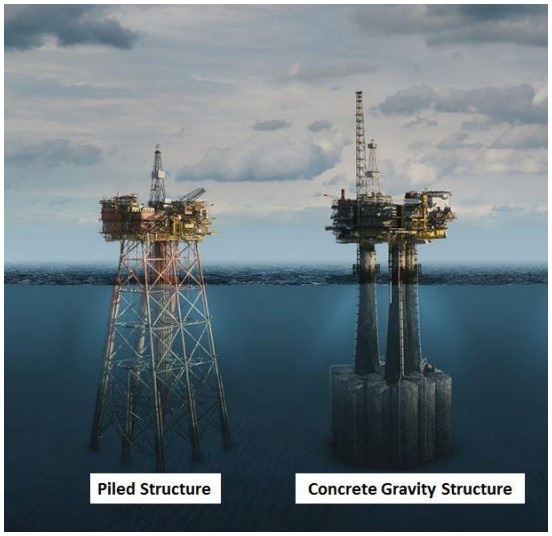


Figure 1 - Piled Structure and Gravity Structure of Brent [4].

Reservoir and fluid characteristics, water depth and ocean environment are the variables that primarily determine the functional requirements for an offshore facility. Besides the structure-function, the site infrastructure, management philosophy and financial strength of the operator as well as the rules, regulations and national law are important aspects to be taken into account as well [4]. Depending on the conditions presented in their site of constriction they may be fixed, complaint or floatable.
Offshore structures are designed to resist continual wave loading which may lead to significant fatigue damage on individual structural members and other types of loads due to severe storms corrosion, fire and explosion, etc.
This gives the best compromise in satisfying the requirements of low drag coefficient, high buoyancy, and high strength to weight ratio [5].

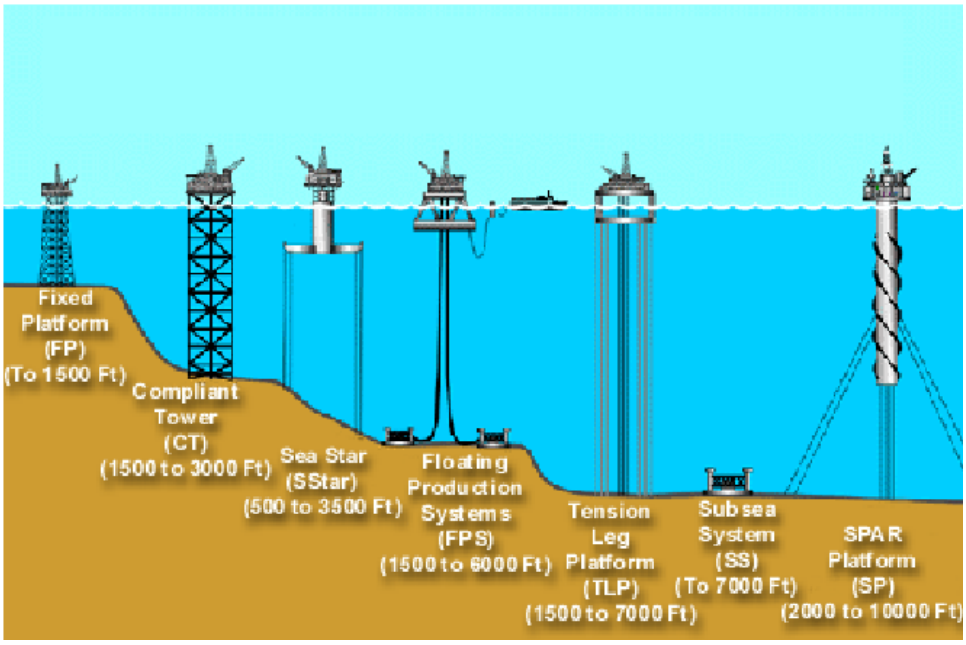


Figure 2 - Types of offshore structures [4].

2.2 Offshore tubular joints

2.2.1 Introduction

The primary basic parts of jacket type platforms, usually utilized for the generation of oil and gas in seaward fields, are created from circular hollow section (CHS) members by welding the prepared end of brace members onto the undisturbed surface of the chord, resulting in what is called a tubular joint [6].
Offshore structures are subjected to multiple environmental cyclic loadings such as wind, wave, ice, and traffic during their service lives. Fatigue failure occurs where the local peak stresses occur. At these high-stress points, cracks will develop and grow until fatigue failure as the structure is being solicited. The two main characteristics that will affect the high peak stresses and therefore the fatigue life of a structure are the geometry and the loading they are subjected to. The most fragile fatigue areas are the welded parts in the tubular joints. Tubular sections are widely used because of their intrinsic properties consisting of the possession of high torsional rigidity and

higher strength to weight ratio when compared to the conventional steel sections as well as the capability of minimizing the hydrodynamic forces with a great quality-cost balance [7]. In Figure 3, different types of tubular joints are shown.

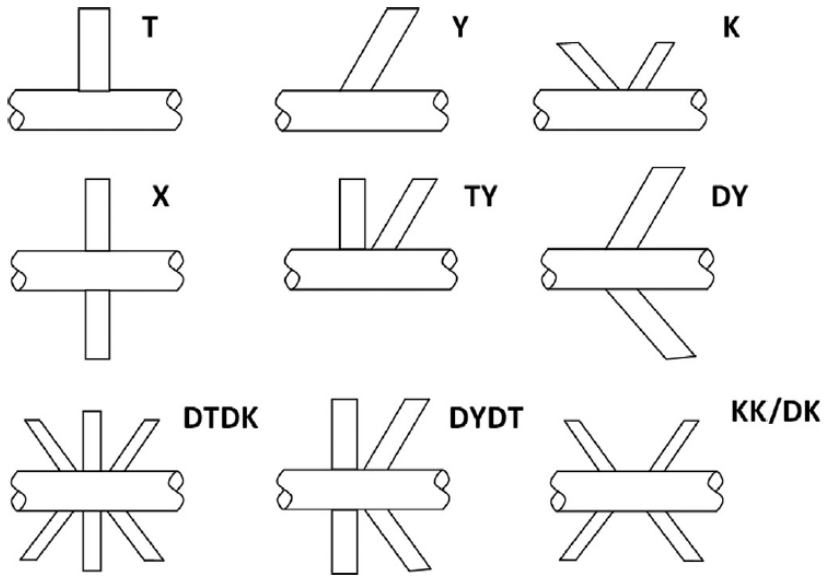


Figure 3 - Types of tubular joints along with their nomenclature [8].

In Figure 4 are presented the geometry of an offshore tubular joint as well as the primary dimensions and how to calculate the non-dimensional parameters commonly used.

The non-dimensional parameters used are the following:

- α: chord length to half chord diameter ratio;
- β: brace diameter to chord diameter ratio;
- γ: radius to wall thickness ratio of chord member;
- τ: brace to chord wall thickness ratio;
- θ: brace to chord intersection angle.

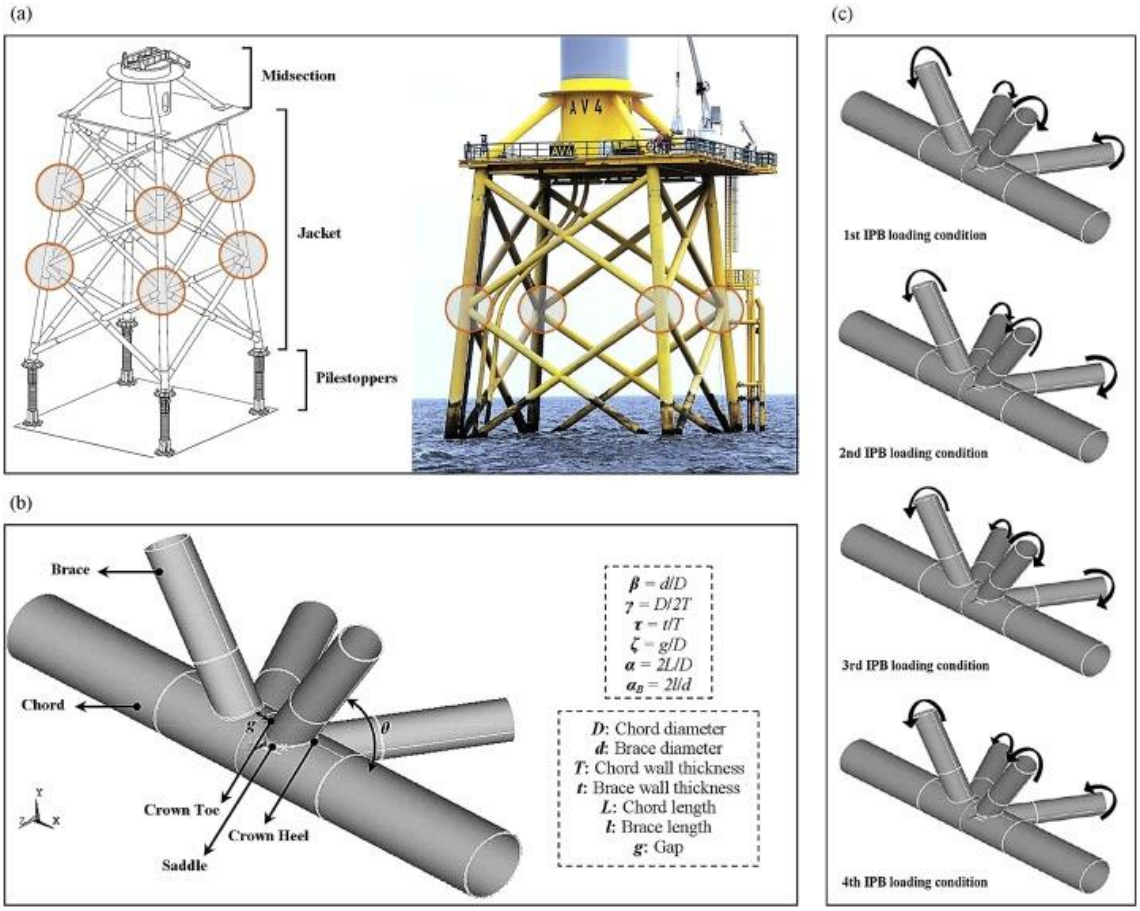


Figure 4 – Offshore tubular joints: (a) Example of offshore jacket structure; (b) Definition of the geometrical parameters of a joint; (c) Different types of IPB loadings [9].

2.3 Fatigue of offshore structures

2.3.1 Introduction

Fatigue analysis may be based on different methodologies depending on what is found most efficient for the considered structural detail. The main difference between these methods relies on the parameters used to estimate the fatigue life or fatigue strength. The fatigue design of welded joints is based on the use of S-N curves (Figure 5), which are obtained from fatigue tests. The design S-N curves which follow are based on the mean-minus-two-standard-deviation curves for relevant experimental data, which are associated with a 97.7% probability of survival [10].

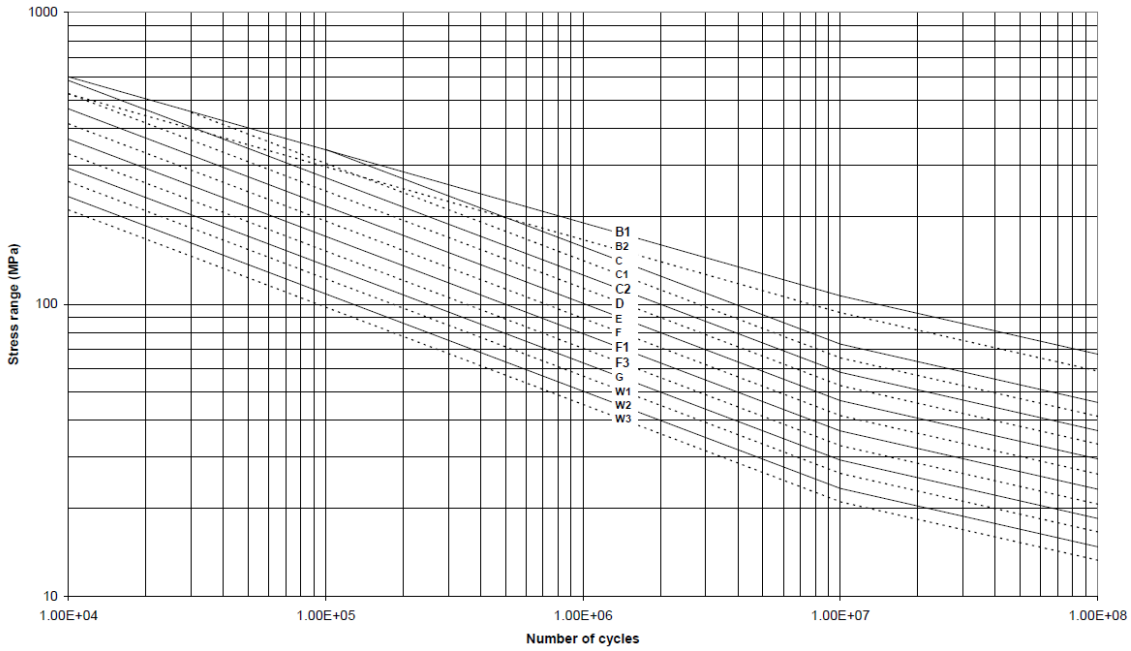


Figure 5 - S-N curves for offshore connections or details based on DNVGL standard [10].

It is thus important that the stresses are calculated in agreement with the definition of the stresses to be used together with a particular S-N curve. Three different concepts of S-N curves are defined below: structural action (nominal stress), compatibility between members (geometric stress) and discontinuity at the joint (local stress).

Nominal stress (σ_{nom}) by definition, it is the maximum stress in a cross-section of the brace member due to forces, moments, or combinations of the two acting at the location of possible cracking, using both the simple beam theory and the superposition principle and ignoring the geometric discontinuity and the weld toe geometry (see Figure 6).

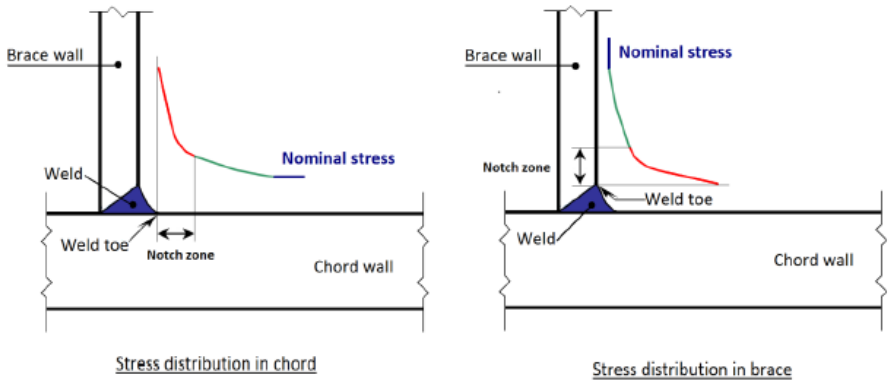


Figure 6 - Definition of nominal stress distribution in chord and brace side [1].

Geometric Stress (σ_G) is interpreted as the fatigue stress at the toe of the weld where fatigue cracking will most likely start because of the high-stress concentration caused by discontinuity and/or notch (see Figure 7). It is used to calculate the fatigue life of tubular/non-tubular joints. The geometric stress is a compromise between membrane stress augmentation due to the complexity of the welded joint and the bending stress towards eccentricity. It does not include the nonlinear stress peak of the exact weld toe geometry.

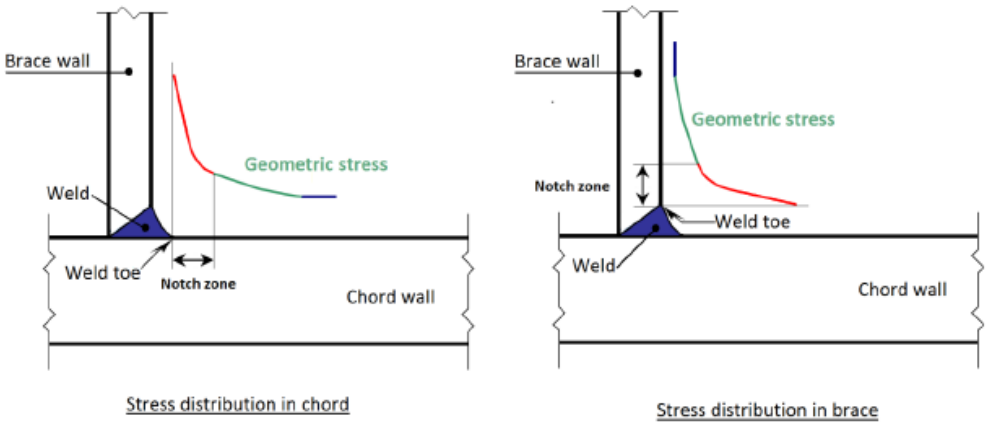


Figure 7 - Definition of geometric stress distribution in chord and brace side [1].

The total stress found at the local notch of the weld toe is called **local notch stress** (see Figure 8). It is dependent on the geometry of the welding which being not accurate, it varies each time it is made. A very tiny change on the local notch causes a significant difference in the local notch stress. Consequently, the non-linear stress distribution is produced, mainly through-thickness direction. Being dependent on the quality of the welding and the workmanship, the value of the local stress is quite random. That is the reason to be excluded from the nominal and hot stress formulation.

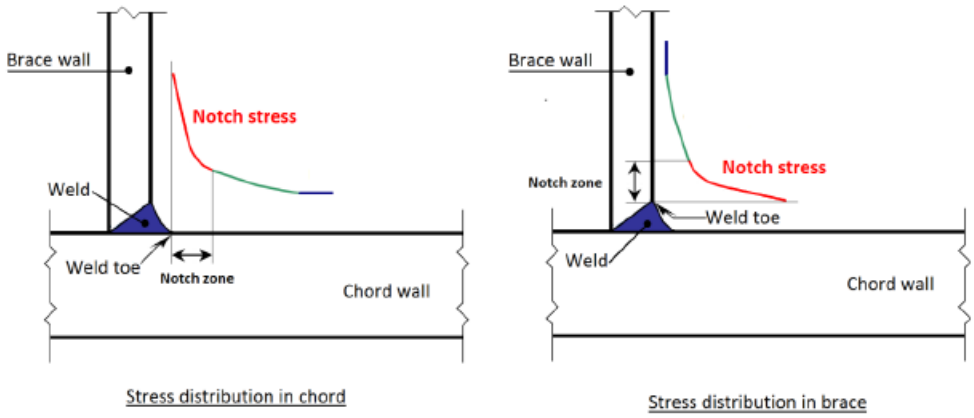


Figure 8 - Definition of notch stress distribution in chord and brace side [1].

2.3.2 Damage accumulation method

The fatigue life may be calculated based on the S-N fatigue approach under the assumption of linear cumulative damage (Palmgren-Miner rule). The linear damage accumulation rule (LDAR) describes the fatigue damage accumulation under variable amplitude load where (D) is the fatigue damage of the material, (n_i) is the number of applied loading cycles corresponding to the *i*th load level, and (N_i) is the number of cycles to failure at the *i*th load level, from constant amplitude experiments [11].

$$D = \sum_{i=1}^{k} \frac{n_i}{N_i} \tag{1}$$

where:

D - Accumulated fatigue damage;

k - Number of stress blocks;

n_i - Number of stress cycles the structural detail endures at range, $\Delta\sigma_i$;

N_i - Number of cycles to failure at stress range, $\Delta\sigma_i$.

2.3.3 Nominal stress approach

For assessing the fatigue strength and service life of non-welded structural members, or in cases where the stress concentrations due to the weld are disregarded, proceeds from the nominal stress amplitudes in the critical cross-section and it is made a comparison with the S-N curve of the sustainable nominal stress amplitudes (see Figure 9). If specific test data are not available, the *S–N* curve can be defined approximately based on the normalized *S–N* curve scheme. The nominal stress *S–N* curve incorporates the influence of the material, its geometry (inclusive of notch and size effect) and surface (inclusive of hardening and residual stresses). The service

life results from the nominal stress *S–N* curve and the nominal stress spectrum according to a simple hypothesis of damage accumulation, mostly according to a modified and relative form of Miner's rule. The nominal stress amplitude spectrum follows from the load amplitude spectrum taking the critical cross-section and the type of loading into account [12].

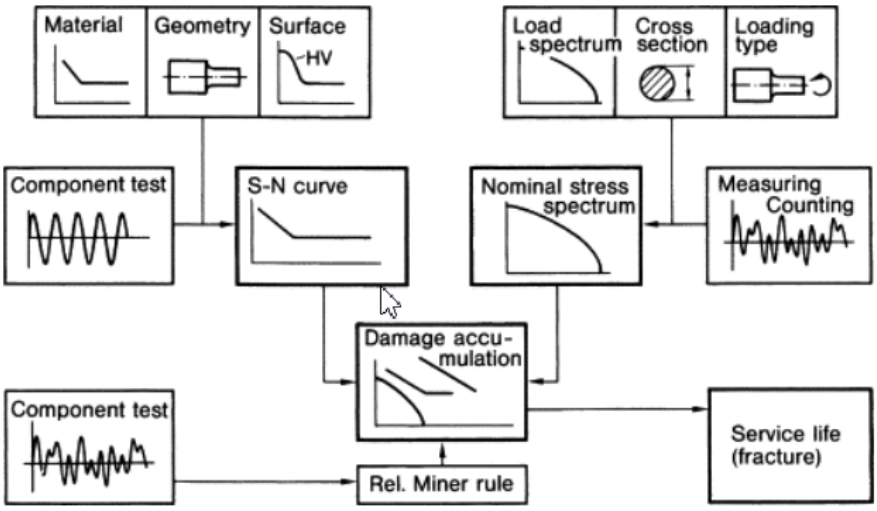


Figure 9 - Nominal stress approach for assessing the fatigue strength and service life of non-welded structural components [12].

The nominal stress approach has two disadvantages for tubular joints. On the first hand, it is not possible to define reasonable nominal stress due to the complex geometry and the applied loading. Secondly, suitable fatigue test data are often not available for large complex tubular joints.
Nominal stress can be determined, in simple components, using elementary theories and structural mechanics based on linear-elastic behavior. Nominal stress is the average stress in the weld throat or plate at the weld toe as the tables of structural details indicate [13].

$$\sigma_{nom} = \frac{P}{A} \pm \frac{M}{I} y \tag{2}$$

where:
P – Applied axial compressive load;
A – Cross-section area;
M – Applied bending moment;
I – Moment of inertia;
y – Position of the extreme fiber.

2.3.4 Hot-Spot stress approach

The hot-spot stress method, also referred to as the geometric stress method, considers the stress raising effect due to structural discontinuity except for the stress concentration due to weld toe, i.e., without considering the localized weld notch stress [8]. Hot- spot stress is the surface value of structural stress at hot-spots. The locations at a welded joint where cracks are most likely to initiate under cyclic loading due to increased stress value are called the hot-spots. Along with research institutes, the offshore platform operators developed this method in the 1970's aiming the fatigue stress assessment of tubular joints [8]. The definition of hot-spot stress (HSS) was drafted by the review panel of the United Kingdom Offshore Steels Research Project (UKOSRP) and adopted by the UK Department of Energy (DEn) Guidance Notes [14] and states that it is the value calculated by the extrapolation to the weld toe of the maximum principal stresses at a distance x_1 and x_2 (Figure 10) [15].

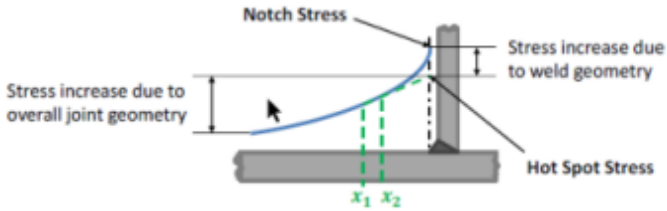


Figure 10 - Definition of hot-spot stress [15].

Radaj [16] demonstrated, more focused on plate and shell structures, that the hot-spot stress is a sum of the membrane and bending stress at the weld toe. These stresses can be determined either by surface extrapolation or inner liberalization of the stress. Figure 11 provides stress distribution through the thickness of the weld plate and its components. Three components of notch stress can be distinguished from the non-linear stress distribution of the figure below: membrane stress (σ_{mem}), shell bending stress (σ_{ben}) and non-linear stress (σ_{nlp}) [8].

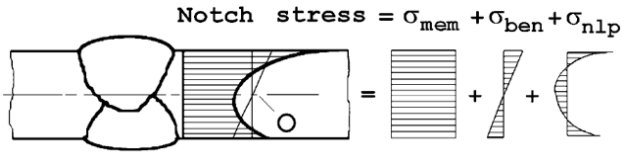


Figure 11 - Stress distribution through the thickness of the weld toe and its components [17].

As shown in Figure 11, the membrane stress is constant and bending stress varies linearly throughout the thickness. The remaining part is the non-linear stress. Hence, in the hot-spot stress method, the latter part (non-linear stress part, σ_{nlp}) is excluded from the structural stress due to the fact that an exact and detailed weld profile during the design phase is quite uncertain. In contrast with the nominal stress, in the hot-

spot stress method, fatigue life is directly related to the hot-spot stresses. It is shown in a S_{hs}-N curve a relation between the hot-spot stress range and the number of cycles to failure. There is an advantage over other methods because there are fewer S_{hs}-N curves needed to evaluate the fatigue life of welded details by the stress concentration factors.
Besides the definitions of structural hot-spot stress as given above, two types of hot-spots are defined according to their location on the plate and their orientation with respect to the weld toe as defined in Table 1.

Table 1 - Types of hot-spots [17].

Type	*Description*	*Determination*
a	Weld toe on plate surface	FEA or measurement and extrapolation
b	Weld toe at plate edge	FEA or measurement and extrapolation

The structural stress acts normal to the weld toe in each case and is determined either by a special FEA procedure or by extrapolation from measured stresses [17]. The structural hot spot stress can either be determined by measurement or calculation. Here the non-linear peak stress is eliminated by linearization of the stress through the plate thickness or by extrapolation of the stress at the surface to the weld toe. Firstly, it is needed to establish the reference points and after determining the structural hot spot stresses of those reference points. The reference point closest to the weld toe must be chosen to avoid any influence of the notch due to the weld itself. Identification of the critical points (hot spots) can be made by:

a) Measuring several different points;

b) Analysing the results of a prior FEM analysis; and,

c) Experience of existing components, especially if they failed.

If the structural hot-spot stress is determined by extrapolation, the element lengths are determined by the reference points selected for stress evaluation. Aiming the avoidance of influence of the stress singularity, the stress closest to the hot spot is usually evaluated at the first nodal point. That way, the length of the element at the hot spot corresponds to its distance from the first reference point [17].

2.3.4.1 Type “a” hot-spots

The structural hot-spot stress, σ_{hs}, is determined using the reference points and extrapolation equations as given by Equations (3) and (5).

Evaluation of nodal stresses at three reference points $0.4t$, $0.9t$ and $1.4t$, for a fine mesh (Figure 12 and Table 2) and using the quadratic extrapolation can be done by

Equation (3). This method is recommended for cases of pronounced non-linear structural stress increase towards the hot-spot, at sharp changes of direction of the applied force or for thick-walled structures.

$$\sigma_{hs} = 2.52 \cdot \sigma_{0.4 \cdot t} - 2.24 \cdot \sigma_{0.9 \cdot t} + 0.72 \cdot \sigma_{1.4 \cdot t} \quad (3)$$

Application of the usual wall thickness correction is required when the structural hot-spot stress of type **"a"** is obtained by surface extrapolation (see Figure 12) [17].
The influence of plate thickness on fatigue strength should be considered when the weld toe is the most likely to fatigue crack. The fatigue resistance values here given correspond to a steel wall with a thickness of up to 25 mm. The lower fatigue strength for thicker members is taken into consideration by multiplying the FAT of the structural detail by the thickness reduction factor, $f(t)$:

$$f(t) = \left(\frac{t_{ref}}{t_{eff}}\right)^n \quad (4)$$

where:

T_{ref} – Reference thickness (tref=25mm);

T_{eff} – Effective thickness; and,

n – Thickness correction exponent.

For circular tubular joints, the wall thickness correction exponent of $n = 0.4$ is recommended [17].

2.3.4.2 Type "b" hot-spots

The stress distribution is not dependent on plate thickness. Therefore, the reference points are given at absolute distances from the weld toe, or from the weld end if the weld does not continue around the end of the attached plate.

For the fine mesh with an element length of not more than 4 mm at the hot-spot, the valuation of nodal stresses at three reference points 4 mm, 8 mm and 12 mm and quadratic extrapolation is made by Equation (5) [17].

$$\sigma_{hs} = 3 \cdot \sigma_{4mm} - 3 \cdot \sigma_{8mm} + \sigma_{12mm} \quad (5)$$

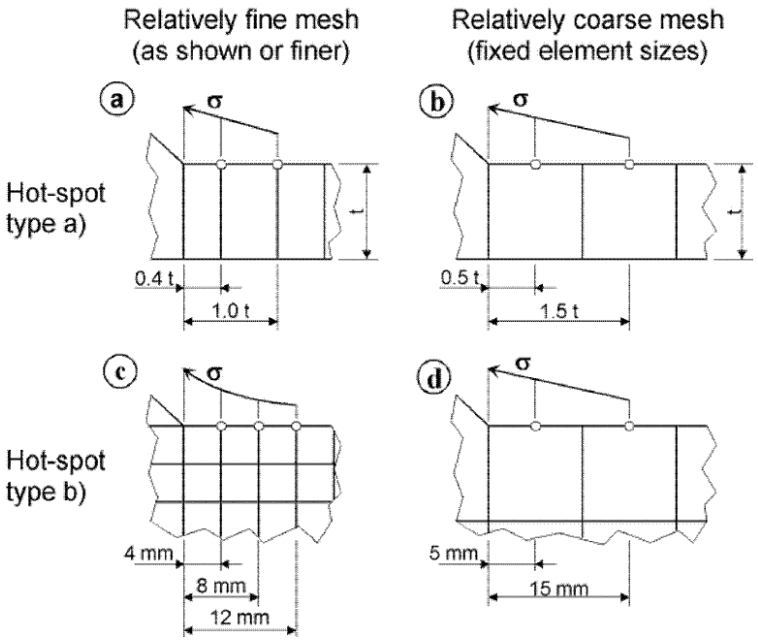


Figure 12 - Reference points at different types of meshing [17].

Table 2 - Recommended meshing and extrapolation [17].

Type of model and weld toe		Relatively coase models		Relatively fine models	
		Type a	Type b	Type a	Type b
Element size	Shells	t x t max t x w/2*)	10 x 10 mm	≤0.4 t x t or ≤0.4 t x w/2	≤ 4 x 4 mm
	Solids	t x t max t x w	10 x 10 mm	≤0.4 t x t or ≤0.4 t x w/2	≤ 4 x 4 mm
Extra-polation points	Shells	0.5 t and 1.5 t mid-side points**)	5 and 15 mm mid-side points	0.4 t and 1.0 t nodal points	4, 8 and 12 mm nodal points
	Solids	0.5 and 1.5 t surface center	5 and 15 mm surface center	0.4 t and 1.0 t nodal points	4, 8 and 12 mm nodal points
*) w = longitudinal attachment thickness + 2 weld leg lengths **) surface center at transverse welds, if the weld below the plate is not modelled (see left part of fig. 2.2-11)					

2.4 Definition of stress concentration factor (SCF)

When in the presence of a welded connection intersection derived from a change of section, it is inherent modification of the stress distribution. Thus, high-stress concentrations appear where the structure is more predisposed to fail. The stress concentration factor (SCF) is a means to quantitatively measure these high-stress concentrations produced in joints subjected to specific loading conditions and can be defined as the ratio of hot spot stress range (σ_{max}, τ_{max}) over nominal stress range (σ_{mon}, τ_{mon}).

For normal stress (tension and bending):

$$SCF = \frac{\sigma_{max}}{\sigma_{nom}} \tag{6}$$

For shear stress (torsion):

$$SCF = \frac{\tau_{max}}{\tau_{nom}} \tag{7}$$

There are different approaches to a welded joint for fatigue life analysis. The main difference between methods lies in the parameters used for the description of fatigue life or fatigue strength. Among all approaches, includes the nominal stress approach, structural or hot-spot stress approach, notch stress or notch intensity approach, notch strain approach, crack propagation approach, and so on. Within all, hot-spot stress is the most widely used and recommended by various fatigue design guidelines (e.g., American Petroleum Institute (API) [18], CIDECT Design Guide No.8 [19]) [8].
In order to deal with the fatigue problem that has been aggravating tubular joints in many offshore structures for the past years it is required the assessment of the magnitude of the SCF [20]. Regarding welded tubular joints, much research has been carried out to improve the estimation of the HSS range through the SCF. It may be obtained analytically from the Elasticity Theory, computationally from the FE method, and experimentally using methods such as photoelasticity or strain measurements. Although some analytical assumptions are not precise, isotropic and homogeneous material, it is possible to achieve quite good agreement with the experimental work.

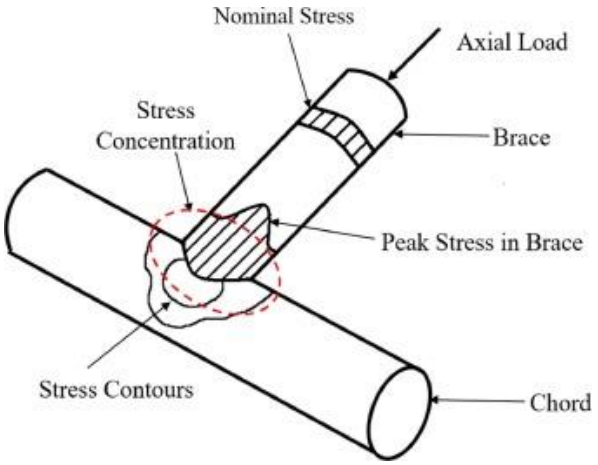


Figure 13 - Stress concentration in tubular joint [8]

2.5 Definition of stress intensity factor (SIF)

Fracture mechanics is used to assessing the behaviour of cracks. It can be used to calculate the growth of an initial crack a_i to a final size a_f. Since crack initiation occupies only a small proportion of the lives of welded joints in structural metals, the

method is suitable for the assessment of fatigue life, inspection intervals, crack-like weld imperfections and the effect of variable amplitude loading. The parameter which describes the fatigue action at a crack tip in terms of crack propagation is the stress intensity factor (SIF) range, ΔK [17].

It is affected by loading conditions, geometric shapes, crack sizes and positions which cause residual stresses (those that remain on the surface of an object even when no external load is applied).

The SIF can generally be obtained by analytical, numerical or test methods. Many studies have been done about the stress intensity factor of welded joints using numerical methods [21]. Al-Mukhtar et al. [22] evaluated the stress intensity factor of load-carrying cruciform welded joints using the 2D finite element method, considering the effects of weld size and plate thickness ratio. Results show that only the weld size has a strong impact on the stress intensity factor while the plate thickness ratio can be disregarded. After comparing the results, it was concluded that there is a good compromise between FE solutions and analytical ones.

Irwin [34] published a solution for fatigue assessments regarding the stress intensity factor as it follows:

$$K = Y(a) \cdot \sigma\sqrt{\pi \cdot a} \tag{8}$$

$$K = (Y_m(a) \cdot \sigma_m + Y_b(a) \cdot \sigma_b) \cdot \sqrt{\pi \cdot a} \tag{9}$$

The geometrical correction factor $Y(a)$ is not only determined with FEM but also analytical solutions are available for $Y(a)$ for many cases in for example BS 7910 standard and IIW recommendations.

Tada [35], like Irwin, published a set of solutions to determine the effective SIF that in the absence of accurate compliance functions can be used to provide pessimistic estimations. In general, the stress intensity factor (SIF) has 3 loading modes required to calculate K_r: tensile loading (mode I), in-plane shear loading (mode II) and out of plane shear loading (mode III). These are designated as follows:

$K_I^p(a)$ and $K_I^s(a)$ are the linear elastic SIFs for the flaw size, a, for loads giving rise, respectively, to primary and secondary stress components which are normal to the plane of the crack.

$$K_I = K_I^p + K_I^s \tag{10}$$

$K_{II}^p(a)$ and $K_{II}^s(a)$ are the linear elastic SIFs for the flaw size, a, for loads giving rise, respectively, to primary and secondary stress components which are in-plane shear.

$$K_{II} = K_{II}^p + K_{II}^s \tag{11}$$

$K_{III}^{p}(a)$ and $K_{III}^{s}(a)$ are the linear elastic SIFs for the flaw size, a, for loads giving rise, respectively, to primary and secondary stress components which are out-of-plane shear (torsion).

$$K_{III} = K_{III}^{p} + K_{III}^{s} \tag{12}$$

The effective SIF (Budden and Jones [23]) can be calculated as follows:

$$\text{If} \quad K_{mat}/\sigma_y \geq 6.3\sqrt{mm}$$
$$K_{eff} = \{K_I^2 + K_{II}^2 + K_{III}^2/(1-\upsilon)\}^{1/2} \tag{13}$$

$$\text{If} \quad K_{mat}/\sigma_y < 6.3\sqrt{mm}$$
refer to Budden and Jones [23] (14)

2.6 Estimation of SCF and SIF values based on design codes

2.6.1 Superposition of stresses in tubular joints

The stresses in tubular joints due to brace loads are calculated at the crown and the saddle points, see Figure 14.

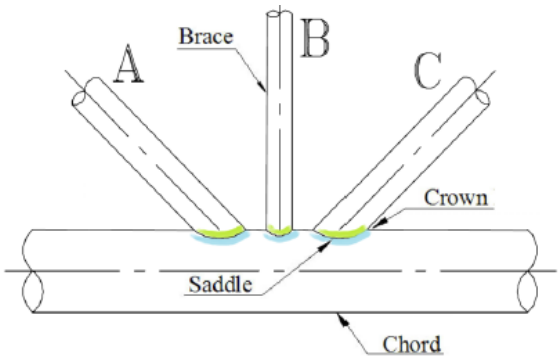


Figure 14 - Illustration of arbitrary KT-Joint with definition of saddle and crown points [1].

It is possible to obtain the hot spot stress at these points by summing up the single stress components from axial, in-plane and out of plane actions. Higher values are possible to get between the saddle and the crown points by using a linear interpolation of the axial action and a sinusoidal bending stress variation from in and out-of-plane bending.

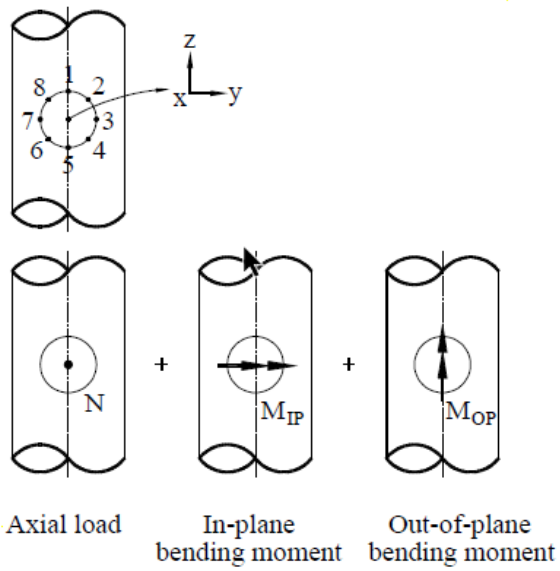


Figure 15 - Superposition of stresses [24].

In such a way, the hot-spot stress should be calculated at 8 different spots circumferencing their intersection, see Figure 15 [24]:

$$\sigma_1 = SCF_{AC}\sigma_x + SCF_{MIP}\sigma_{my} \tag{15}$$

$$\sigma_2 = \frac{1}{2}(SCF_{AC} + SCF_{AS})\sigma_x + \frac{1}{2}\sqrt{2}SCF_{MIP}\sigma_{my} - \frac{1}{2}\sqrt{2}SCF_{MOP}\sigma_{mz} \tag{16}$$

$$\sigma_3 = SCF_{AS}\sigma_x - SCF_{MOP}\sigma_{mz} \tag{17}$$

$$\sigma_4 = \frac{1}{2}(SCF_{AC} + SCF_{AS})\sigma_x - \frac{1}{2}\sqrt{2}SCF_{MIP}\sigma_{my} - \frac{1}{2}\sqrt{2}SCF_{MOP}\sigma_{mz} \tag{18}$$

$$\sigma_5 = SCF_{AC}\sigma_x - SCF_{MIP}\sigma_{my} \tag{19}$$

$$\sigma_6 = \frac{1}{2}(SCF_{AC} + SCF_{AS})\sigma_x - \frac{1}{2}\sqrt{2}SCF_{MIP}\sigma_{my} + \frac{1}{2}\sqrt{2}SCF_{MOP}\sigma_{mz} \tag{20}$$

$$\sigma_7 = SCF_{AS}\sigma_x + SCF_{MOP}\sigma_{mz} \quad (21)$$

$$\sigma_8 = \frac{1}{2}(SCF_{AC} + SCF_{AS})\sigma_x + \frac{1}{2}\sqrt{2}SCF_{MIP}\sigma_{my} + \frac{1}{2}\sqrt{2}SCF_{MOP}\sigma_{mz} \quad (22)$$

where:

σ_x, σ_{my} and σ_{mz} are the maximum nominal stresses derived from axial load and in plane and out of plane bending respectively;

SCF_{AS} and SCF_{AC} are the stress concentration factor for axial load at the saddle and crown respectively;

SCF_{MIP} and SCF_{MOP} are the stress concentration factor for in plane and out of plane moment respectively.

The stress concentration factors for tubular joints shown in Table 3 are subjected to loads in the braces. Still in the axial direction, for significant dynamic stresses, the hot spot stresses at the crown toe and at the crown heel should be added to the corresponding hot spot-stresses resulting from the brace loads before the S-N curve is entered for calculation of fatigue damage. Braces may be considered attachments to the chord when axial loading in the chord is applied. As a consequence, the axial stress in the chord should be increased by a SCF=1.20 for calculation of additional hot-spot stress at the crown toe and the crown heel for dynamic loading in the axial direction of the chord [24].

2.6.2 Parametric equations

The hot-spot stress method requires an accurate prediction of SCFs. In this section, a brief description of the commonly used parametric equation is provided with an emphasis on how the hot-spot stress is defined and their range of applicability [8].

2.6.2.1 Efthymiou equations

Efthymiou [25] published 1988 a complete and thorough set of simple joint parametric equations covering T/Y, X, K, and KT simple combined setups. These equations were designed using influence functions to describe K, KT, and multi-planar joints in terms of simple T braces with carry-over effects from the additionally loaded braces. [26] In Table 3 are presented, by way of example, different parametric formulas to calculate

the SCF in a KT-joint. These parametric equations are based on Efthymiou's research and are frequently used in the fatigue design code [10]. These equations presented are for the chord and brace outer surface only. The disadvantage of this study is that the SCFs are only given at certain positions around the weld such as the saddle and the crown disregarding any possible useful further information. However, these equations are widely accepted and used in the offshore industry.

For the design of simple tubular joints, it is standard practice to use parametric equations for the derivation of stress concentration factors (SCF) to obtain hot-spot stress for the actual geometry. Then this hot-spot stress is entered into a relevant hot-spot stress S-N curve for tubular joints [24].

Table 3 - Stress concentration factors for simple KT tubular joints and overlap KT joints [24].

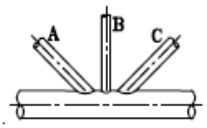
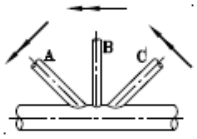
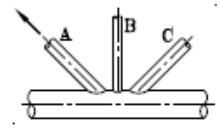
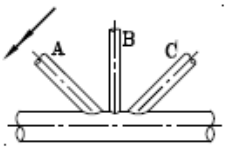
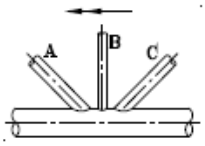
Load type	*SCF equation*
Balanced axial load  	Chord: (Eqn. (20)) Brace: (Eqn. (21)) For the diagonal braces A & C use $\zeta = \zeta_{AB} + \zeta_{BC} + \beta_B$ For the central brace, B, use ζ = maximum of ζ_{AB}, ζ_{BC}
In-plane bending	Chord crown: (Eqn. (8)) Brace crown: (Eqn. (9))
Unbalanced out-of-plane bending  	Chord saddle SCF adjacent to diagonal brace A: $(\text{Eqn.}(10))_A \cdot \left(1-0.08(\beta_B\gamma)^{0.5}\exp(-0.8x_{AB})\right)\left(1-0.08(\beta_C\gamma)^{0.5}\exp(-0.8x_{AC})\right)+$ $(\text{Eqn}(10))_B \cdot \left(1-0.08(\beta_A\gamma)^{0.5}\exp(-0.8x_{AB})\right)\left(2.05\beta_{max}^{0.5}\exp(-1.3x_{AB})\right)+$ $(\text{Eqn}(10))_C \cdot \left(1-0.08(\beta_A\gamma)^{0.5}\exp(-0.8x_{AC})\right)\left(2.05\beta_{max}^{0.5}\exp(-1.3x_{AC})\right)$ where $x_{AB} = 1+\frac{\zeta_{AB}\sin\theta_A}{\beta_A}$ $x_{AC} = 1+\frac{(\zeta_{AB}+\zeta_{BC}+\beta_B)\sin\theta_A}{\beta_A}$ Chord saddle SCF adjacent to central brace B: $(\text{Eqn.}(10))_B \cdot \left(1-0.08(\beta_A\gamma)^{0.5}\exp(-0.8x_{AB})\right)^{P_1} \cdot$ $\left(1-0.08(\beta_C\gamma)^{0.5}\exp(-0.8x_{BC})\right)^{P_2} +$ $(\text{Eqn.}(10))_A \cdot \left(1-0.08(\beta_B\gamma)^{0.5}\exp(-0.8x_{AB})\right)\left(2.05\beta_{max}^{0.5}\exp(-1.3x_{AB})\right)+$ $(\text{Eqn.}(10))_C \cdot \left(1-0.08(\beta_B\gamma)^{0.5}\exp(-0.8x_{BC})\right)\left(2.05\beta_{max}^{0.5}\exp(-1.3x_{BC})\right)$ where $x_{AB} = 1+\frac{\zeta_{AB}\sin\theta_B}{\beta_B}$ $x_{BC} = 1+\frac{\zeta_{BC}\sin\theta_B}{\beta_B}$ $P_1 = \left(\frac{\beta_A}{\beta_B}\right)^2$ $P_2 = \left(\frac{\beta_C}{\beta_B}\right)^2$

Table 4 - Stress concentration factors for simple KT tubular joints and overlap KT joints [24] (continued).

Out-of-plane bending brace SCFs	Out-of-plane bending brace SCFs are obtained directly from the adjacent chord SCFs using: $\tau^{-0.54}\gamma^{-0.05}\left(0.99-0.47\beta+0.08\beta^{4}\right)\cdot SCF_{chord}$ where SCFchord = (Eqn. 27)) or (Eqn. (28))
Axial load on one brace only 	Chord saddle: (Eqn. (5)) Chord crown: (Eqn. (6)) Brace saddle: (Eqn. (3)) Brace crown: (Eqn. (7))
Out-of-plane bending on one brace only 	Chord SCF adjacent to diagonal brace A: $(\text{Eqn. (10)})_{A}\cdot\left(1-0.08(\beta_{B}\gamma)^{0.5}\exp(-0.8x_{AB})\right)\left(1-0.08(\beta_{C}\gamma)^{0.5}\exp(-0.8x_{AC})\right)$ where $x_{AB}=1+\frac{\zeta_{AB}\sin\theta_{A}}{\beta_{A}}$ $x_{AC}=1+\frac{(\zeta_{AB}+\zeta_{BC}+\beta_{B})\sin\theta_{A}}{\beta_{A}}$
	Chord SCF adjacent to central brace B: $(\text{Eqn. (10)})_{B}\cdot\left(1-0.08(\beta_{A}\gamma)^{0.5}\exp(-0.8x_{AB})\right)^{P_1}\cdot$ $\left(1-0.08(\beta_{C}\gamma)^{0.5}\exp(-0.8x_{BC})\right)^{P_2}$ where $x_{AB}=1+\frac{\zeta_{AB}\sin\theta_{B}}{\beta_{B}}$ $x_{BC}=1+\frac{\zeta_{BC}\sin\theta_{B}}{\beta_{B}}$ $P_1=\left(\frac{\beta_{A}}{\beta_{B}}\right)^{2}$ $P_2=\left(\frac{\beta_{C}}{\beta_{B}}\right)^{2}$
Out-of-plane brace SCFs	Out-of-plane brace SCFs are obtained directly from the adjacent chord SCFs using: $\tau^{-0.54}\gamma^{-0.05}\left(0.99-0.47\beta+0.08\beta^{4}\right)\cdot SCF_{chord}$

2.6.2.2 Lloyd’s Register equations

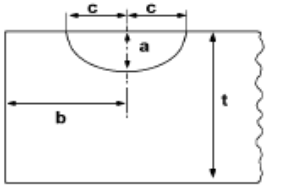
The Lloyd’s Register equations were developed in 1991 for T/Y, X, K, and KT joint configurations [1].

UK Health and Safety Executive report arranged by Lloyd's Register gave a complete appraisal of existing parametric conditions for basic tubular joints. It likewise secured the new arrangement of parametric conditions created by Lloyd's Register. These new conditions depended on trial examination on steel and acrylic cylindrical joint examples. A survey on trial and numerical demonstrating methods to decide SCF in straightforward tubular joints were as well given in this report. The joints with geometric parameters having applications in seaward stages were incorporated into the database i.e., $\tau \leq 1.05$, $\gamma \leq 40$, $SCFs \geq 1.5$, and $\beta \leq 1.0$. Further, Lloyd's Register arranged a report UK Health and Safety Executive, which covers the exploratory database of SCF in multiplanar K and KK/DK joints. These conditions have a constrained degree and the SCF esteems are given distinctly at crown and seat focuses. These conditions depend on acrylic and steel joint example just, and thus, the SCF esteems may not be solid by and large. In any case, these conditions are appropriate to assess fatigue life utilizing the S-N approach [8].

2.6.3 Calculation of SIF by IIW standards

The international institute of welding, more specifically the Commissions XIII and XV transferred to the joint working group XIII-XV where it was discussed and drafted in the years 1990 to 1996 and then updated in the years 2002-2007.
The IIW, and every other body or person involved in the preparation and publication of this document aimed to provide a basis for the design and analysis of welded components loaded by fluctuating forces, to avoid failure by fatigue. In addition, they may assist other bodies who are establishing fatigue design codes.
The purpose of designing a structure against the limit state due to fatigue damage is to ensure, with an adequate survival probability, that the performance is satisfactory during the design life. The required survival probability is obtained by the use of appropriate partial safety factors. It is shown in the figure below an example of a set of equations regarding the calculation of SIF in surface cracks [17]. In Figure 16, the procedure to calculate the stress intensity factor values for a surface cracks under shell bending and membrane stress are presented.

Surface cracks under shell bending and membrane stress



b = distance to nearest edge

The formula for the stress intensity factor K_1 is valid for a/c < 1,
for more details see ref.[4-2].

$K_1 = (\sigma_{mem} + H \cdot \sigma_{ben}) \sqrt{(\pi \cdot a / Q)} \cdot F_s$

$Q = 1 + 1.464\ (a/c)^{1.65}$

$F_s = [M_1 + M_2 \cdot (a/t)^2 + M_3 \cdot (a/t)^4] \cdot g \cdot f \cdot f_w$

$M_1 = 1.13 - 0.09\ (a/c)$

$M_2 = -0.54 + 0.89 / (0.2 + a/c)$

$M_3 = 0.5 - 1 / (0.65 + a/c) + 14\ (1 - a/c)^{24}$

$f_w = [\sec(\pi \cdot c \sqrt{(a/t)} / (2 \cdot b))]^{1/2}$

g and f are dependent to direction

"a"-direction: g = 1 f = 1

"c"-direction: $g = 1 + [0.1 + 0.35\ (a/t)^2]$ $f = \sqrt{(a/c)}$

The function H is given by the formulae:

"a"-direction: $H = 1 + G_1(a/t) + G_2(a/t)^2$

where $G_1 = -1.22 - 0.12 \cdot (a/c)$

$G_2 = 0.55 - 1.05 \cdot (a/c)^{0.75} + 0.47(a/c)^{1.5}$

"c"-direction: $H = 1 - 0.34\ (a/t) - 0.11\ (a/c)\ (a/t)$

Figure 16 - Stress intensity factor for surface cracks [17].

2.6.4 Calculation of SIF by BS 7910 standards

This British Standard has been set up by Technical Committee WEE/37 in 2005 which overrides the BS7910: 1999. As the number of application standards determining prerequisites for weld flaw acceptance levels dependent on fitness purposes increases, so it is important to refresh and stretch out the guidance to be utilized in planning and supporting those necessities. This update joins late improvements in crack mechanics appraisal techniques. While subjective control levels will keep on being utilized for quality control purposes, the corresponding utilization of the techniques portrayed in this guide allows the adequacy of known or proposed defects specifically circumstances to be assessed in a balanced way. It has been accepted in drafting BS 7910 that the execution of its arrangements is endowed to properly qualified and experienced individuals, having fitting learning of assessment innovation, NDT, materials conduct and break mechanics. Despite the fact that accentuation is put on welded manufactures in ferritic and austenitic steels and aluminium compounds, the techniques created can be utilized for breaking down defects in structures produced using other metallic materials and in non-welded parts or structures. The methods described can be applied at the design, fabrication and operational phases of a structure's life [27]. In Figure 17, examples of welded joints according to BS7910 standard are shown. Additionally, as for example, a graphic for calculating the stress intensity magnification factor M_b for surface flaws in bending is

presented. This kind of parameter, M, and other related to geometric configurations are extremely important for the evaluation of the stress intensity factor according to BS7910 standard. Normally, M and Y parameters depend on the geometry of the detail under consideration.

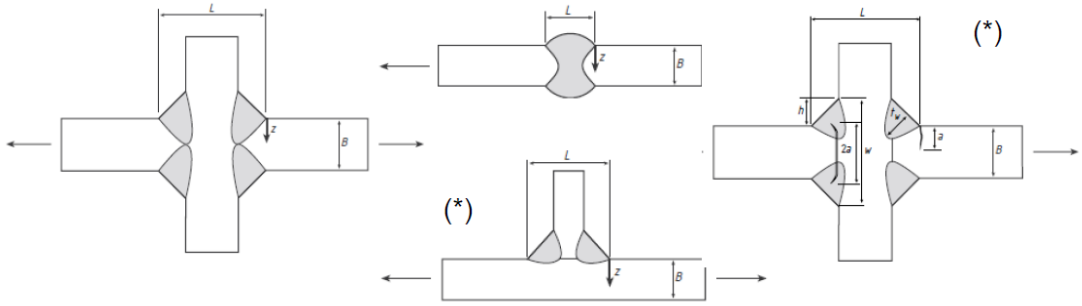


Figure 17 - Examples of welded joints [28].

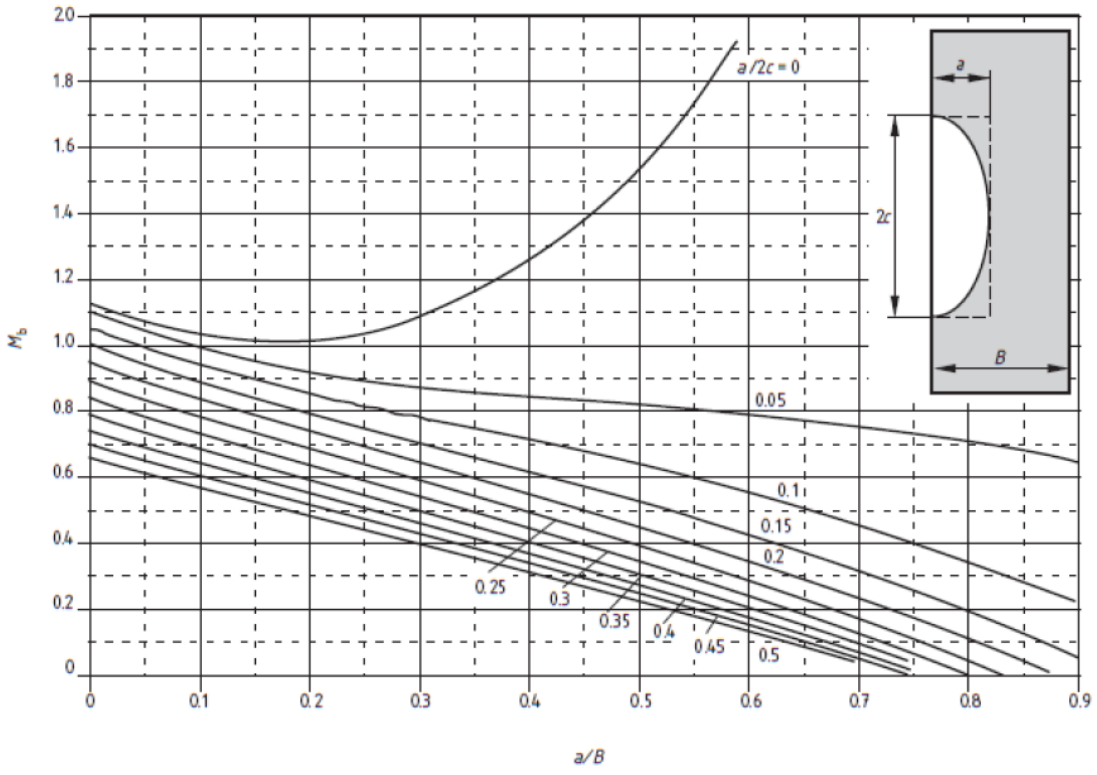


Figure 18 - Stress intensity magnification factor M_b for surface flaws in bending [28].

2.7 Review on finite element analysis to evaluate the SCF and SIF values of tubular joints

FEA is a powerful technique, able to produce solutions to challenging structural analysis problems. The technology and computational efficiency of the method, together with the rapid increases in computer processing power means that today the scope and size of simulations far exceed the capabilities of even a few years ago. There is, however, a steep learning curve to overcome in order to improve designs or achieve certification of new products. There are a bewildering array of element types, solution types, meshing methods and pre-post processing options that have to be faced. The assessment, validation, and interpretation of FEA results are vital for delivering safe, effective products. A process is shown which provides confidence in the results and aims to provide conservative, reliable and qualified results [29].

The Finite Element Method has been combined throughout the most recent four decades as the most flexible numerical procedure for the investigation of strong mechanics 40 issues. It might be characterized as a guess methodology of continuum issues, and is portrayed by the accompanying procedure [15]:

- Domain discretization, the continuum is separated into a limited number of units or gatherings (known as components) interconnected at determined focuses (known as hubs);
- Element Analysis, the nearby solidness framework of every component is resolved, and any stacking is changed into proportional nodal powers;
- System Analysis, gather a worldwide firmness lattice dependent on the blend of the nearby solidness networks. The static harmony conditions and all states of similarity (congruity of the removals) must be fulfilled;
- Equation framework goals, the nodal dislodging vector is resolved;
- Results post-preparing, component stresses and strains can be determined from the nodal relocations.

Numerous authors did heaps of researches with simulated models so as to see how the geometrical parameters and the loads related impact the assessment of the stress concentration factor on various tubular joints. Minguez [15] built up a finite element analysis of a T-Joint (Figure 19) where it was looked at the primary contrasts between a shell model and a solid model in the assessment of the stress concentration factor. Along these lines, all degrees of freedom in the models were fixed at the chord ends.

Shell elements are commonly used for tubular joint stress analysis; for this reason, initial models were formed by thin four-node quadrilateral elements. Models were subjected to axial, IPB and OPB load cases. The stresses were measured at the mid-section, without considering the effect of a weld fillet. The SCFs were estimated by dividing the maximum principal stress obtained at the brace/chord intersection by the appropriate nominal stress.

In order to reduce computational time, the mesh of all the models is characterised by fine elements near the intersection and coarser elements in regions where the stresses are more evenly distributed. Elongated or distorted elements were avoided. T-joints with a brace length of about $0.4L$ were used in order to avoid the effect of short brace length. Chord lengths greater than $6D$ were used to ensure that stresses at the brace/chord intersection were not affected by the boundary conditions. The density, Young's modulus, and Poisson's ratio were taken to be 7850 kg/m3, 207 GPa and 0.3, respectively.

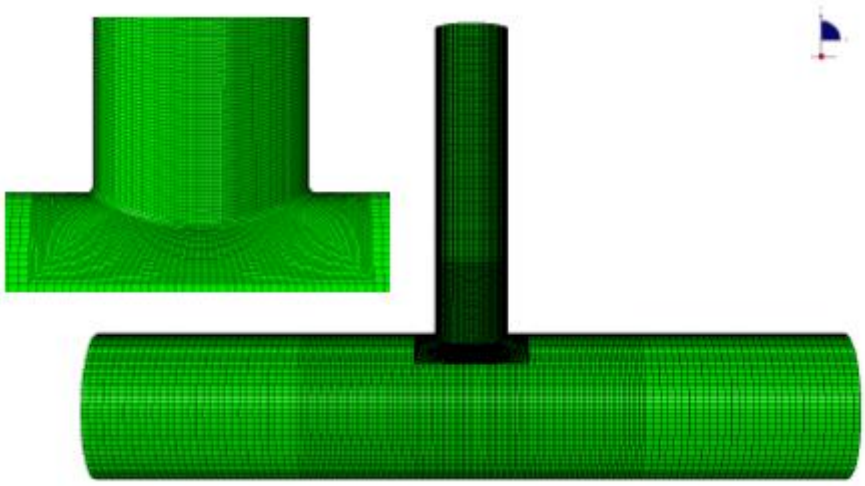


Figure 19 – Complete profile solid FE T-joint model [15].

A convergence test was carried out aiming to verify that the meshes used for this research were sufficiently fine to accurately predict the SCFs. Four meshes with 32, 64, 112, and 160 elements respectively around the joint intersection were analysed. Once the mesh was selected, the T-joint model was subjected both to IPB and OPB loading. Solid models were characterised by eight-node hexahedral elements. Models were subjected to axial, IPB and OPB load cases, and both chord ends were rigidly fixed. The SCF values for the solid FE models without fillet weld were estimated directly from the values obtained at the brace/chord intersection in the same manner as for the Shell FE models, except that the maximum principal stresses were measured at the external surface [15]. Minguez [15] presented a comparison of SCF values between numerical simulation and analytical formulations, shown in Table 4.

Table 5 - SCFs comparison [15].

		CHORD		BRACE	
		CROWN	SADDLE	CROWN	SADDLE
Axial	Kuang et al. Eq. [18]		6.106		8.553
	Efthymiou et al. Eq. [254]	2.203	6.602	2.400	6.407
	Hellier et al. Eq. [256]	2.833	7.047	2.579	8.109
	Lloyds's Register of Shipping Eq. [250]	2.596	5.960	1.883	4.707
	Chang et al. [257]	2.199	7.497	2.813	9.171
	Shell FE results	1.788	5.805	2.681	8.218
IPB	Kuang et al. Eq. [18]	1.633		2.169	
	Efthymiou et al. Eq. [254]	2.175		2.494	
	Hellier et al. Eq. [256]	2.505	0.000	3.035	0.087
	Lloyds's Register of Shipping Eq. [250]	1.895		1.067	
	Chang et al. [257]	2.578	0.056	3.330	0.181
	Shell FE results	2.020	0.064	2.865	0.247
OPB	Kuang et al. Eq. [18]		4.457		5.586
	Efthymiou et al. Eq. [254]		5.060		5.391
	Hellier et al. Eq. [256]	0.000	5.348	0.000	4.522
	Lloyds's Register of Shipping Eq. [250]		4.380		3.390
	Chang et al. [257]	0.177	5.553	0.434	6.621
	Shell FE results	0.092	4.591	0.391	6.097

As observed for the shell FE models, the higher stress concentration is located at the saddle for axial and OPB cases, and close to the crown for the IPB case. If the shell FEA results are compared with these results, it can be observed that there is an increase of the SCF of 14.8% for axial loading and 11.8% for OPB loading at the saddle. At the crown, there is an increase in the SCF of 11.7% for IPB loading. It is reasonable that the solid SCFs are slightly higher, since the shell results are measured at the mid-section, whereas the solid results are measured on the external surface [15].

Numerous studies have been carried out for assessing and modelling the uncertainty in fatigue crack growth in tubular joints, since cracks may compromise the integrity of the structure, and because crack growth estimations are needed for maintenance and safety requirements. The shape of the crack changes during growth, extending around the circumference and increasing in crack depth, depending on: the initial crack shape, the crack initiation site, the geometry of the structure, the loading modes, the material's anisotropy, and the environmental conditions. The crack shape development can be determined by plotting the crack aspect ratio (a/c) versus the normalised crack depth (a/T).

The restrictions of the brace and chord lengths, and the recommendations provided by the AWS Welding code used for the complete weld profile solid FE tubular T-joint models, were also applied to the cracked tubular T-joint models. The density, Young's modulus and Poisson's ratio were taken to be 7850 kg/m3, 210 GPa and 0.3 respectively. All the models were axially loaded and subjected to a nominal stress of 6 MPa. The nominal stress was defined as the total applied load divided by the hollow cross-sectional area of the brace. Both chord ends were rigidly fixed.

Once the cracked geometry is built, the T-joint part is divided into several regions using different partition tools to create mesh boundaries in order to help the refinement.

Linear elements with reduced integration were applied to be consistent with the previous SCF studies, but in this part of the research the aim is to derive the optimum SIF value. Clearly, the greater the number of elements and the more Gaussian integration points per element there are, the more accurate the output will be. A comparison has been made between four element types: linear elements with reduced integration (C3D8), linear elements with full integration (C3D8R), quadratic elements with reduced integration (C3D20R), and quadratic elements with full integration (C3D20). It was concluded that C3D20 elements are the most favourable option since 8-node elements does not provide accurate results and the difference in running time is not significant enough as for not selecting the most precise elements (see Table 5 and Table 6) [15].

Table 6 - Cost of computation comparison [15].

	K_I (Pa $m^{1/2}$)	N° Elements	N° Nodes	Wall time (Sec)
C3D8R	6.212E+06	42156	49937	20
C3D8	5.285E+06	42156	49937	28
C3D20R	6.954E+06	42156	191851	109
C3D20	6.940E+06	42156	191851	126

Table 7 - Comparative analysis of submodel accuracy [15].

	K_I (Pa $m^{1/2}$)	Elements	Nodes
C3D20 Reference model	6.940E+06	42156	191851
C3D20 Global model	7.826E+06	22610	107193
C3D20 Submodel1	6.947E+06	12897	59175
C3D20 Submodel2	6.946E+06	11049	50951
C3D20 Submodel3	6.945E+06	9663	44783

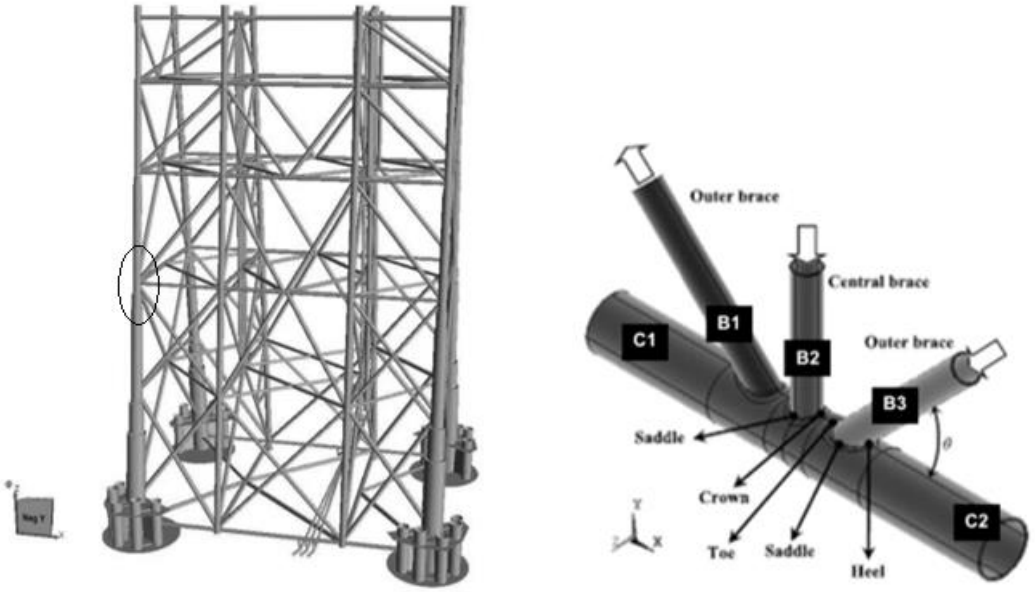
3. Evaluation of SCF values of a typical tubular KT-joint based on numerical simulation

3.1. Introduction

During the 70's, which coincided with the boom in the offshore oil sector in Norway, the increasing development of the hot spot stress S-N approach to fatigue joint life estimation has made it clear that the determination of reliable SCF's for tubular joints is quite fundamental to this methodology's accuracy. Toprac and Beale in 1967, in [30], derived the first parametric SCF equations covering simple tubular joints using a limited steel joint database.
The prohibitive cost of testing scaled steel models led Reber, Visser and Kuang et al to use finite element (FE) analyses based on analytical models of cylindrical shells. Subsequent equations by Wordsworth and Smedley using acrylic model specimens and the works of Efthymiou and Durkin employing 3-D shell FE analyses, have made considerable advances both in the accuracy of parametric equations and in the range of joints covered. [31]

3.2. Geometry of the Tubular KT-joint under consideration

Usually the go to solution when it comes to offshore fixed structures, particularly in the North Sea, jacket-type offshore structure are comprised of tubular structural elements, in any pair combination of 4, 6 or 8 legs, extending from the connection to the topside, on the surface, to the piles attached to the sea bed.
Depending on the structure overall design, there are several possibilities for tubular joints, either X-, K- or KT- shaped, amongst others. From these, the KT-type joints are the subject of the work, as such, only these will be addressed in this document.
For this research, an offshore fixed substructure case study was selected from the Norwegian sector of the North Sea, off the west coast of Norway with a considered depth of 115.67m depth for hydrodynamic calculations, see [32], and is presented in Figure 20a.
Even though all the KT-type joints could be subject of study, is was determined that the critical joint, i.e. connection with the highest stress ranges, would suffice and provide sufficient data, this way this study focuses on the joint presented in Figure 20b with the respective geometrical properties included in Table 7 below.



a) b)

Figure 20 – Case study a) Jacket-type offshore structure and b) KT-type tubular joint [26].

Table 8 - Geometric properties of the KT-type joint case study [26].

Member	Diameter (m)	Thickness (m)
C1	2.300	0.095
C2	2.300	0.095
B1	1.200	0.040
B2	1.000	0.030
B3	1.100	0.025

3.3. SCF evaluation based on DNVGL code/Efthymiou parametric equations

To study the SCF in tubular joints, Efthymiou used a Finite Element program and cross-checked with either full scale or model tests [8]. The hot spot stress was obtained by linear extrapolation of the maximum principal stresses of the weld toe. As a result, he published a comprehensive set of equations covering the tubular KT-joint configuration.

In order to access the stress concentration factors, present around the weld for each of the structural elements in question, certain geometrical parameters relating to the tubular elements geometric proportions must first be calculated. Afterwards, and depending on the loading conditions under considerations the SCF are given considering both the previous geometrical parameters, as well as the relative alignment of the pipes.

For balanced axial loading conditions, such as the case presented in Figure 20b, Equations (23) and (24) provide an expedite solution to obtain the SCF values around the weld (both crown and saddle) in the chord and brace, respectively.

For the balanced in-plane and out-of-plane bending cases, the SCF elements can be resolved utilizing the Equations (25) and (26), and Equations (27) to (33), respectively.

$$SCF_{AC/AS} = \tau^{0.9}\,\gamma^{0.5}\,(0.67 - \beta^2 + 1.16\beta)\,sin\theta\left(\frac{sin\theta_{max}}{sin\theta_{min}}\right)^{0.3}\left(\frac{\beta_{max}}{\beta_{min}}\right)^{0.3}(1.64 + 0.29\beta^{-0.38}ATAN(8\zeta)) \quad (23)$$

$$SCF_{AC/AS} = 1 + (1.97 - 1.57\beta^{0.25})\tau^{-0.14}(sin\theta)^{0.7}SCF_{AC/AS} + sin\theta^{1.8}(\theta_{max} + \theta_{min})\big(0.131 - 0.084\,ATAN(14\zeta + 4.2\beta)\big)C\beta^{1.5}\gamma^{0.5}\tau^{-1.22} \quad (24)$$

where:
C = 0, for gap joints;
C = 1, for the through brace;
C = 0.5, for the overlapping brace

In the cases where both in- and out-of-plane bending are concerned the two equations groups, Eq. (25)-(26) as well as Eq. (27)-(33), respectively, provide an adequate answer.

$$SCF_{MIP} = 1.45\beta\tau^{0.85}\gamma^{(1-0.68\beta)}(sin\theta)^{0.7} \tag{25}$$

$$SCF_{MIP} = 1 + 0.65\beta\tau^{0.4}\gamma^{(1.09-0.77\beta)}(sin\theta)^{(0.06\gamma-1.16)} \tag{26}$$

$$SCF_{MOP,chord} = \gamma\tau\beta(1.7 - 1.05\beta^3)(sin\theta)^{1.6} \cdot F3 \tag{27}$$

$$\begin{aligned} SCF_{MOP,brace(B1/B3)} &= \tau^{-0.54}\gamma^{-0.05}(0.99 - 0.47\beta + 0.08\beta^4)SCF_{MOP,chord(A)} \\ &\cdot (1 - 0.08(\beta_B\gamma)^{0.5}\exp(-0.8 \cdot x_{AB}))(1 \\ &- 0.08(\beta_C\gamma)^{0.5}\exp(-0.8 \cdot x_{AC})) + SCF_{MOP,chord(B)} \cdot (1 \\ &- 0.08(\beta_A\gamma)^{0.5}\exp(-0.8 \\ &\cdot x_{AB}))(2.05{\beta_{max}}^{0.5}\exp(-1.3x_{AB}) + SCF_{MOP,chord(C)} \\ &\cdot (1 \\ &- 0.08(\beta_A\gamma)^{0.5}\exp(-0.8 \\ &\cdot x_{AC}))(2.05{\beta_{max}}^{0.5}\exp(-1.3x_{AC}) \end{aligned} \tag{28}$$

$$\begin{aligned} SCF_{MOP,brace(B2)} &= \tau^{-0.54}\gamma^{-0.05}\big(0.99 - 0.47\beta \\ &+ 0.08{\beta^4}_B\big)SCF_{MOP,chord(B)} \\ &\cdot (1 \\ &- 0.08(\beta_A\gamma)^{0.5}\exp(-0.8 \cdot x_{AB}))^{P1}(1 \\ &- 0.08(\beta_C\gamma)^{0.5}\exp(-0.8 \cdot x_{AC}))^{P2} + SCF_{MOP,chord(A)} \\ &\cdot (1 \\ &- 0.08(\beta_B\gamma)^{0.5}\exp(-0.8 \\ &\cdot x_{AB}))(2.05{\beta_{max}}^{0.5}\exp(-1.3x_{AB}) + SCF_{MOP,chord(C)} \\ &\cdot (1 \\ &- 0.08(\beta_B\gamma)^{0.5}\exp(-0.8 \\ &\cdot x_{BC}))(2.05{\beta_{max}}^{0.5}\exp(-1.3x_{BC})) \end{aligned} \tag{29}$$

where:

$$x_{AB} = 1 + \frac{\zeta_{AB}sin\theta_B}{\beta_B} \tag{30}$$

$$x_{BC} = 1 + \frac{\zeta_{BC}sin\theta_B}{\beta_B} \tag{31}$$

$$P_1 = \left(\frac{\beta_A}{\beta_B}\right)^2 \quad (32)$$

$$P_1 = \left(\frac{\beta_A}{\beta_B}\right)^2 \quad (33)$$

As previously mentioned, the geometrical parameters are paramount to calculating the SCF in the joint, as such the relative angle between tubular elements is provided in Table 8. Also necessary for the calculating of the geometrical parameters present in Table 9 are the gaps are as follows:

- B1/B2 - 0.15304 m;
- B2/B3 – 0.03156 m;

Table 9 - Angles between joint elements according to Figure 20b, [26].

θ	**C2**	**C1**	**B2**
C2	-	-	-
C1	180º	-	-
B2	90º	90º	-
B1	-	38.41849º	51.58151º
B3	38.41849º	-	51.58451º

Table 10 - Geometrical parameters and stress concentration factors calculation [26]

	Member	**β**	**T**	**Ɣ**	**α**	**$SCF_{AC/AS}$**	**SCF_{MIP}**	**SCF_{MOP}**
B1						1.600	1.299	1.836
B2	C1/C2	1	1	12.10	6.83	2.949	1.370	2.591
B3						1.368	0.859	1.082
B1	B1	0.52	0.42	12.10	6.83	1.823	1.623	2.689
B2	B2	0.43	0.31	12.10	6.83	3.408	2,171	3.785
B3	B3	0.47	0.26	12.10	6.83	1.785	1.514	2.943

where:

SCF_{AS} - SCF at the saddle for axial load;
SCF_{AC} - SCF at the crown for axial load;
SCF_{MIP} - SCF for the in-plane moment;
SCF_{MOP} - SCF for out-of-plane moment.

3.4. SCF evaluation based on Lloyd's register (LR) equations

The "*SCFs for simple tubular joints*", a project funded by the HSE in 1991, developed the Lloyd's Register (LR), where several equations aimed at determining the SCF are proposed. These equations intended to apply influence functions in order to be able to transpose a generic formulation of the SCF from one type joint to another using a series of factors concerning the stiffness effect of additional tubular elements.

In addition, a concern had been raised for joints with *b=1* where problems due to the degree of cut-back of the weld in the saddle. Even though not achieved for the data available to the LR, the derivation of shot chord correlation factors in order to account for short chord effects was attempted.

The LR SCF derivation database is similar to the SCF assessment database that was used in this project to assess SCF formulae. It includes both steel and acrylic joint data and has the same parametric and geometric limitations. Hence, comparisons between the SCF assessment database and the LR equations should be taken into consideration in the knowledge that the equations themselves were largely developed from the dataset against which they are being compared.

With regards to the LR equations, the following considerations should be noted, [31]:

- The LR equations generally give the SCF at the saddle and crown locations (except for IPB) and may underestimate a larger SCF if located between these locations. This is most likely to be the case for K/KT joints under axial load, although it was considered that the differences would be small;

- The LR equations use the Efthymiou short chord correction factors, which have not been independently verified;

- The LR equations are limited to c ratios greater than c = 12, while a significant number of tubular joints are designed with c values below this limitation;

- Short chord length effects, chord bending effects and the weld influence have been considered in deriving these equations;

- The form of the equations, while being more complex for 'hand calculations', gives a more logical influence function format, which largely removes the problem of joint classification.

Not unlike the formulations presented in Section 3.3, the Lloyd's Registry also presents a variety of equations based on the respective type of loading. The following groups,

Eqs. (34) to (37) and Eqs. (38) to (41) present the formulas for balanced axial loading conditions for braces B2 and B1, respectively.

$$SCF_{CS} = MAX[(T1_B S1_{BA} S1_{BC} - T1_A S1_{AB} S1_{AC} IF1_{BA}), (T1_B S1_{BC} S1_{BA} - T1_C S1_{CB} S1_{CA} IF1_{BC})] \cdot (F1_B \; or \; F2_B) \quad (34)$$

$$SCF_{CC} = MAX[(T2_B S2_B - T2_A S2_A IF2_{BA}) + B0_B \cdot B1_B, (T2_B S2_B - T2_C S2_C IF2_{BC}) + B0_B \cdot B1_B] \quad (35)$$

$$SCF_{BS} = MAX[(T3_B S1_{BA} S1_{BC} - T3_A S1_{AB} S1_{AC} IF3_{BA}), (T3_B S1_{BC} S1_{BA} - T3_C S1_{CB} S1_{CA} IF3_{BC})] \cdot (F1_B \; or \; F2_B) \quad (36)$$

$$SCF_{BC} = MAX[(T4_B S2_B - T4_A S2_A IF4_{BA}), (T4_B S2_B - T4_C S2_C IF4_{BC})] \quad (37)$$

$$SCF_{CS} = (T1_A S1_{AB} S1_{AC} - T1_C S1_{CB} S1_{CA} IF1_{AC}) \cdot (F1_A \; or \; F2_A) \quad (38)$$

$$SCF_{CC} = (T2_A S2_{AB} - T2_C S2_{CB} IF2_{AC}) + B0_A \cdot B1_A \quad (39)$$

$$SCF_{BS} = (T3_A S1_{AB} S1_{AC} - T3_C S1_{CB} S1_{CA} IF3_{AC}) \cdot (F1_A \; or \; F2_A) \quad (40)$$

$$SCF_{BC} = (T4_A S2_{AB} - T4_C S2_{CB} IF4_{AC}) \quad (41)$$

where:

$$S2_A = MAX(S2_{AB} S2_{AC}) \quad (42)$$

$$S2_B = MAX(S2_{BA} S2_{BC}) \quad (43)$$

$$S2_C = MAX(S2_{CB} S2_{CA}) \quad (44)$$

For the parametric equations from (45) to (48) are for the central brace B2 and the parametric equations from (49) to (52) are for the outer brace are the following:

$$SCF_{CS} = MAX[(T1_B S1_{BA} S1_{BC} - T1_A S1_{AB} S1_{AC} IF1_{BA}), (T1_B S1_{BC} S1_{BA} - T1_C S1_{CB} S1_{CA} IF1_{BC})] \cdot (F1_B \; or \; F2_B) \quad (45)$$

$$SCF_{CC} = MAX[(T2_B S2_B - T2_A S2_A IF2_{BA}) + B0_B \cdot B1_B, (T2_B S2_{BC} - T2_C S2_C IF2_{BC}) + B0_B \cdot B1_B] \quad (46)$$

$$SCF_{BS} = MAX[(T3_B S1_{BA} S1_{BC} - T3_A S1_{AB} S1_{AC} IF3_{BA}), (T3_B S1_{BC} S1_{BA} - T3_C S1_{CB} S1_{CA} IF3_{BC})] \cdot (F1_B \; or \; F2_B) \quad (47)$$

$$SCF_{BC} = MAX[(T4_B S2_B - T4_A S2_A IF4_{BA}), (T4_B S2_B - T4_C S2_C IF4_{BC})] \quad (48)$$

$$SCF_{CS} = (T1_A S1_{AB} S1_{AC} - T1_C S1_{CB} S1_{CA} IF1_{AC}) \cdot (F1_A \; or \; F2_A) \quad (49)$$

$$SCF_{CC} = (T2_A S2_{AB} - T2_C S2_{CB} IF2_{AC}) + B0_A \cdot B1_A \quad (50)$$

$$SCF_{BS} = (T3_A S1_{AB} S1_{AC} - T3_C S1_{CB} S1_{CA} IF3_{AC}) \cdot (F1_A \; or \; F2_A) \quad (51)$$

$$SCF_{BC} = (T4_A S2_{AB} - T4_C S2_{CB} IF4_{AC}) \quad (52)$$

where:

$$S2_A = MAX(S2_{AB} S2_{AC}) \quad (53)$$

$$S2_B = MAX(S2_{BA} S2_{BC}) \quad (54)$$

$$S2_C = MAX(S2_{CB} S2_{CA}) \quad (55)$$

With the objective to complete the application of the Lloyd's register equations for KT-joints it is essential to use complementary equations given by Eqs. (56) to (74), given below.

$$T1 = \tau\gamma^{1.2}\beta(2.12 - 2\beta)(sin\theta)^2 \quad (56)$$

$$T2 = \tau\gamma^{0.2}\beta(3.5 - 2.4\beta)(sin\theta)^{0.3} \quad (57)$$

$$T3 = 1 + \tau^{0.6}\gamma^{1.3}\beta(0.76 - 0.7\beta)(sin\theta)^{2.2} \quad (58)$$

$$T4 = 2.6\beta^{0.65}\gamma^{(0.3-0.5^{\beta})} \quad (59)$$

$$T5 = \tau\gamma\beta(1.4 - \beta^5)(sin\theta)^{1.7} \quad (60)$$

$$T6 = 1 + \tau^{0.6}\gamma^{1.3}\beta(0.27 - 0.2\beta^5)(sin\theta)^{1.7} \quad (61)$$

$$T7 = 1.22\tau^{0.8}\beta\gamma^{(1-0.68\beta)}(sin\theta)^{(1-\beta^3)} \quad (62)$$

$$T8 = 1 + \tau^{0.2}\gamma\beta(0.26 - 0.21\beta)(sin\theta)^{1.5} \quad (63)$$

$$S1_{ij} = \left[1 - 0.4 \cdot \exp\left(-30{x^2}_{ij} \cdot \left((\frac{\beta_i}{\beta_j})^2 \cdot \left(\frac{sin\theta_i}{Y}\right)\right)\right)\right] \quad (64)$$

$$S2_{ij} = \left[1 + exp - \left(2{x^2}_{ij} \cdot \sin\left(\theta_j \cdot \gamma^{-0.5}\right)^{-2}\right)\right] \quad (65)$$

where:

$$X_{ij} = 1 + \frac{\zeta_{ij}\, sin\theta_i}{\beta_i} \quad (66)$$

$$IF1_{ij} = \beta_i(2.13 - 2\beta_i)\gamma^{0.2}(sin\theta_i)\left(\frac{sin\theta_i}{sin\theta_j}\right)^{p} exp(-0.3x_{ij}) \quad (67)$$

with:

$$P = 1 \;\; if \;\; \theta_i > \theta_j \quad (68)$$

$$P = 5 \;\; if \;\; \theta_i < \theta_j \quad (69)$$

and where:

$$IF2_{ij} = [20 - 8(\beta_i + 1)^2]\exp(-3x_{ij}) \quad (70)$$

$$IF3_{ij} = \beta_i(2 - 1.8\beta_i)\gamma^{0.2}\left(\frac{\beta_{min}}{\beta_{max}}\right)\left(\frac{sin\theta_i}{sin\theta_j}\right)^{p}\exp(-0.5x_{ij}) \quad (71)$$

with:

$$P = 2 \;\; if \;\; \theta_i > \theta_j \quad (72)$$

$$P = 4 \;\; if \;\; \theta_i < \theta_j \quad (73)$$

$$IF4_{ij} = [20 - 8(\beta_i + 1)^2]\exp(-3x_{ij}) \quad (74)$$

In this analysis the $IF4_{ij}$ parameter was assumed equal to $IF2_{ij}$ parameter. The OTH 354 report does not present the equation for the $IF4_{ij}$ variable.

Table 11 - Lloyd's SCF calculation [26].

BRACE	SCF_{CS}	SCF_{CC}	SCF_{BS}	SCF_{BC}
B1	1.733	1.772	1.596	1.861
B2	0.935	1.598	0.216	1.479
B3	1.047	1.117	1.249	1.861

where:

SCF_{CS} – Stress concentration on chord saddle;

SCF_{CC} - Stress concentration on chord crown;

SCF_{BS} – Stress concentration on brace saddle;

SCF_{BC} – Stress concentration on brace chord.

3.5. SCF evaluation based on numerical analysis

Following the works of Mendes [26], where a determination of the SCF of the case study offshore substructure where a respective critical joint is studied using FEA in order to compare with results taken from normative formulations providing a localized assessment of the degree of over-conservatism present in both Efthymiou and the LR.

With a strong 3D FE model a FEA was conducted using the ANSYS R19.0 student version software, not considering the weld fillet effects, and with loading/boundary conditions based on the stresses obtained via global model with a deterministic environmental loading conditions, local hot-spot stresses can be manually taken and the SCFs indirectly obtained.

The selection of components type for the examination relies upon the geometry of the joint and the reason for which the aftereffects of the investigation will be utilized. The 3D numerical model was constructed utilizing solid finite elements and a linear-elastic stresses analysis was utilized. The mechanical properties used in the numerical analysis of the KT-type joint are given in Table 11, for the S420 structural steel.

Table 12 - Material properties

Density, ρ_{steel}	7.850E-06 kg/mm^3
Modulus of Elasticity, *E*	210000 N/mm^2
Shear Modulus, *G*	80770 N/mm^2
Poisson´s ratio, *υ*	0.3

The achievement of a suitable strength whilst maintaining other properties has been the driving force behind the development of modern steel making and rolling processes. Designers should note that yield strength reduces with increasing plate or section thickness, as such different variations of the yield stress for several thicknesses' ranges are provided in Table 12, [25].

Table 13 - The variation of minimum yield strength (N/mm2) with thickness for S420

Type of steel	**Nominal thickness (mm)**					
	≤ 16	**> 16 ≤ 40**	**> 40 ≤ 63**	**> 63 ≤ 80**	**> 80 ≤ 100**	**> 100 ≤ 150**
S420	420	400	390	370	360	340

The chemical properties of the same S420 structural steel used in the offshore platform case study is provided below in Table 13.

Table 14 - Chemical properties of S420 steel [33]

Chemical elements	S420
C	0.14
Si	0.15-0.55
Mn	≤ 1.65
P	0.02
S	0.007
Al	0.15-0.055
Cr	0.25
Mo	0.25
Ni	0.7
Cu	0.3
N	0.01
Nb	0.04
Ti	0.025
V	0.08

After having all the data related to the joint constitution it is possible to assemble the FEA model of the case study. Following the same nomenclature for the braces as presented in Figure 20b, Figure 21 provides a first overview of the FE 3D model, whereas Figure 22 provides a general location of the principal stress points. The type of mesh elements (8 nodes solid element) used on the braces and the appropriate boundaries conditions to accurately refine and extract results from the most sensitive are presented with a green highlighted zone in Figures 23 and 24 respectively.

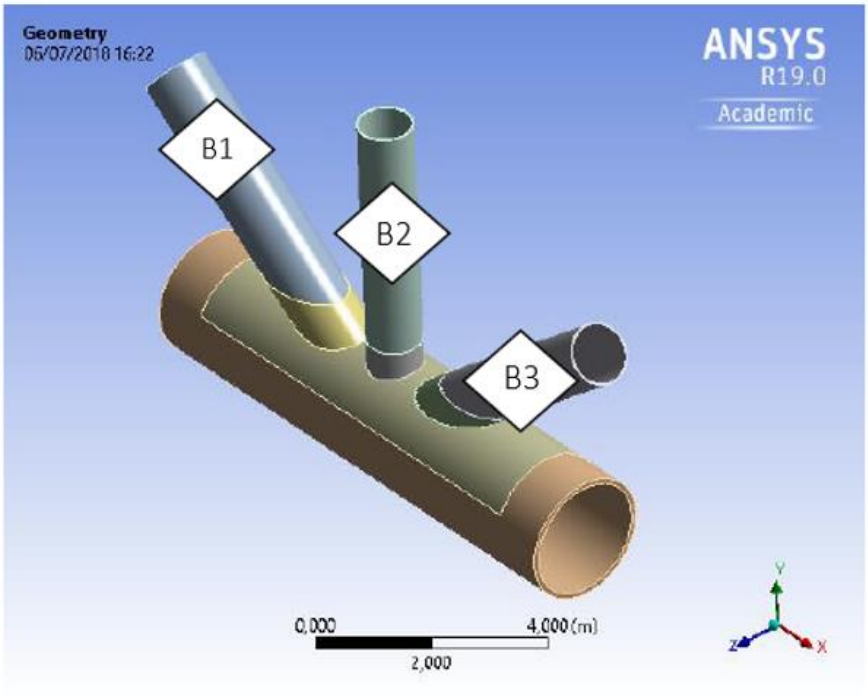


Figure 21 - Solid model with designation of the braces [26].

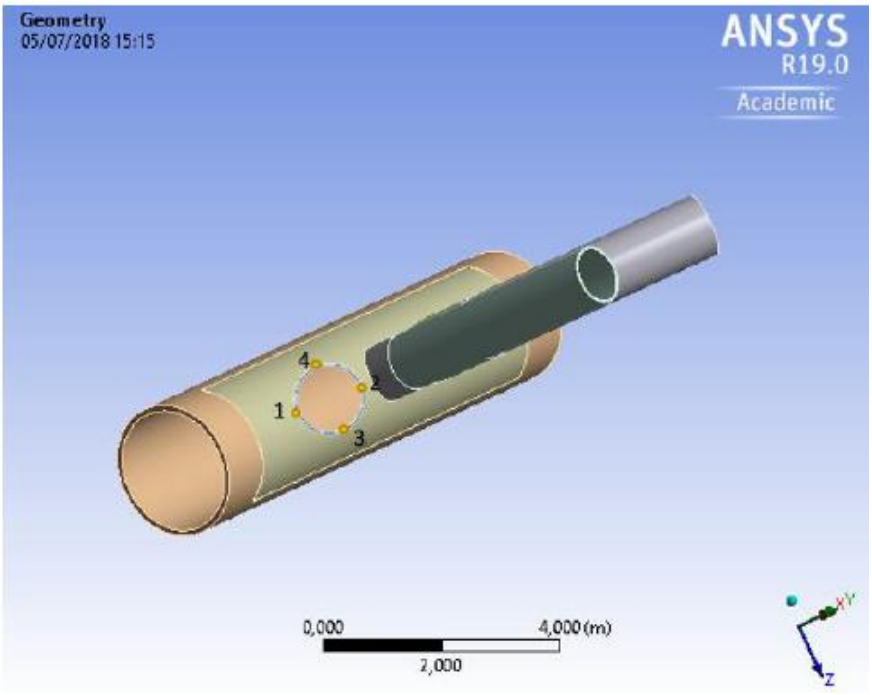


Figure 22 - Solid model with the principal stress points [26].

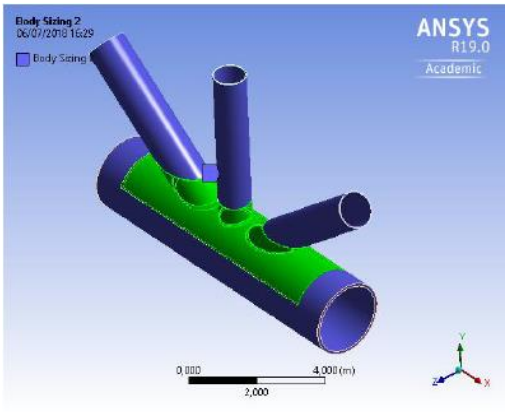


Figure 23 - Solid model with the details of the size of the 8-nodes cube solid elements and 6-nodes triangular solid elements in braces and chord, respectively in the blue zone, 0.15m (Exterior zone) [26].

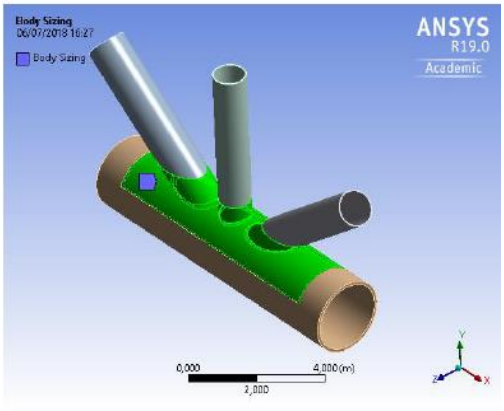


Figure 24 - Solid FE model with the details of the size of the 8-nodes solid elements in green with 5E-2 meters in size [26].

The 3D finite element model of the KT-joint under consideration is presented in Figures 25 to 27, with a front, side and top view, respectively.

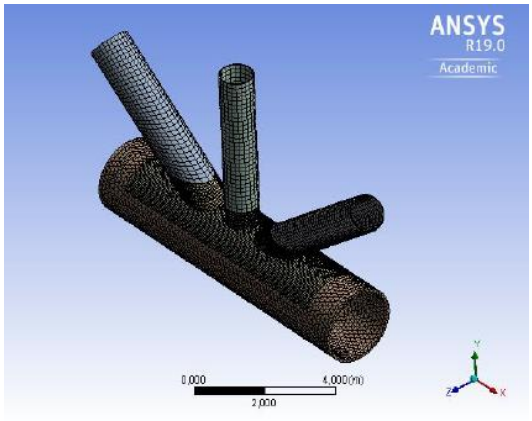


Figure 25 - Solid FE model with the designed meshing refinement (Front view) [26].

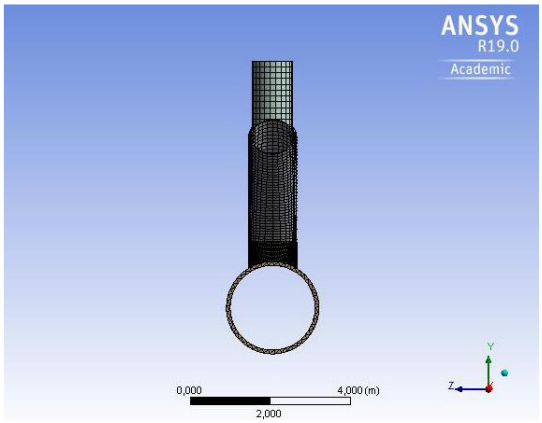


Figure 26 - Solid FE model with the designed meshing refinement (Side view) [26].

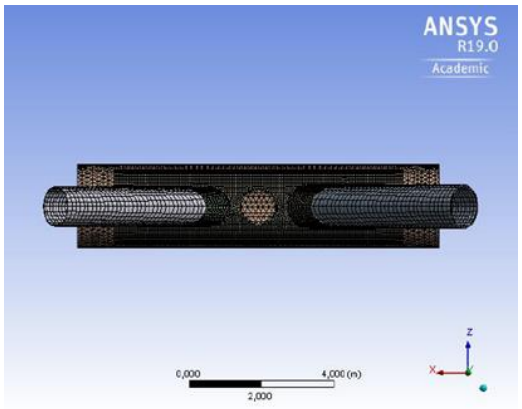


Figure 27 - Solid FE model with the designed meshing refinement (Top view) [26].

With aims to estimate the SCFs, a mesh convergence study is required to obtain a convergence of the linear-elastic stresses around of the intersection between chord and braces. Important to highlight is the fact that the element size used in the analysis is lower when compared to the IIW recommendations.

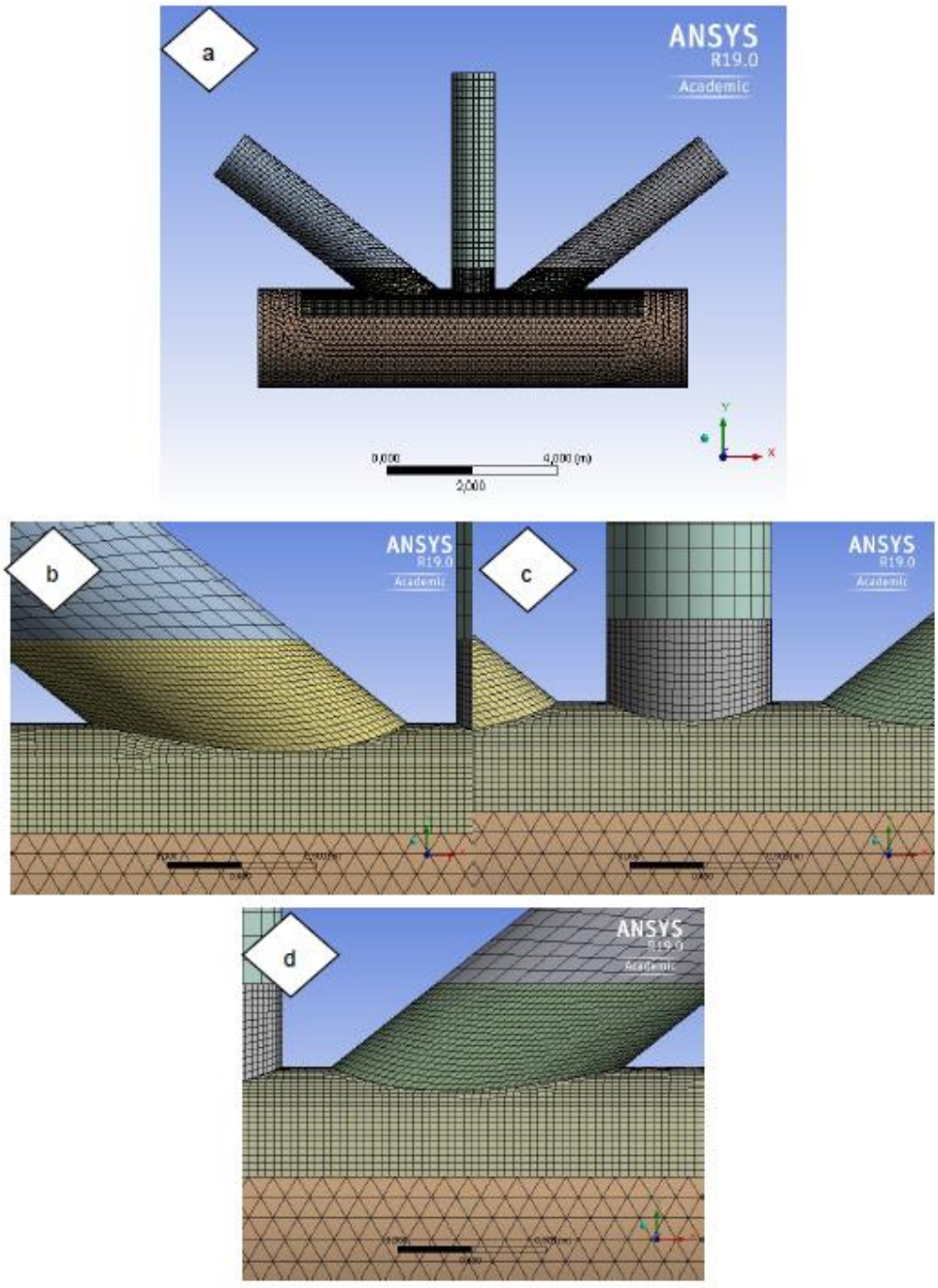


Figure 28 - 3D FE model of the KT-Joint under consideration [26].

As mentioned before, the loads applied in the model are originated from the global model and are presented below in Table 14.

Table 15 - Loads used in numerical model of the KT-joint [26]

Members	ΔF[MN]
C1	9.241
C2	1.659
B1	1.1001
B2	0.575
B3	0.269

In Table 15 are presented the nominal stresses applied in the KT-joint based on the loads considered in this study (see Table 14). To calculate the nominal stresses, it's is essential to calculate the section properties as well using Equation (75) for purely axial loading.

$$\Delta\sigma_x = \frac{\Delta F_x}{A} \tag{75}$$

where:
$\Delta\sigma_x$ – Nominal stress due to axial load;
ΔF_x – axial loading;
A – cross section area.

Table 16 - Nominal stresses and section properties [26].

A [m^2]	$\Delta\sigma_x$ [MPa]
0.336	27.495
0.336	4.937
0.0741	13.515
0.0427	13.471
0.0464	5.819

For axial loading condition, such as presented in Figure 29, the model with the axial forces for each associated brace is displayed according to the loads presented previously in Table 14.

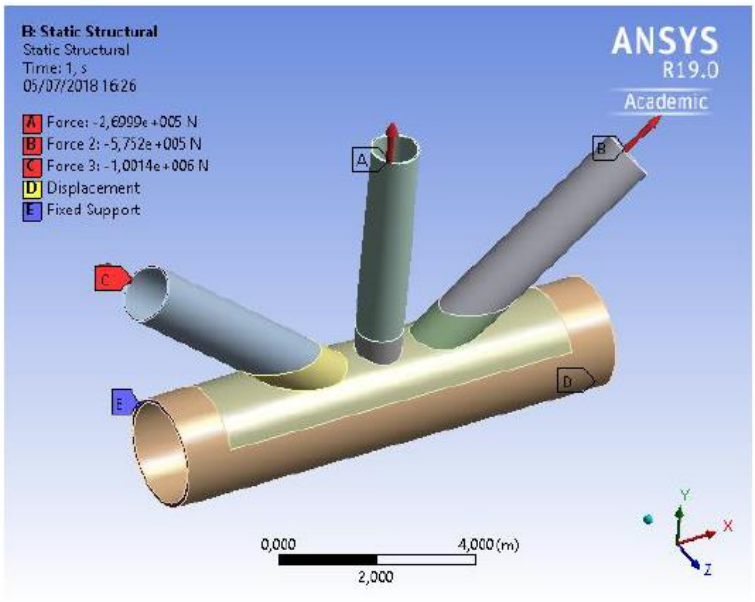


Figure 29 - Solid model with the representation of the axial forces [26].

The chord end boundary conditions of tubular joints in offshore structures may range from almost fixed to almost pinned, while generally being closer to almost fixed. On one side of the rope, all nodes were restricted in all directions, while on the opposite side, the Y and Z directions were restricted, and the X direction considered free from constraints. Figures 31 to 33 provide all the information regarding the supports of the joint. [15]

Details of "Fixed Support"

Scope	
Scoping Method	Geometry Selection
Geometry	1 Face
Definition	
Type	Fixed Support
Suppressed	No

a)

Details of "Displacement"

Scope	
Scoping Method	Geometry Selecti...
Geometry	1 Face
Definition	
Type	Displacement
Define By	Components
Coordinate System	Global Coordinat...
X Component	Free
Y Component	0, m (ramped)
Z Component	0, m (ramped)
Suppressed	No

b)

Figure 30 - Details about the support conditions used in the FE model: a) Fixed support; b) Displacement. [26].

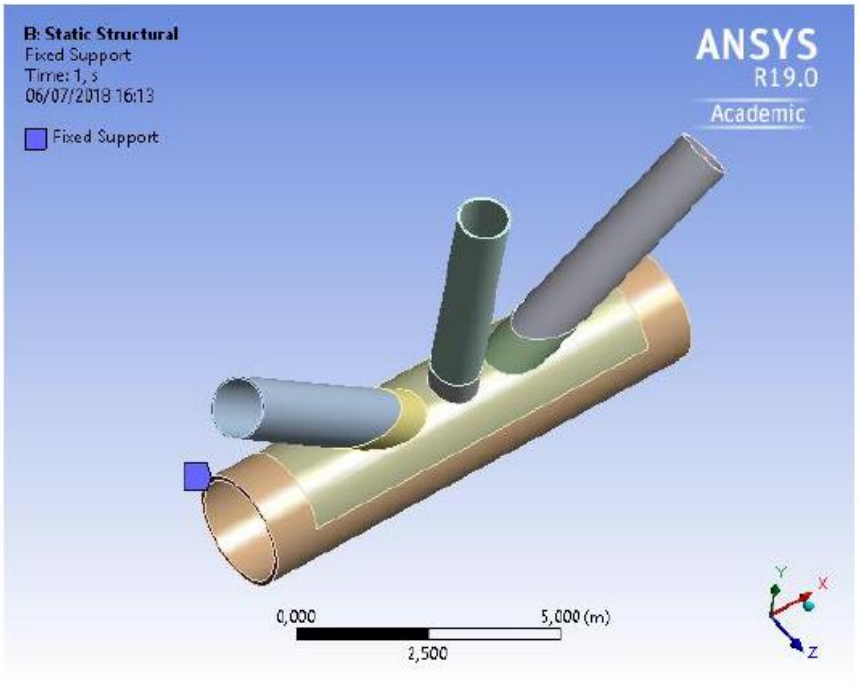


Figure 31 - Solid model with identification of fixed support [26].

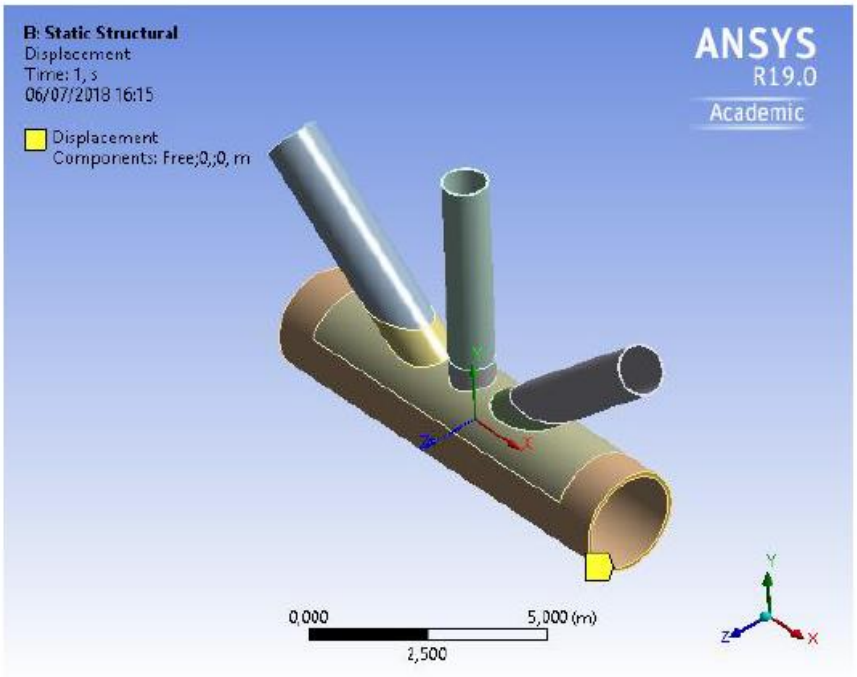


Figure 32 - Solid model with identification of restricted and free directions [26].

In Figures 33 and 34 are shown the stress fields considering the axial loading case. It is noticeable that within the intersection of the chord and braces (crown and saddle) is where it is found the higher stresses. By using the principal stress points present in Figure 24, a path can be drawn along each of the tubular member and the stress

distribution along the path converging on the nominal stress can be seen in Figures 35 to 47 for each of the loading conditions.

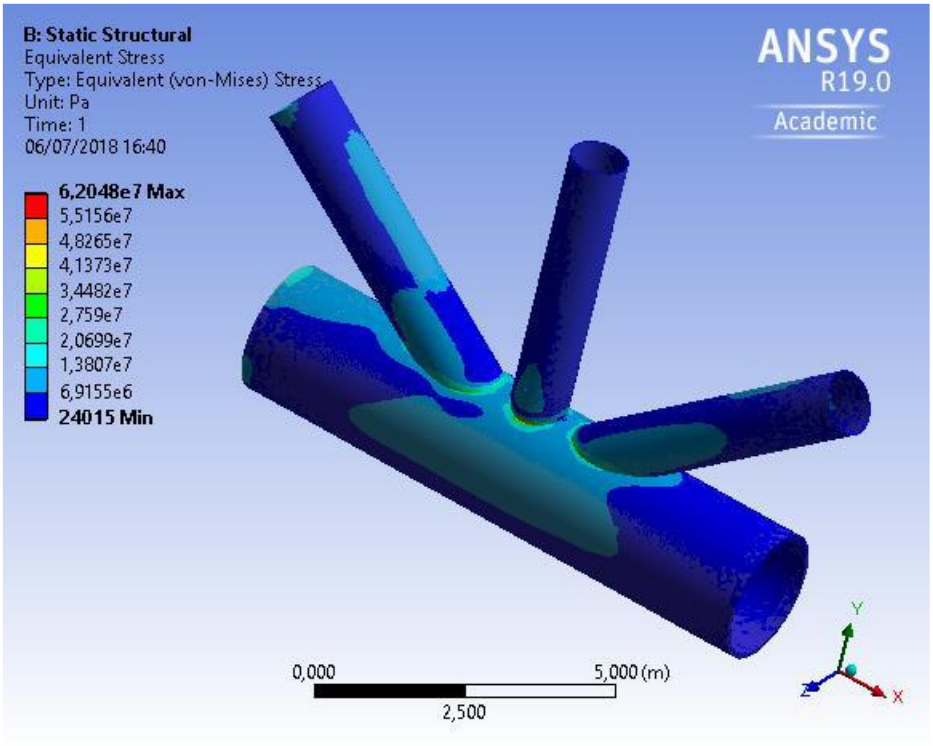


Figure 33 - Stress fields for axial loading case in the KT-joint under consideration [26].

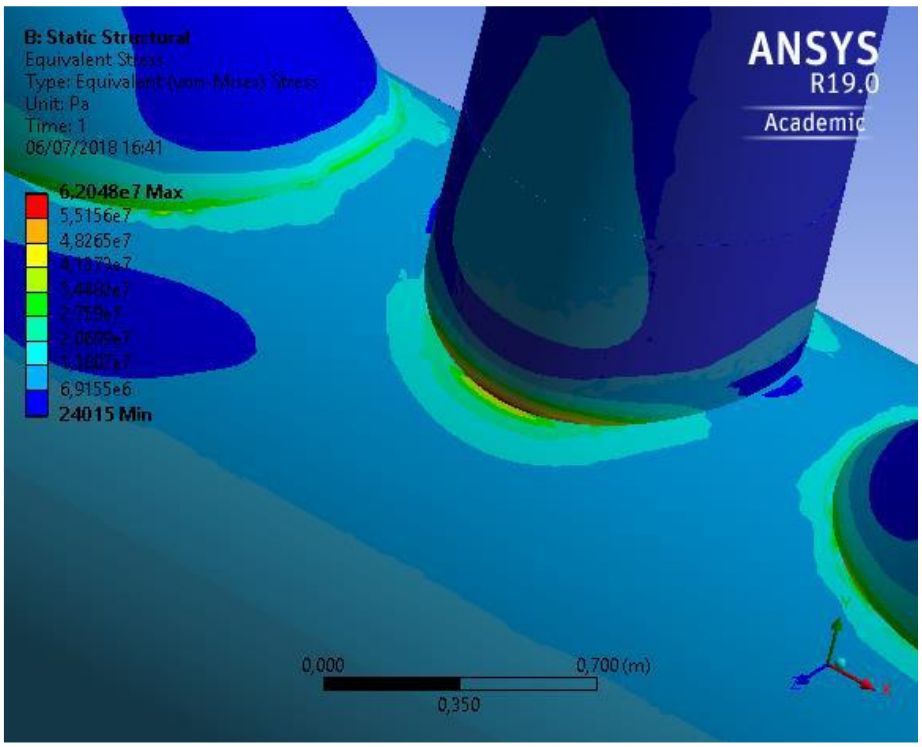


Figure 34 - Stress fields for axial loading case in the KT-joint under consideration (Closer look) [26].

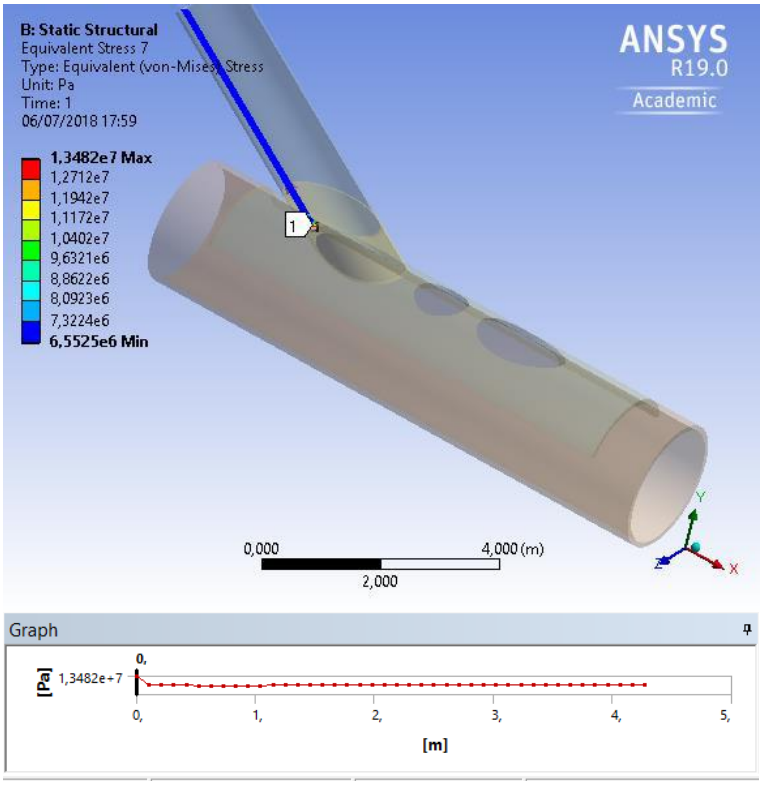


Figure 35 - Stress distribution in brace B1 for axial loading case: Side 1 [26].

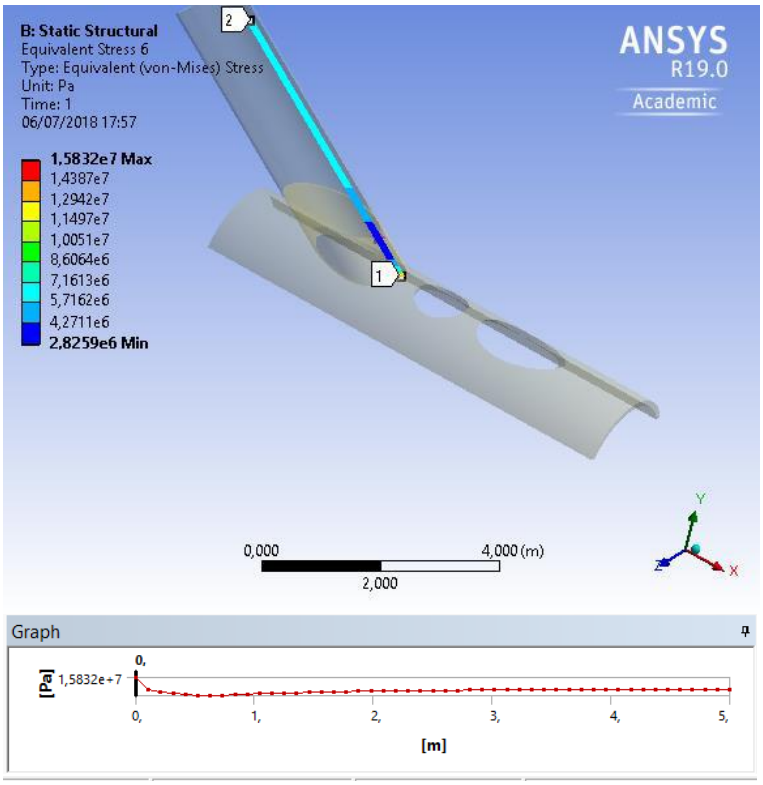


Figure 36 - Stress distribution in brace B1 for axial loading case: Side 2 [26].

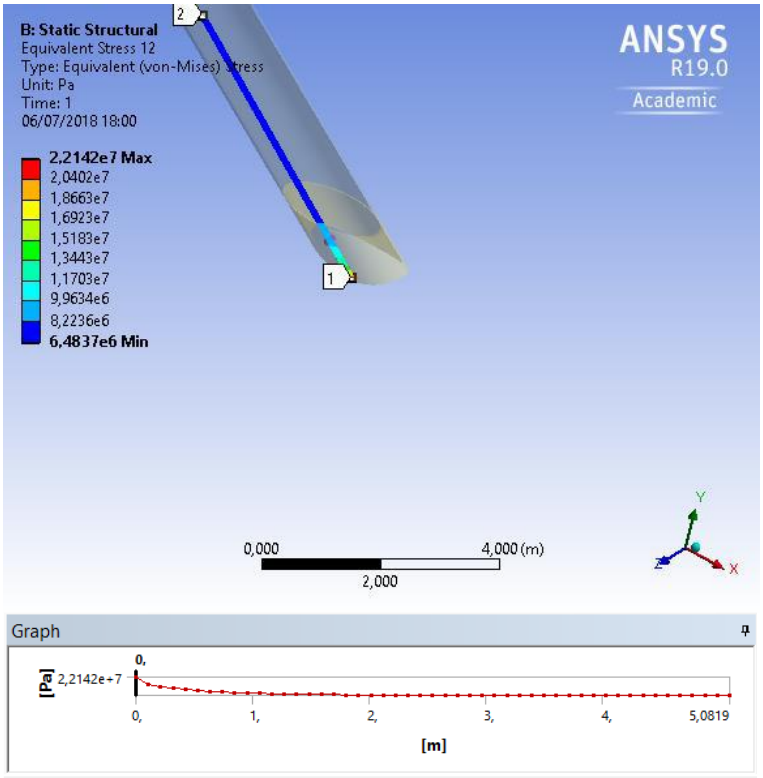


Figure 37 - Stress distribution in brace B1 for axial loading case: Side 3 [26].

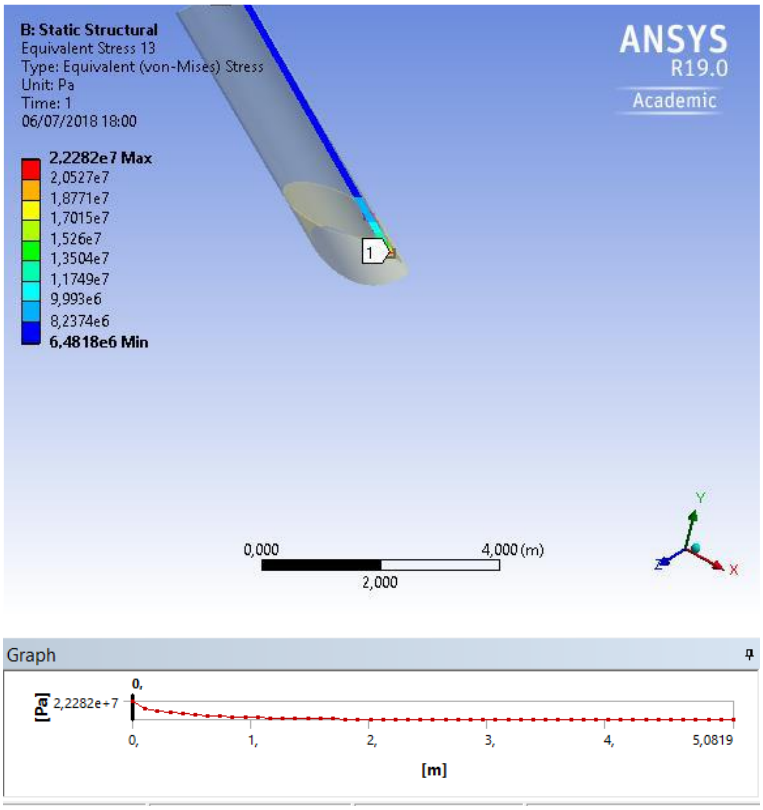


Figure 38 - Stress distribution in brace B1 for axial loading case: Side 4 [26].

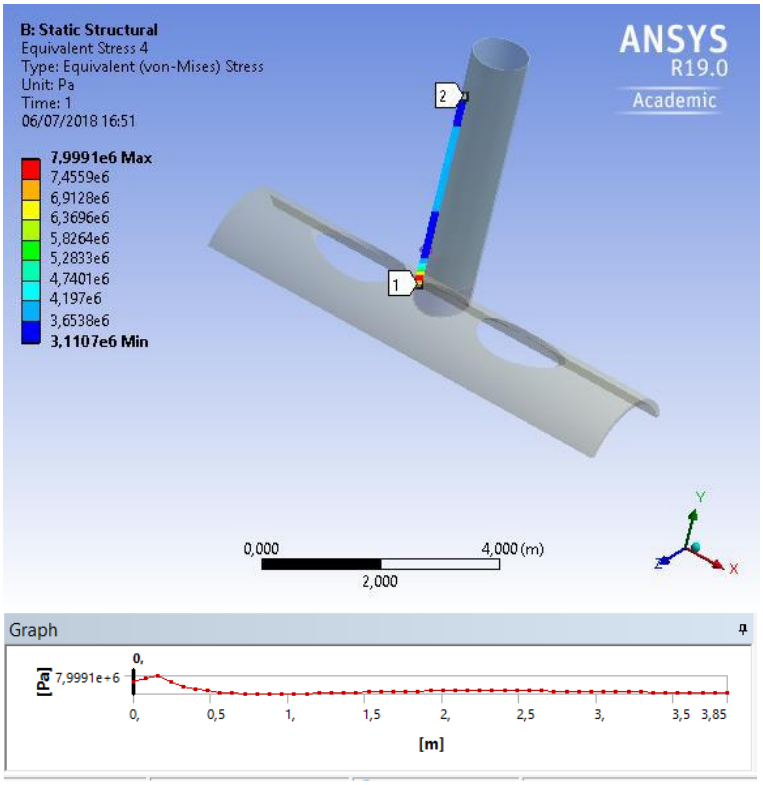


Figure 39 - Stress distribution in brace B2 for axial loading case: Side 1 [26].

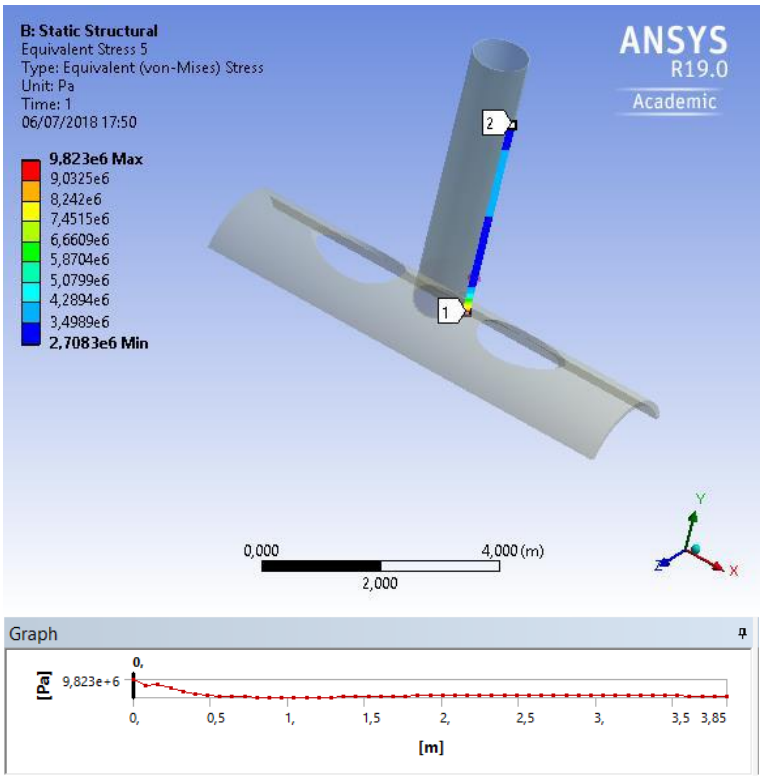


Figure 40 - Stress distribution in brace B2 for axial loading case: Side 2 [26].

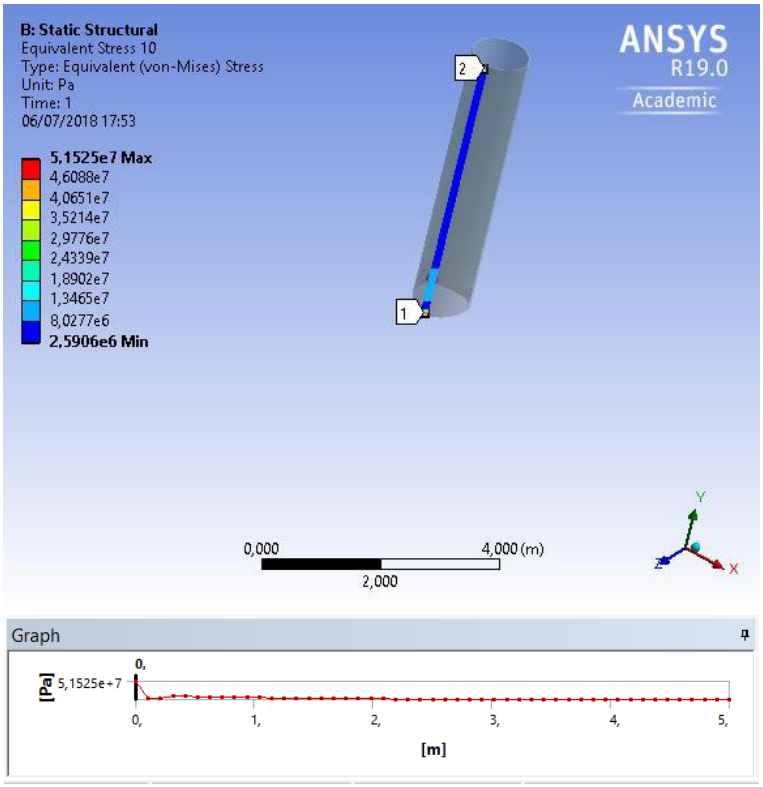


Figure 41 - Stress distribution in brace B2 for axial loading case: Side 3 [26].

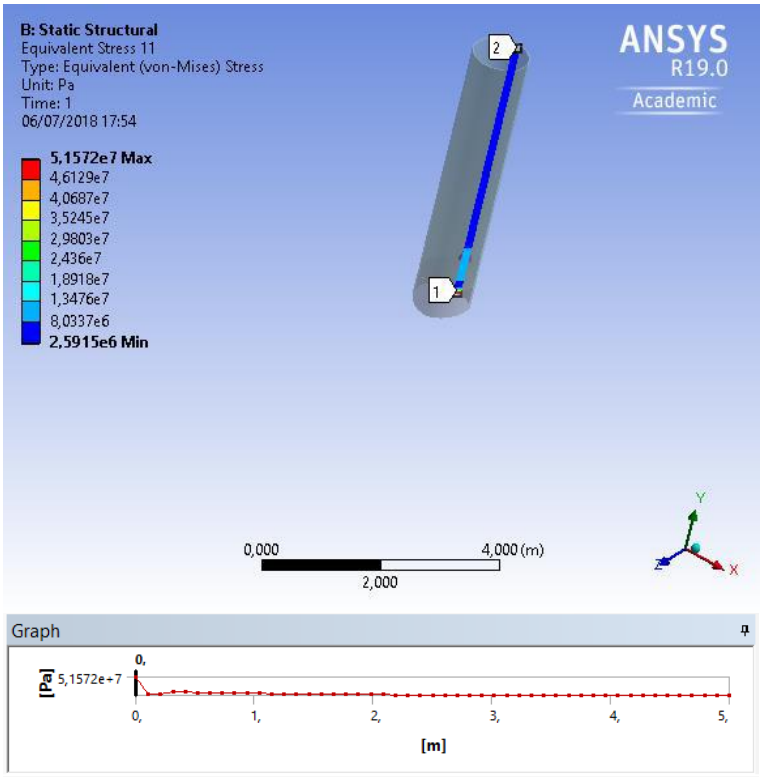


Figure 42 - Stress distribution in brace B2 for axial loading case: Side 4 [26].

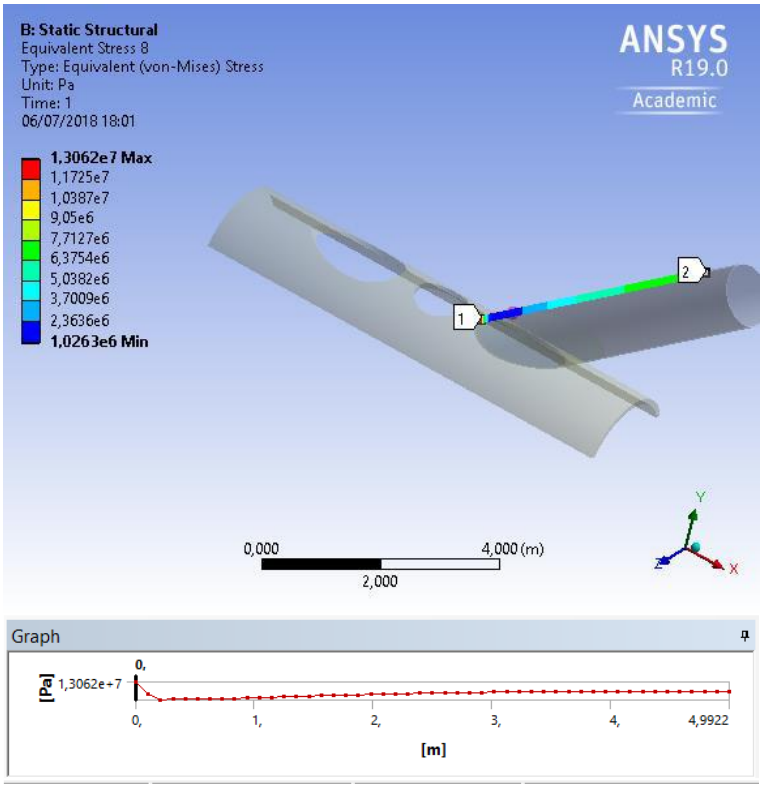


Figure 43 - Stress distribution in brace B3 for axial loading case: Side 1 [26].

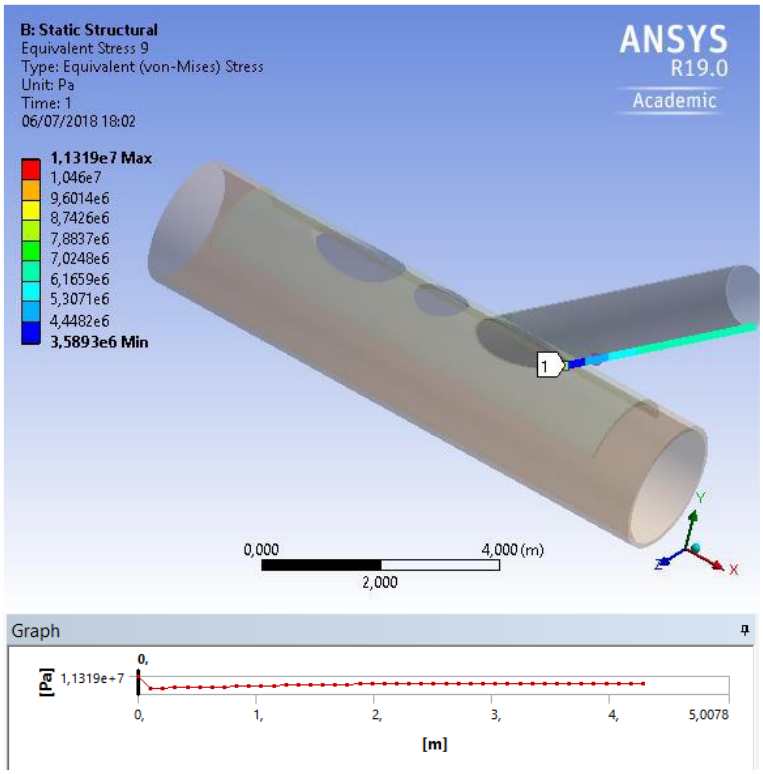


Figure 44 - Stress distribution in brace B3 for axial loading case: Side 2 [26].

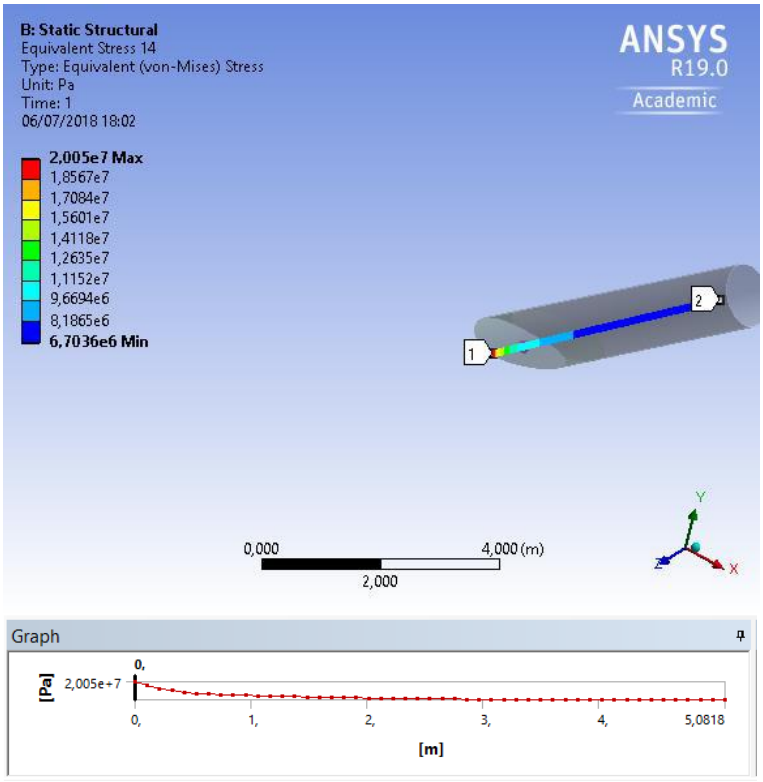


Figure 45 - Stress distribution in brace B3 for axial loading case: Side 3 [26].

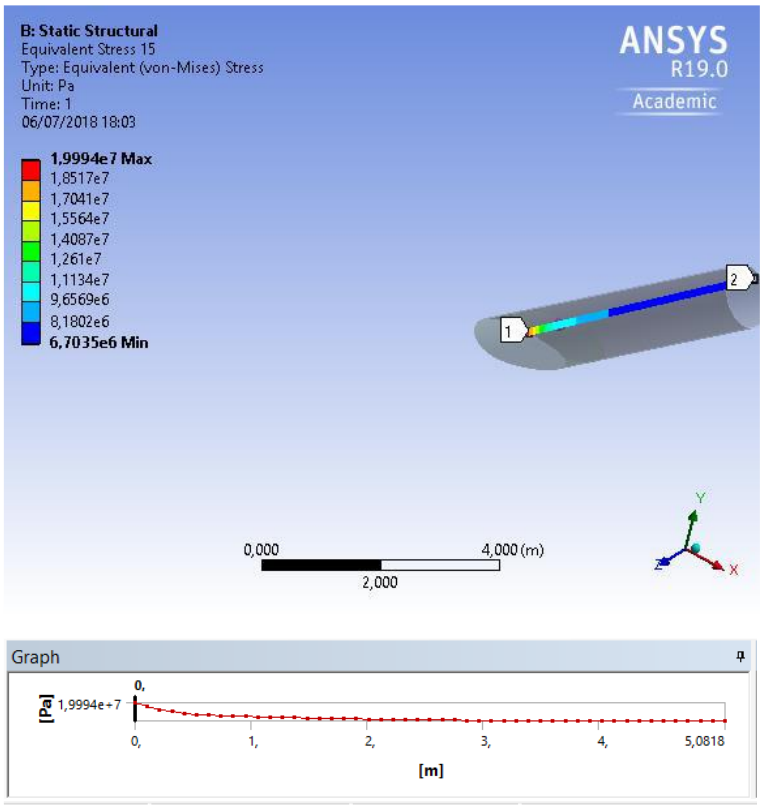


Figure 46 - Stress distribution in brace B3 for axial loading case: Side 4 [26].

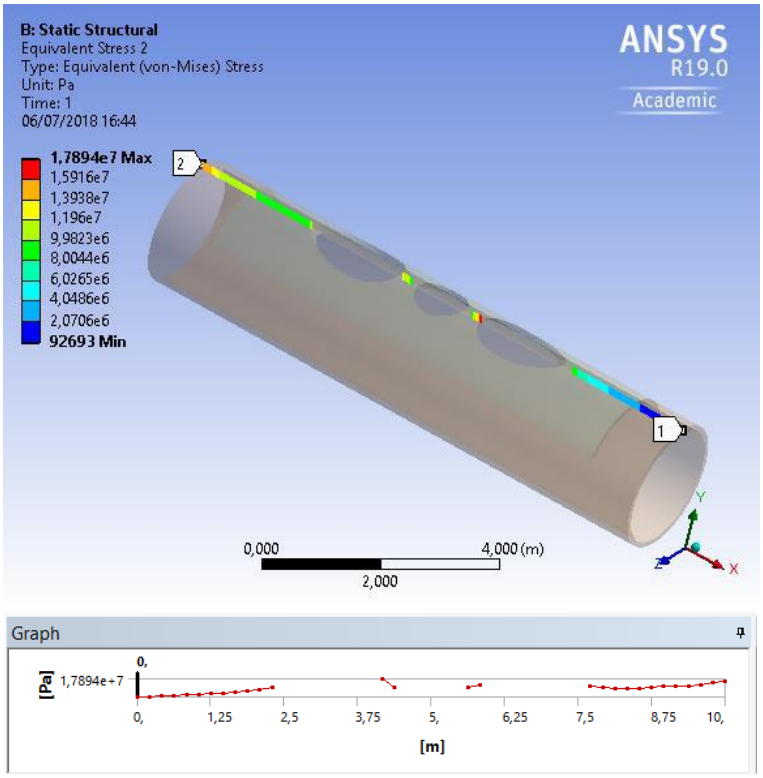


Figure 47 - Stress distribution in chord for axial loading case [26].

The accuracy of the results obtained strongly relies on the types of elements used along with the mesh size in the vicinity of the weld. It is reasonable that the SCFs taken from solid FEA provide higher values, since the results from shell elements are measured at the mid-section, whereas the solid results are measured on the external surface [15]. The loading sustained in service lead to displacements of rotary translation of the platform surface. The numerical simulations carried out in this study only considered the axial loading where the hotspots coincide with the crown ad saddle locations.

It is clearly noticeable from analyzing Figures 47 and 48, that the gaps in results are localized at the hollow tubular structural elements positions, and thus makes sense to point out that the stresses tend to increase until they reach a peak around the weld filet due to discontinuities in the geometry.

Stresses at the chord were only taken from the crown alignment, as can be seen in Figure 47, since these represent the location of highest stresses were as the minimum are around the location of the saddle. In addition, the stresses for axial loading conditions reach a peak at the chords C1 end, which is to be expected given the boundary conditions put forwards previously in this chapter.

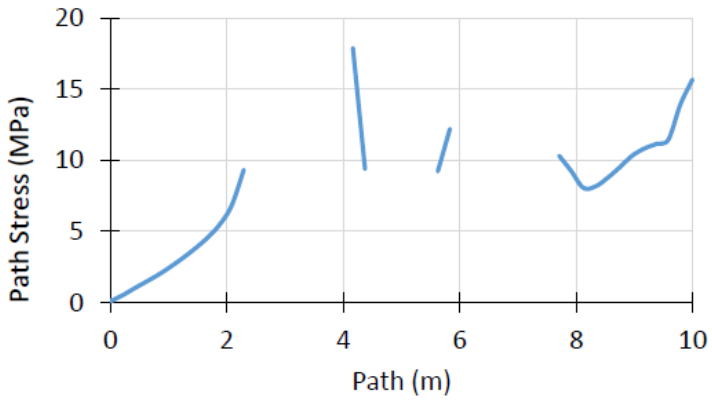


Figure 48 - Path stresses in chord crown for axial loading case [26]

As mentioned before in this document, once the hot-spot stresses are available, the SCF can be easily obtained via nominal stresses (see Table 16), as presented in Equation (76).

$$SCF = \frac{\sigma_{Hss}}{\sigma_n} \tag{76}$$

Where:

σ_{Hss} – Hot-spot stress

σ_n – Nominal stress

SCF – Stress concentration factor

Following the methodology presented above the SCF presented in Tables 16 to 19 for the chord and braces 1 to 3, along with each of the stress paths for every structural member in Figures 48 to 54, respectively.

Table 17 - Stress concentration factors in chord crown (axial) [26]

σ_{HSS}[MPa]	SCF
17.89	3.624

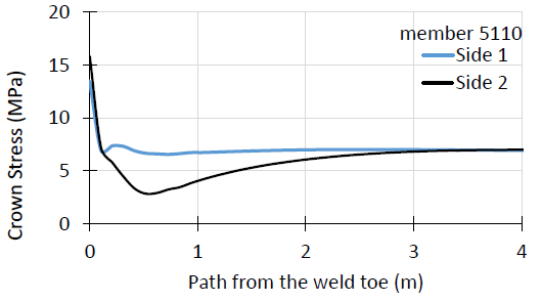


Figure 49 - Path stress in brace crown B1 for axial loading case (Side 1 and 2) [26]

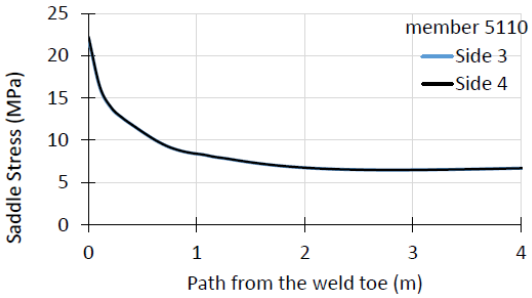


Figure 50 - Path stress in brace saddle B1 for axial loading case (Side 3 and 4) [26]

Table 18 - Results of the hot-spot stress distribution and stress concentration factor for Brace B1 due to axial loading [26]

		σ_{HSS}	SCF (Eq.77)
crown	Side 1	13.48	0.998
	Side 2	15.83	1.171
saddle	Side 3	51.53	1.638
	Side 4	51.57	1.649

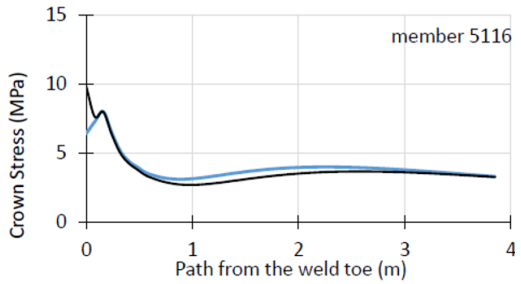


Figure 51 - Path stress in brace crown B2 for axial loading case (Side 1 and 2) [26].

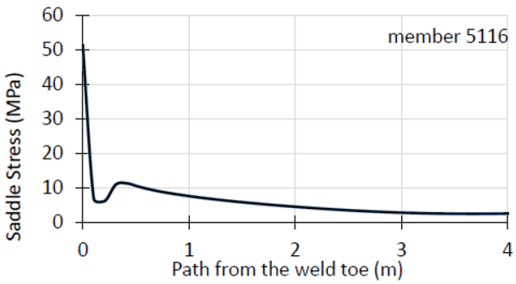


Figure 52 - Path stress in brace saddle B2 for axial loading case (Side 3 and 4) [26]

Table 19 - Results of the hot spot stress distribution and stress concentration factor for Brace B2 due to axial loading [26]

		σ_{HSS}	SCF (Eq.77)
crown	Side 1	8	1.375
	Side 2	9.82	1.688
saddle	Side 3	51.53	8.855
	Side 4	51.57	8.863

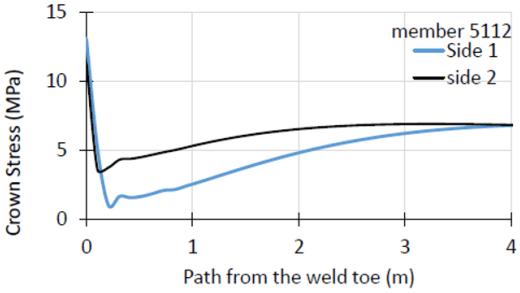


Figure 53 - Path stress in brace crown B3 for axial loading case (Side 1 and 2) [26]

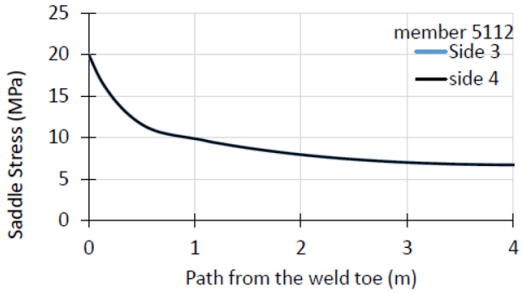


Figure 54 - Path stress in brace saddle B3 for axial loading case (Side 3 and 4) [26]

Table 20 - Results of the hot spot stress distribution and stress concentration factor for Brace B3 due to axial loading

		σ_{HSS}	SCF (Eq.77)
crown	Side 1	13.06	0970
	Side 2	11.32	0.840
saddle	Side 3	20.05	1.488
	Side 4	19.99	1.484

3.6. Conclusions

This dissertation continues the research work performed by P. Mendes, in [26], where the comparison of the SCF regarding several normative and other sources such as numerical modelling where compared, thus, this chapter aims to provide an introduction towards the following evaluation of the stress concentration factors and stress intensity factors values.

When trying to estimate the SCF values for both Efthymiou and Lloyd's parametric equations it was observed that there is a range of values regarding the geometrical parameters that need to be fulfilled, included in Table 20.

Table 21 - Validity range of values for both parametric equations [26]

	β		τ		γ		θ		ζ	
Relations	Min.	Max.	Min.	Max.	Min.	Max.	Min.	Max.	Min.	Max.
Efthymiou	0.2	1	0.2	1	8	32	20º	90º	$-0.6\beta/_{sin\theta}$	1
Lloyd	0.13	1	0.25	1	10	35	30º	90º	0	1

Table 22 - SCF comparison between DNV code and Lloyd [26]

		Lloyd's	DNV	DNV vs Lloyd's
Chord	B1	1.773	1.601	-9.70%
	B2	1.598	2.949	88.05%
	B3	1.117	1.369	22.53%
Brace	B1	1.861	1.823	-2.02%
	B2	1.480	3.409	130.49%
	B3	1.861	1.786	-4.07%

A comparison was established between the results obtained from Efthymiou's and Lloyd's parametric equations, see Table 21. For the axial loading conditions, it is possible to conclude that even though there is a different, which in the case of the B1/chord intersection the highest values tends towards the LR, the majority of the results show that DNV provides higher SCF values for axial loading conditions, particularly for the intermediate brace where the different is significant.

After the parametric equations results an FEA model was developed, a comparison and discussion on the stress concentration factor results between Lloyd's register KT-type joint equations, DNV parametric equations and FEA analysis was made. In Table 22, presented below, the maximum values obtained in all three different approaches are shown. The deviation obtained from the DNVGL equations for the Lloyd's register equations and finite element analysis is presented in Table 23, where a palpable overestimation of the parametric equations can be seen, even though further studies with the weld should be conducted.

Overall, DNV recommended practices provide the highest values for SCF with the lowest being found through FEA, with exception for the saddle in the intermediate brace, B2, where an increase of 3984.3% and 160.0% was found regarding the Lloyd's registry and DNV, respectively.

Table 23 - Stress concentration factors for axial loading case from the Lloyd and DNVGL parametric equations and finite element analysis [26]

Comparison		$SCF_{AS/AC}$				
		DNV	Lloyd		FEA	
			Crown	Saddle	Crown	Saddle
Chord	B1	1.601	1.773	1.733	3.624	
	B2	2.949	1.598	0.935	0.341	
	B3	1.369	1.117	1.047	0.444	
Saddle	B1	1.823	1.861	1.596	1.171	1.649
	B2	3.409	1.480	0.217	1.688	8.863
	B3	1.786	1.861	1.250	0.970	1.488

The DNVGL standard does not specify a lower limit for the SCF. However, values lower than 1 should not be considered. However, the DNVGL standard states that due to the axial stress in the chord the SCF should be increased by a factor of 1.20 for calculation of additional hot-spot stress at the crown toe and the crown heel for dynamic loading in the axial direction of the chord.

Table 24 - Deviation of stress concentration factors between DNV-FEA and between Lloyd-FEA for axial loading case [26]

Deviation	SCF AS/AC		
Chord	DNV vs FEA	Loyd vs FEA	
		Crown	Saddle
B1	55.8%	104.4%	109.1%
B2	-764.7%	-78.7%	-63.5%
B3	-208.2%	-60.2%	-57.6%
Brace	DNV vs FEA	Crown	Saddle
B1	-11.4%	-37.1%	3.3%
B2	160.0%	14.0%	3984.3%
B3	-16.7%	-47.9%	19.0%

4. Evaluation of SIF values of a typical tubular KT-joint

4.1. Introduction

The use of T-butt joints to calculate stress intensity factors (SIFs) for weld toe cracks in tubular joints has been proposed by many researchers, including Dijkstra et al. (TNO, Delft), Pang (Nanyang Technological University), Fu et al. (British Gas), Maddox (TWI) and Burdekin et al. (UMIST), as described in ref. [33]. The reasons for using T-butt joint solutions to approximate tubular joint SIFs are, first, because tubular joint solutions only exist for a few very basic tubular joint configurations, and, secondly, because to derive solutions for the many different geometries and configurations of tubular joint used in practice would require an unmanageable number of analyses [33]. According to Section 2.2.1, different types of tubular joints (K, KT, X, Y, etc.) can be used in offshore applications. Normally, the stress intensity factor values are determined based on analytical formulations suggested by BS7910 standard, IIW recommendations, SINTAP standard, among others. However, these analytical formulations are based on geometric configurations not exactly fitted to tubular joints, except for the expressions proposed by SINTAP standard, where the SIF values can be evaluated for T tubular joints. Alternatively, the numerical simulations seem to be more suitable for the SIF evaluation of tubular joints.
In this way, the stress intensity factors evaluation based on BS7910 standard, IIW recommendations and SINTAP standard for a typical KT tubular joints are made. Additionally, a comparison and discussion of the obtained SIF values are done.

4.2. SIF evaluation based on BS7910 standard

4.2.1 BS7910 standard rules

According to BS 7910 standard (annex M), the stress intensity factor (K_I) solutions for a range of flaw types that are likely to arise in welded joints are calculated by the following equation:

$$K = (Y \cdot \sigma) \cdot \sqrt{\pi \cdot a} \tag{77}$$

where, σ is a general stress term, Y is the geometric function, and a is the crack depth.

Additional, the stress intensity factor solutions have been published in the form of handbooks, for a wide range of geometry and loading configurations. Alternatively,

numerical analysis methods (e.g. finite elements) or weight function techniques can be used to derive stress intensity factors, but the basis of the method and the results should be fully documented. The validity of the solutions given in the annex M of the BS7910 standard is limited strictly to the ranges stated. No extrapolation outside these limits should be carried out.
For fatigue assessments, the corresponding stress intensity factor range is given by

$$\Delta K = Y \cdot (\Delta\sigma) \cdot \sqrt{\pi \cdot a} \tag{78}$$

For fracture assessments at Level 1 the following equation applies

$$Y\sigma = M f_w M_m \sigma_{max} \tag{79}$$

For fracture assessments at Levels 2 and 3 the following equation applies

$$Y\sigma = (Y\sigma)_p + (Y\sigma)_s \tag{80}$$

where, $(Y\sigma)_p$ e $(Y\sigma)_s$ represent contributions from primary and secondary stresses, respectively. They are calculated as follows:

$$(Y\Delta\sigma)_p = M f_w [k_{tm} \cdot M_{km} \cdot M_m \cdot P_m + k_{tb} \cdot M_{kb} \cdot M_b \cdot \{P_b + (k_m - 1) \cdot P_m\}] \tag{81}$$

$$(Y\sigma)_s = M_m Q_m + M_b Q_b \tag{82}$$

For fatigue assessments the following equation applies

$$(Y\Delta\sigma)_p = M[K_{tm} \cdot M_{km} \cdot M_m \cdot \Delta\sigma_m + K_{tb} \cdot M_{kb} \cdot M_b \cdot \{\Delta\sigma_b + (K_m - 1) \cdot \Delta\sigma_m\}] \tag{83}$$

Expressions for M, f_w, M_m and M_b are given on a case-by-case basis. The factors M_{km} and M_{kb} apply when the crack is in a region of local stress concentration such as close to the toe of a weld. For k_t, k_{tm}, k_{tb}, and k_m, reference should be made according to the literature. To determine M_{km}, it has to be taken into consideration that depending on the weld profile its value may differ [27].

For a geometry of the crack with a surface flaw, for the membrane loading situation, as given by Figure 55, the Equations (84) to (99) are applied.

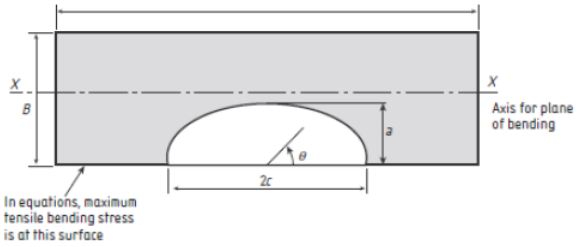


Figure 55 - Surface flaw [27].

Thus, the following conditions are applied:

$$0 \leq a/2c \leq 1.0 \tag{84}$$

$$0 \leq \theta \leq \pi \tag{85}$$

for $0 \leq a/2c \leq 0.1$

$$a/B < 1.25(a/c + 0.6) \tag{86}$$

for $0.1 \leq a/2c \leq 1.0$

$$a/B < 1.0 \tag{87}$$

The stress intensity factor is given by Equations (88) to (103), where $M = 1$:

$$f_w = \left(\sec\left[\left(\frac{\pi c}{W}\right)\left(\frac{a}{B}\right)^{0.5}\right]\right)^{0.5} \tag{88}$$

Equation (89) defines M_m whereas M_b is null since it is only applied membrane loading, not bending loading.

$$M_m = (M_1 + M_2(a/B)^2 + M_3(a/B)^4) g f_\theta / \Phi \tag{89}$$

where, for $0 \leq a/2c \leq 0.5$:

$$M_1 = 1.13 - 0.09(a/c) \tag{90}$$

$$M_2 = [0.89/(0.2 + (a/c))] - 0.54 \tag{91}$$

$$M_3 = 0.5 - 1/(0.65 + (a/c)) + 14(1 - (a/c))^{24} \tag{92}$$

$$g = 1 + (0.1 + 0.35(a/B)^2)(1 - sin\theta)^2 \tag{93}$$

$$f_\theta = ((a/c)^2 cos\theta^2 + sin\theta^2)^{0.25} \tag{94}$$

and, where, for $0.5 \leq a/2c \leq 1.0$:

$$M_1 = (c/a)^{0.5}(1 + 0.04(c/a)) \tag{95}$$

$$M_2 = 0.2(c/a)^4 \tag{96}$$

$$M_3 = -0.11(c/a)^4 \tag{97}$$

$$g = 1 + (0.1 + 0.35(c/a)(a/B)^2)(1 - sin\theta)^2 \tag{98}$$

$$f_\theta = ((c/a)^2 sin\theta^2 + cos\theta^2)^{0.25} \tag{99}$$

Φ, the complete elliptic integral of the second kind, may be determined from standard tables or from the following solution, which is sufficiently accurate:

for $0 \leq a/2c \leq 0.5$

$$\Phi = (1 + 1.464(a/c)^{1.65})^{0.5} \tag{100}$$

for $0.5 < a/2c \leq 1.0$

$$\Phi = (1 + 1.464(c/a)^{1.65})^{0.5} \tag{101}$$

Having into consideration the weld toe profile, the value M_k is given by the Equations (102) and (103) and using the Table 24:

$$M_k = \upsilon_{(*)} \cdot \left(\frac{Z}{B}\right)^w \tag{102}$$

$$\upsilon_{(*)} = \upsilon \cdot \left(\frac{B}{t_w}\right)^{0.5} \tag{103}$$

Table 25 - Values of v and w for axial and bending loading [28]

Loading Mode	*L/B*	*z/B*	*v*	*w*
Axial	≤ 2	$\leq 0.05(L/B)^{0.55}$ $>0.05(L/B)^{0.55}$	$0.51(L/B)^{0.27}$ 0.83	-0.31 $-0.15(L/B)^{0.46}$
	> 2	≤0.073 >0.073	0.615 0.83	-0.31 -0.20
Bending	≤ 1	$\leq 0.03(L/B)^{0.55}$ $>0.03(L/B)^{0.55}$	$0.45(L/B)^{0.21}$ 0.68	-0.31 $-0.9(L/B)^{0.21}$
	> 1	≤0.03 >0.03	0.45 0.68	-0.31 -0.19

After having all the information regarding the equations are calculated the stress intensity factors.

4.2.2 Results

After having all the information regarding the equations needed to correctly calculate the stress intensity factor, it is possible to build $SIF\ vs\ a$ curves for both outer and central braces, and chord sections whenever possible, based on SCF values obtained according to Lloyd's register, DNV standard and FEA (see Chapter 3).

4.2.2.1 Brace B1

In Figures 56 to 60 are displayed the stress intensity factor (SIF) values as a function of the crack size (a), Brace B1 (see Figure 20), for several a/c ratios, based on SCF values obtained using Lloyd's Register, DNV standard, and FEA. According to Figures 56 to 60, it is possible to conclude that the SIF vs. a curves obtained for SCF values calculated based on Lloyd (crown and saddle points) and DNV are very close. When comparing SIF results using SCF values from Lloyd and FEA, for crown point, it can be assumed that the SIF values are somewhat close. Already saddle location that fact is not

verified.

For the Brace B1 (see Figure 20), the *SIF vs. a* curves based on DNV standard for $\sigma_n = 12.5MPa$, for $0.1 \leq a/c \leq 0.5$, $0.6 \leq a/c \leq 1$, and $1.2 \leq a/c \leq 2$, are illustrated in Figures 61 to 63, respectively. These curves were obtained to support the designers in their analysis, since the calculation form is too long.

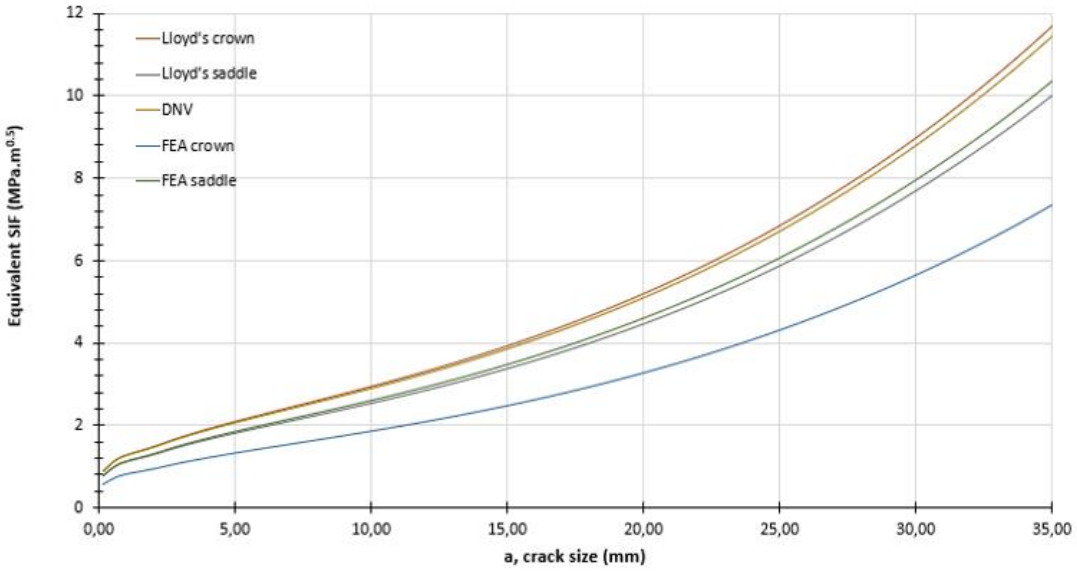


Figure 56 - *SIF vs. a* curves for the Brace B1 using BS7910 standard based on Lloyd's Register, DNV standard, and FEA: $a/c = 0.1$.

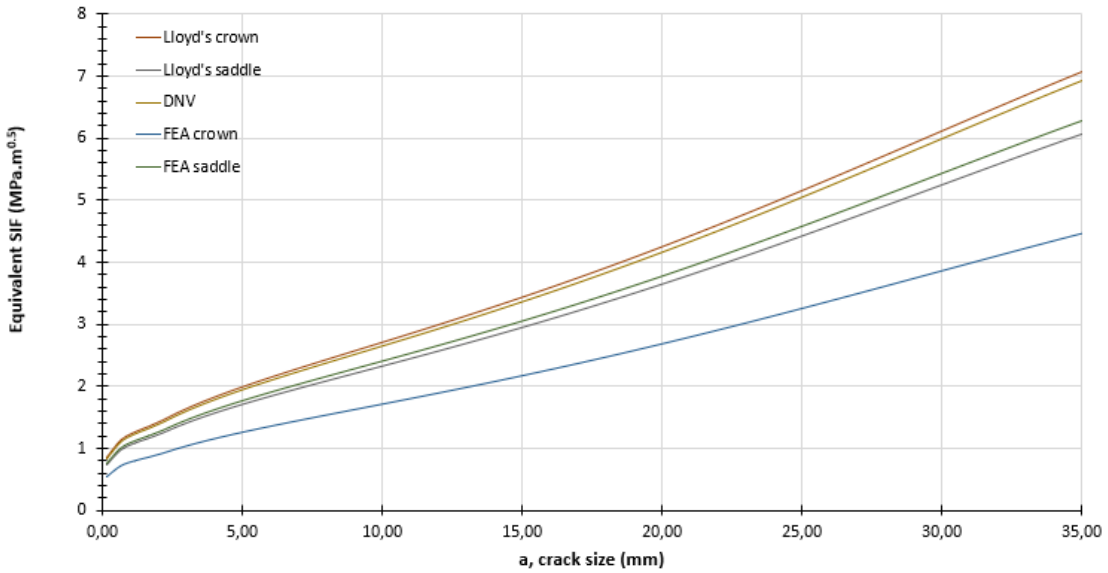


Figure 57 - *SIF vs. a* curves for the Brace B1 using BS7910 standard based on Lloyd's Register, DNV standard, and FEA: $a/c = 0.2$.

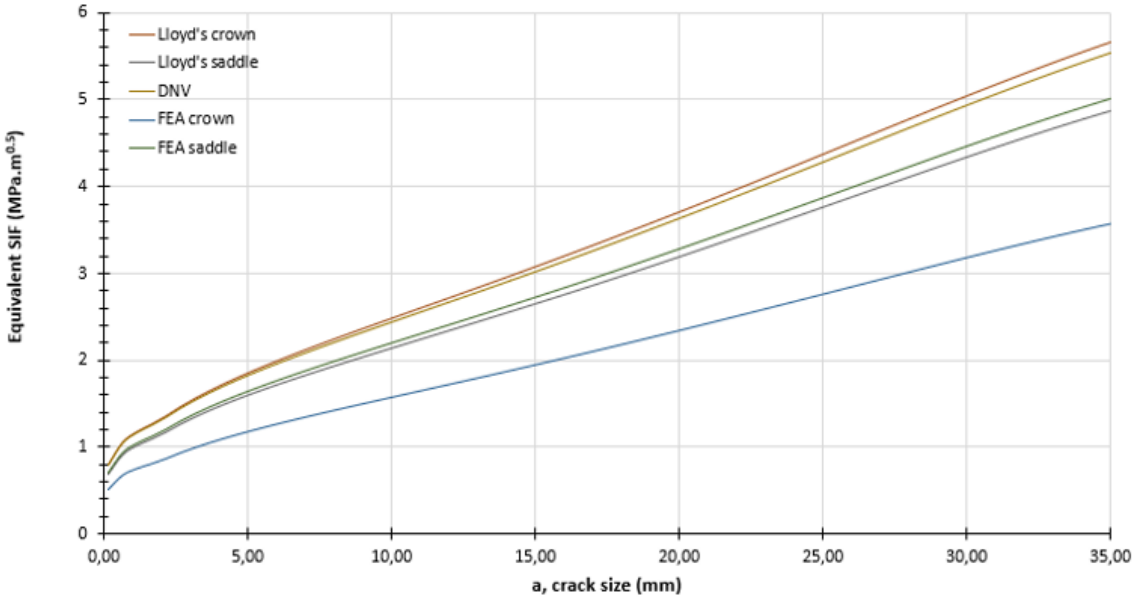


Figure 58 - *SIF vs. a* curves for the Brace B1 using BS7910 standard based on Lloyd's Register, DNV standard, and FEA: $a/c = 0.3$.

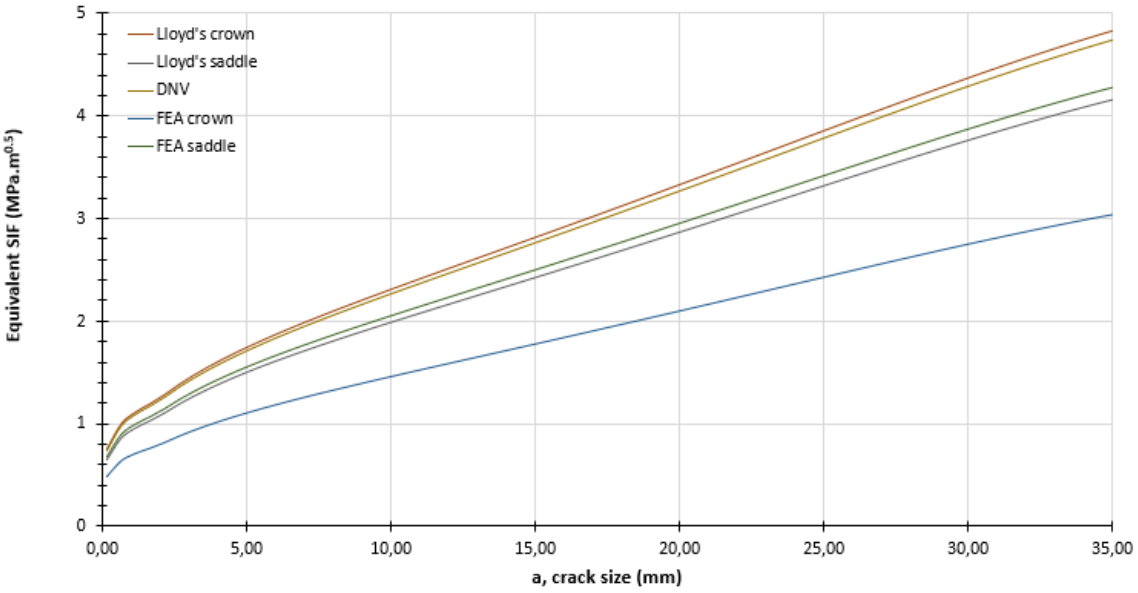


Figure 59 - *SIF vs. a* curves for the Brace B1 using BS7910 standard based on Lloyd's Register, DNV standard, and FEA: $a/c = 0.4$.

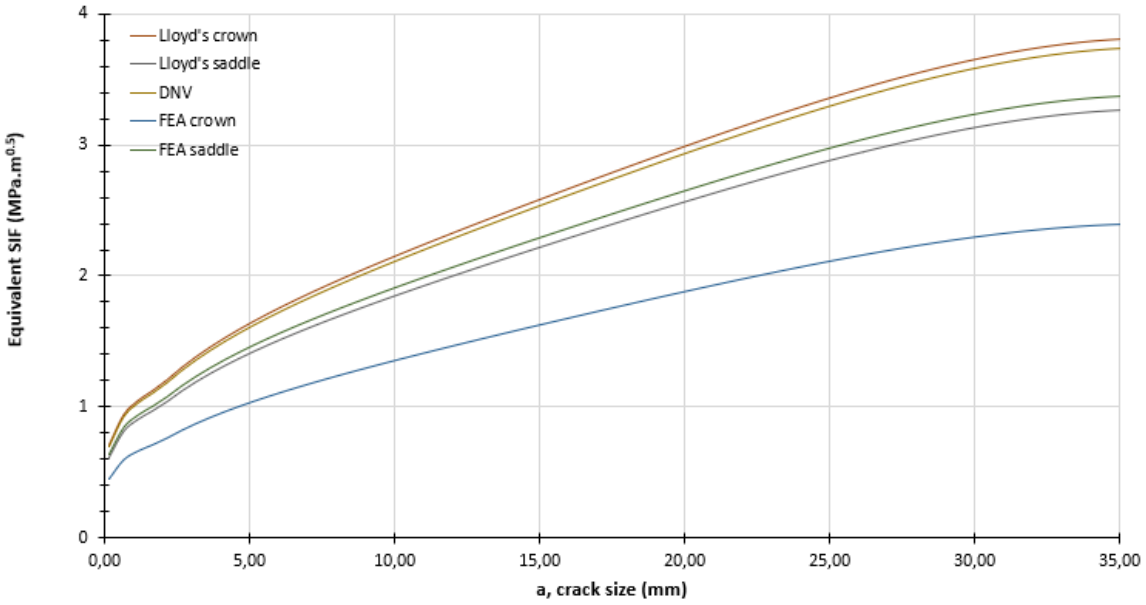


Figure 60 - *SIF vs. a* curves for the Brace B1 using BS7910 standard based on Lloyd's Register, DNV standard, and FEA: $a/c = 0.5$.

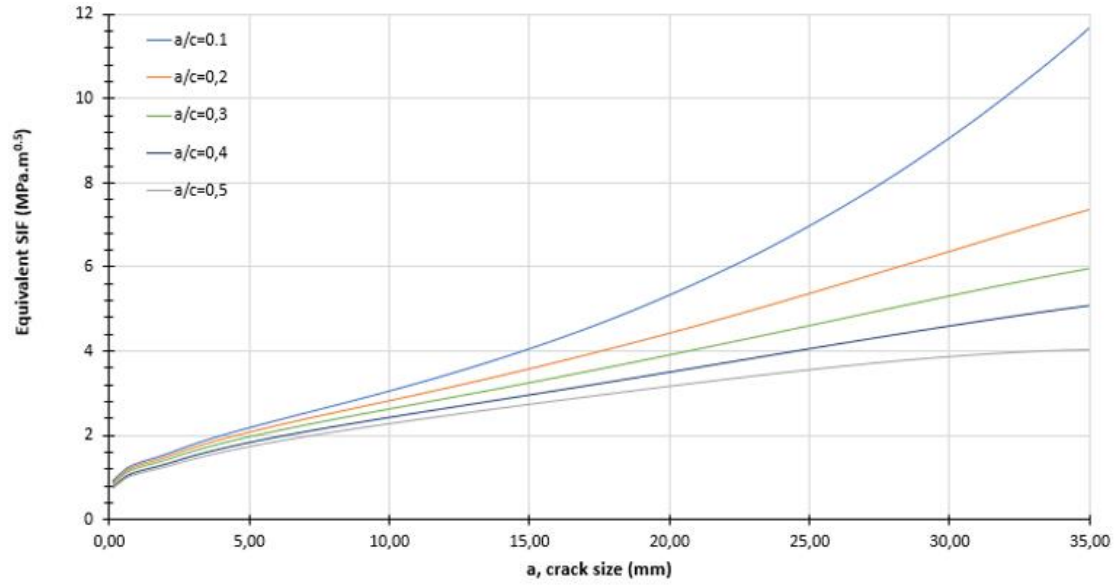


Figure 61 - *SIF vs. a* curves for the Brace B1 using BS7910 standard based on DNV standard for $\sigma_n = 12.5MPa$: $0.1 \leq a/c \leq 0.5$.

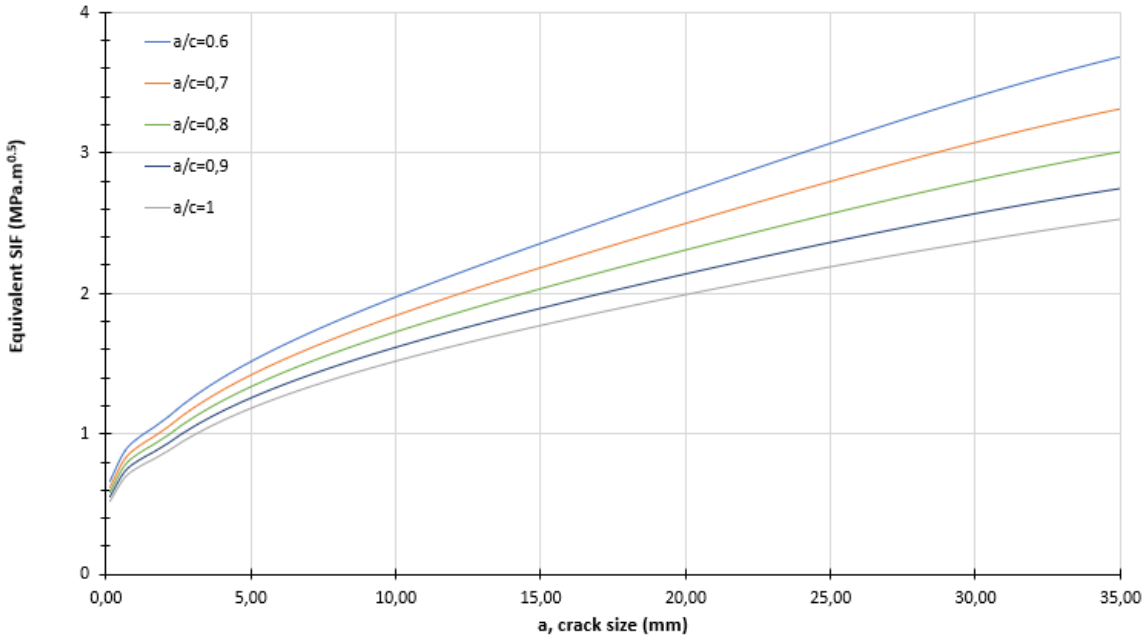


Figure 62 - *SIF vs. a* curves for the Brace B1 using BS7910 standard based on DNV standard for $\sigma_n = 12.5MPa$: $0.6 \leq a/c \leq 1.0$.

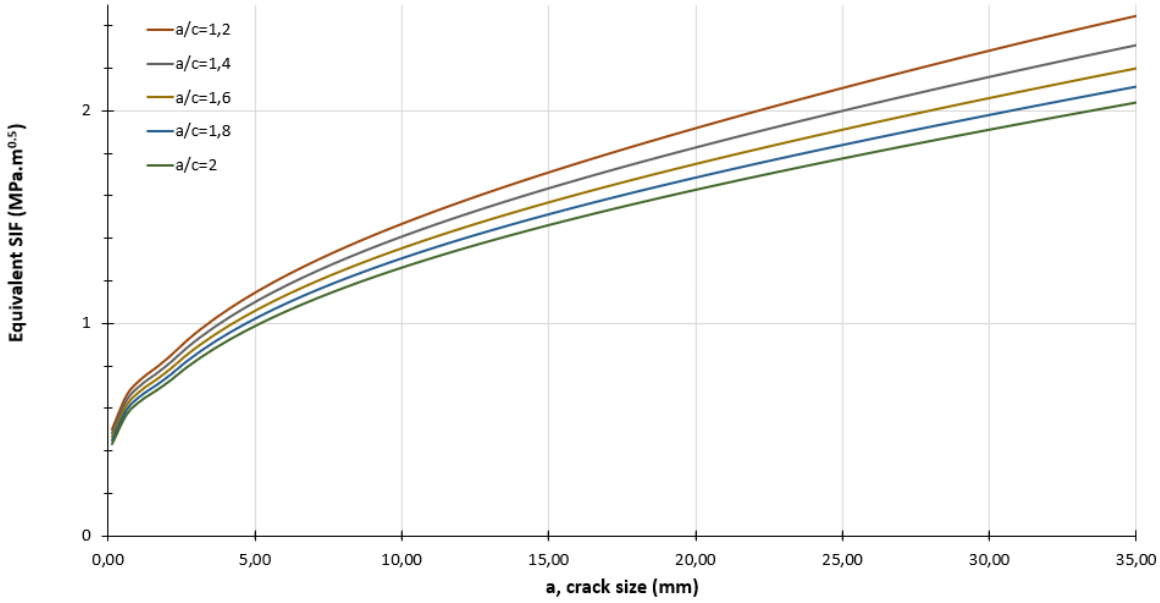


Figure 63 - *SIF vs. a* curves for the Brace B1 using BS7910 standard based on DNV standard for $\sigma_n = 12.5MPa$: $1.2 \leq a/c \leq 2$.

4.2.2.2 Brace B2

In Figure 64 is presented the stress intensity factor (SIF) values as a function of the crack size (a), Brace B2 (see Figure 20), for several $a/c = 0.1$, based on SCF values obtained using Lloyd's Register, DNV standard, and FEA. According to Figure 64, it is possible to conclude that the SIF vs. a curves obtained for SCF values calculated based on Lloyd and FEA, crown point, are very close. The same can be verified when is compared the SIF results obtained for SCF values based on DNV and FEA (saddle point). SIF values obtained using the SCF values from the Lloyd, for the saddle point, are far from the rest of the curves.

For the Brace B2 (see Figure 20), the *SIF vs. a* curves based on DNV standard for $\sigma_n = 37.3MPa$, for $0.6 \leq a/c \leq 1$ and $1.2 \leq a/c \leq 2$, are illustrated in Figures 65 and 65, respectively. These curves were obtained to support the designers in their analysis, since the calculation form is too long.

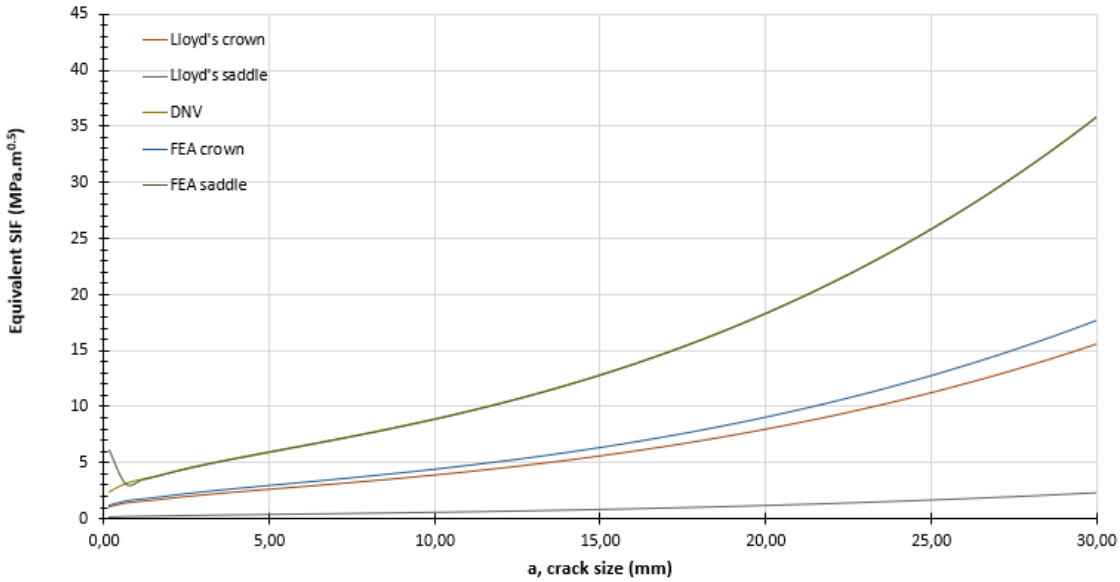


Figure 64 - *SIF vs. a* curves for the Brace B2 using BS7910 standard based on Lloyd's Register, DNV standard, and FEA: $a/c = 0.1$.

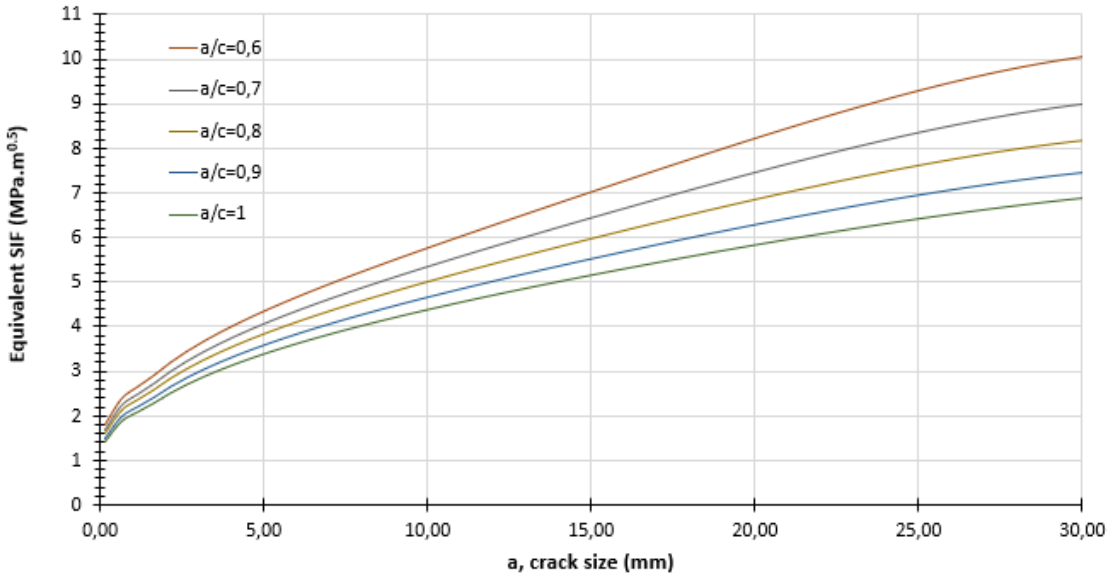


Figure 65 - *SIF vs. a* curves for the Brace B2 using BS7910 standard based on DNV standard for $\sigma_n = 37.3MPa$: $0.6 \leq a/c \leq 1.0$.

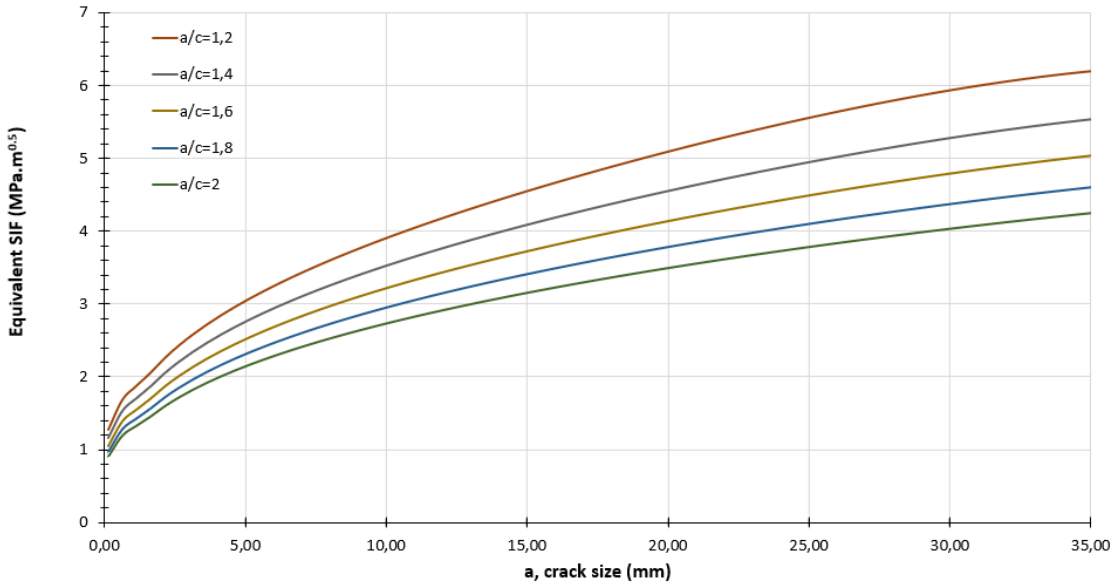


Figure 66 - *SIF vs. a* curves for the Brace B1 using BS7910 standard based on DNV standard for $\sigma_n = 37.3MPa$: $1.2 \leq a/c \leq 2.0$.

4.2.2.3 Brace B3

Figures 67 to 71 are displayed the stress intensity factor (SIF) values as a function of the crack size (a), Brace B3 (see Figure 20), for several a/c ratios, 0.1 to 0.5, based on SCF values obtained using Lloyd's Register, DNV standard, and FEA. According to Figures 67 to 71, it is possible to conclude that the SIF vs. a curves obtained for SCF values calculated based on Lloyd (crown point) and DNV are very close. When comparing SIF results using SCF values from Lloyd and FEA, for saddle point, it can be assumed that the SIF values are somewhat close. Comparing the SIF results obtained, for the crown point, using the SCF values based on FEA and Lloyd solutions, it is observed a poor agreement between the curves.

For the Brace B3 (see Figure 20), the *SIF vs. a* curves based on DNV standard for $\sigma_n = 21.2MPa$, for $0.6 \leq a/c \leq 1$ and $1.2 \leq a/c \leq 2$, are illustrated in Figures 72 and 73, respectively. These curves were obtained to support the designers in their analysis, since the calculation form is too long.

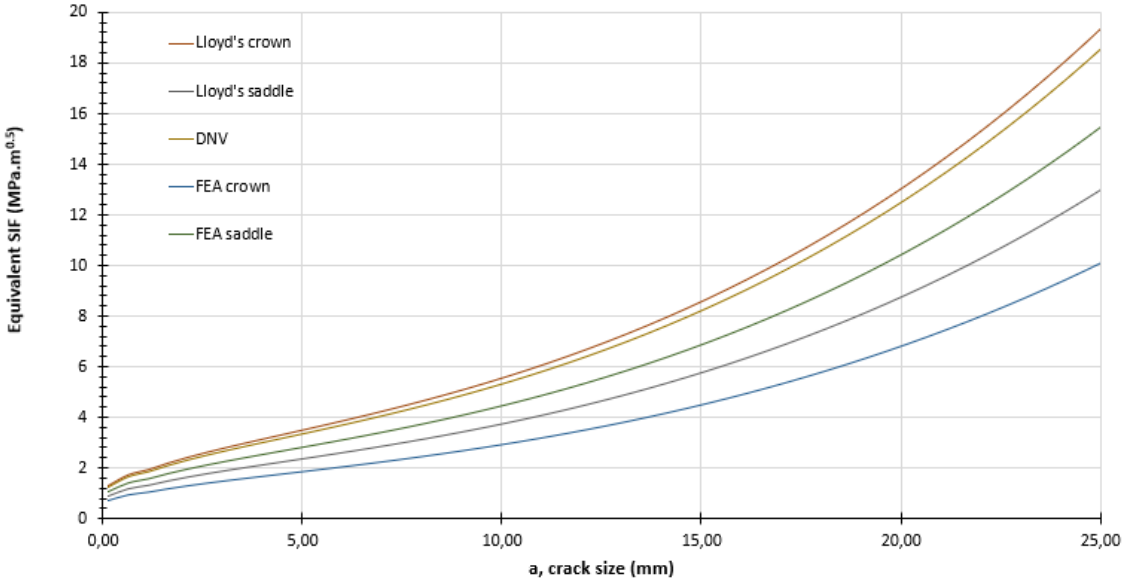


Figure 67 - *SIF vs. a* curves for the Brace B3 using BS7910 standard based on Lloyd's Register, DNV standard, and FEA: $a/c = 0.1$.

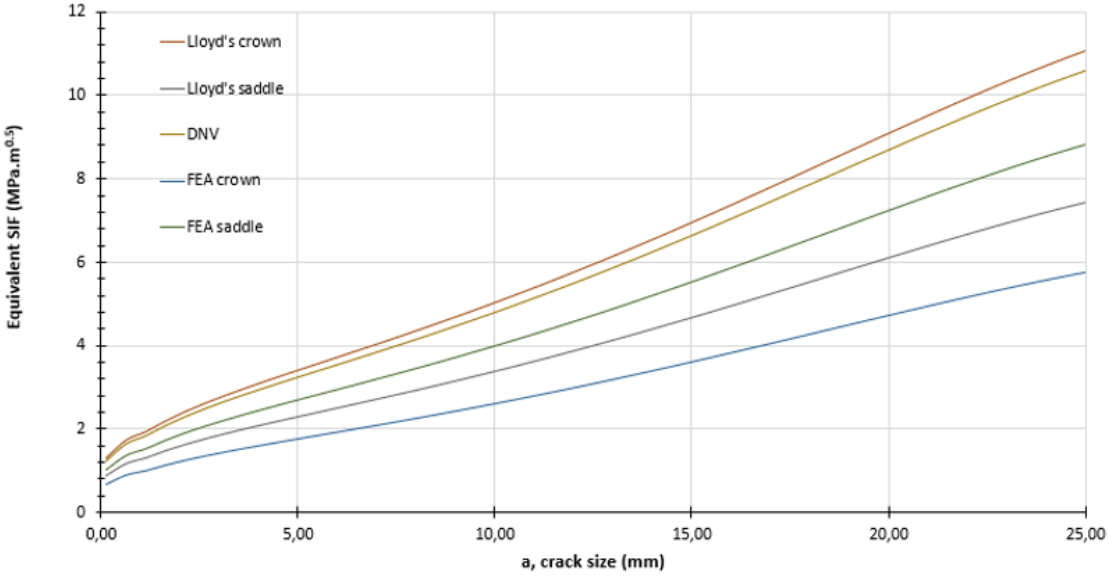


Figure 68 - *SIF vs. a* curves for the Brace B3 using BS7910 standard based on Lloyd's Register, DNV standard, and FEA: $a/c = 0.2$.

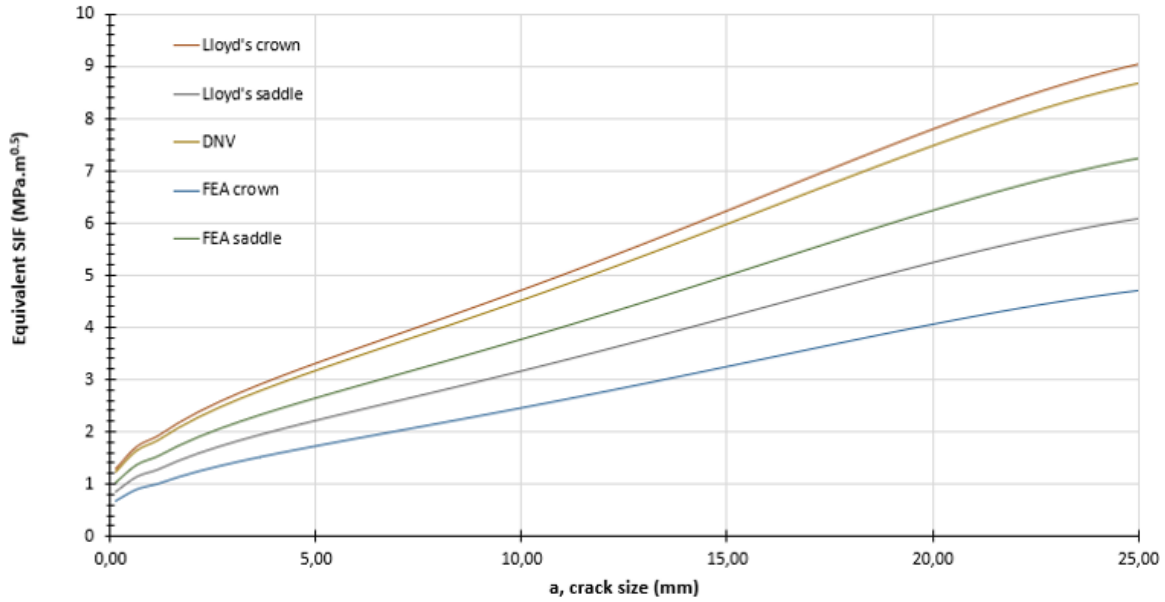


Figure 69 - *SIF vs. a* curves for the Brace B3 using BS7910 standard based on Lloyd's Register, DNV standard, and FEA: $a/c = 0.3$.

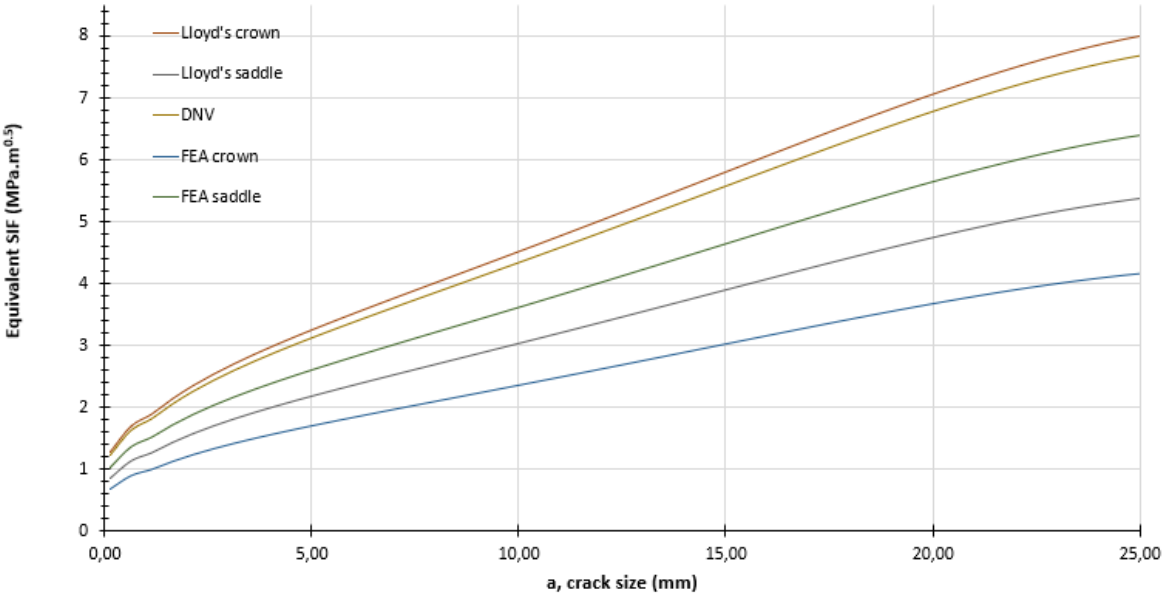


Figure 70 - *SIF vs. a* curves for the Brace B3 using BS7910 standard based on Lloyd's Register, DNV standard, and FEA: $a/c = 0.4$.

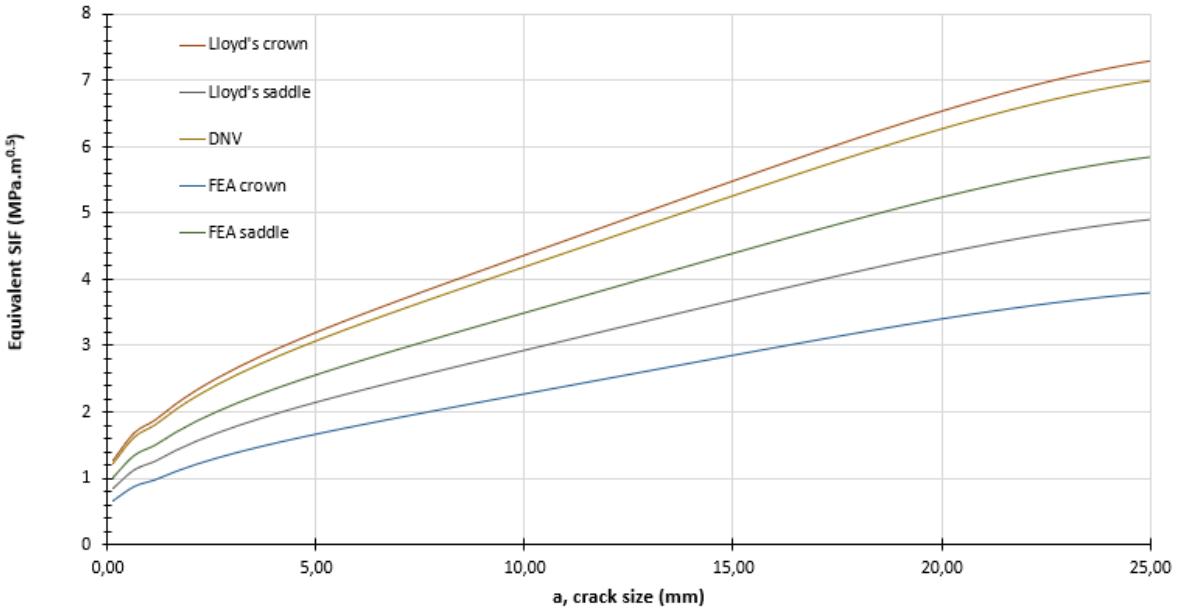


Figure 71 - *SIF vs. a* curves for the Brace B3 using BS7910 standard based on Lloyd's Register, DNV standard, and FEA: $a/c = 0.5$.

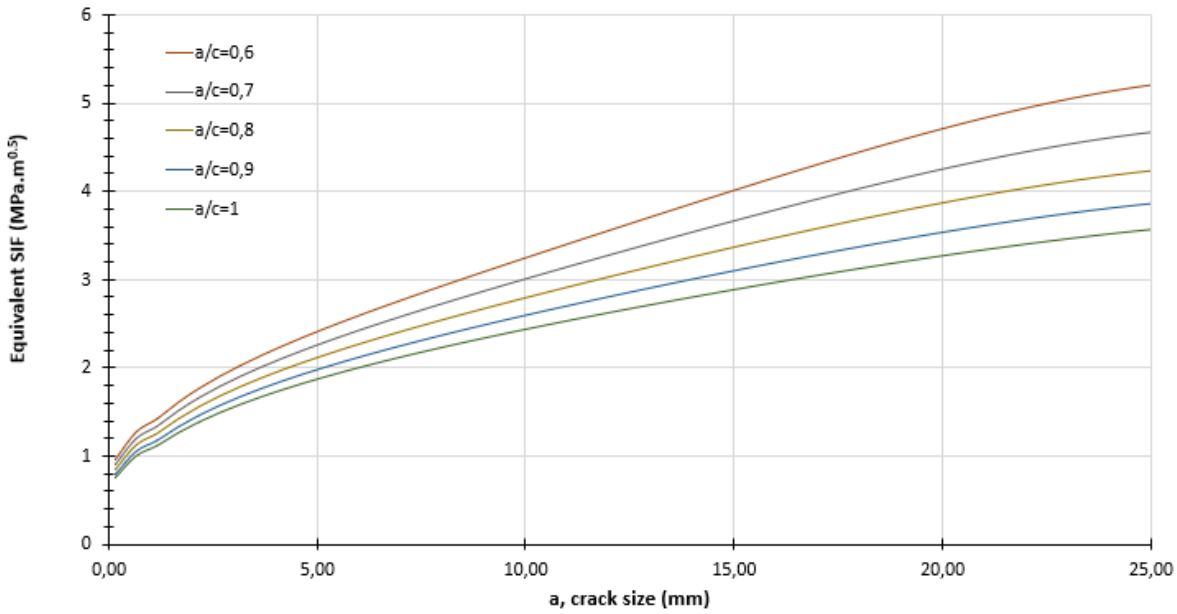


Figure 72 - *SIF vs. a* curves for the Brace B3 using BS7910 standard based on DNV standard for $\sigma_n = 21.2MPa$: $0.6 \leq a/c \leq 1.0$.

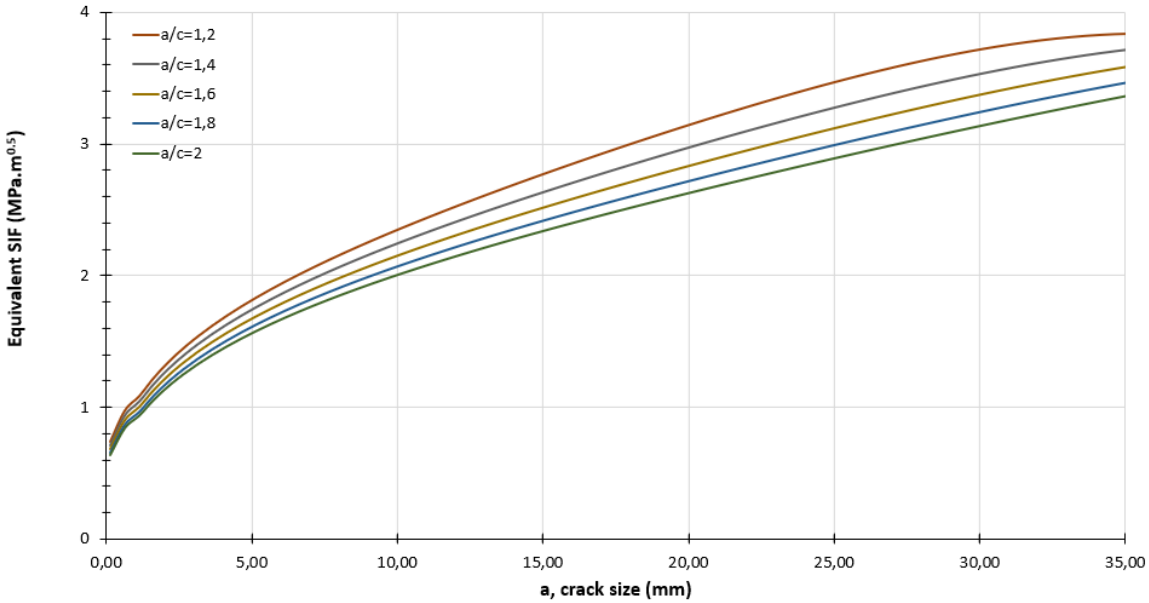


Figure 73 - *SIF vs. a* curves for the Brace B3 using BS7910 standard based on DNV standard for $\sigma_n = 21.2MPa$: $1.2 \leq a/c \leq 2$.

4.3. SIF evaluation based on IIW recommendations

4.3.1 Rules from IIW recommendations

At First, it is supposed that at the location of the crack when the relevant applied stress is determined, there is no actual crack [17]. The stress, preferably, is divided into membrane and shell bending stress components. SIF, also symbolized by K, results from the superposition of the effects of both stress components. Crack shape and size effects are accounted for correction function, Y. The stress remaining caused by the discontinuity or notch of the structure (non-linear peak stress) is contained in an additional factor M_k.

$$K = \sqrt{\pi \cdot a} \cdot \left(\sigma_m \cdot Y_m \cdot M_{k,m} + \sigma_b \cdot Y_b \cdot M_{k,b}\right) \tag{104}$$

where:

K - stress intensity factor;

σ_m - membrane stress;

σ_b - shell bending stress;

Y_m - correction function for membrane stress intensity factor;

Y_b - correction function for shell bending stress intensity factor;

$M_{k,m}$ - correction for non-linear stress peak in terms of membrane action; and,

$M_{k,b}$ - correction for non-linear peak in terms of shell bending.

For the calculation of the stress intensity factor of a surface crack under shell bending and membrane stresses by the IIW recommendations, the following equations are applied:

The formula for the stress intensity factor K1 is valid for a/c < 1,

$$K = (\sigma_{mem} + H \cdot \sigma_{ben})\sqrt{\pi \cdot a/Q} \cdot F_s \quad (105)$$

$$Q = 1 + 1.464 \cdot (a/c)^{1.65} \quad (106)$$

$$F_s = [M_1 + M_2 \cdot (a/t)^2 + M_3 \cdot (a/t)^4] \cdot g \cdot f \cdot f_w \quad (107)$$

$$M_1 = 1.13 - 0.09(a/c) \quad (108)$$

$$M_2 = -0.54 + 0.89/(0.2 + a/c) \quad (109)$$

$$M_3 = 0.5 - 1/(0.65 + a/c) + 14(1 - a/c)^{24} \quad (110)$$

$$f_w = [\sec(\pi \cdot c \cdot \sqrt{a/t}/(2 \cdot b))]^{1/2} \quad (111)$$

The variables g and f are dependent to direction:

"a"-direction: $g = 1$ and $f = 1$

"c"-direction:

$$g = 1 + [0.1 + 0.35 \cdot (a/t)^2] \quad (112)$$

$$f = \sqrt{a/c} \quad (113)$$

The function H is given by the formulae:
"a"-direction:

$$H = 1 + G_1 \cdot (a/t) + G_2 \cdot (a/t)^2 \quad (114)$$

where:

$$G_1 = -1.22 - 0.12 \cdot (a/c) \quad (115)$$

$$G_2 = 0.55 - 1.05 \cdot (a/c)^{0.75} + 0.47 \cdot (a/c)^{1.5} \quad (116)$$

"c"-direction:

$$H = 1 - 0.34\,(a/t) - 0.11\,(a/c)\,(a/t) \quad (117)$$

For a variety of welded joints parametric formulae of the M_k functions have been established and published. For the majority of cases, the formulae given below are sufficient [17].
For the membrane stress case, the stress intensity factor for the brace for $M_k > 1$ (see Equations (119) to (122)) is given by the following equations:

For $l/t \leq 2$:

$$M_K = 0.51 \cdot (l/t)^{0.27} \cdot (a/t)^{-0.31} \qquad \text{for } (a/t) \leq 0.05 \cdot (l/t)^{0.55} \tag{118}$$

$$M_K = 0.83 \cdot (a/t)^{-0.15(l/t)^{0.46}} \qquad \text{for} (a/t) > 0.05 \cdot (l/t)^{0.55} \tag{119}$$

For $l/t > 2$:

$$M_K = 0.615 \cdot (a/t)^{-0.31} \tag{120}$$

$$M_K = 0.83 \cdot (a/t)^{-0.2} \tag{121}$$

For the bending stress case, the stress intensity factor for the brace for $M_k > 1$ (see Equations (122) to (125)) is given by the following equations:

For $l/t \leq 1$:

$$M_K = 0.45 \cdot (l/t)^{0.21} \cdot (a/t)^{-0.31} \tag{122}$$

$$M_K = 0.68 \cdot (a/t)^{-0.19(l/t)^{0.21}} \tag{123}$$

For $l/t > 1$:

$$M_K = 0.45 \cdot (a/t)^{-0.31} \tag{124}$$

$$M_K = 0.68 \cdot (a/t)^{-0.19} \tag{125}$$

A simplified method can be used to calculate M_K factors. In this case, it is presented a derivation from the non-linear stress peak distribution $\sigma_{nlp}(x)$ along the anticipated crack path x assuming that no crack is present.

$$M_k = \frac{2}{\pi} \cdot \int_{x=0}^{x=a} \frac{K_{t,nlp}(x)}{\sqrt{a^2 - x^2}} dx \tag{126}$$

For different crack lengths a, a function $M_k(a)$ can be established, which is preferably presented in the form:

$$M_k(a) = \frac{const}{a^{exp}} \quad for\ (a) > 1 \tag{127}$$

4.3.2 Results

In this section, the $SIF\ vs\ a$ curves for the Braces B1, B2 and B3 of the KT tubular joint presented in Figure 20 (Chapter 3) based on the SCF and/or hot-spot stress values calculated using the Lloyd's register, DNV standard and FEA, are shown.

4.3.3.1 Brace B1

Figures 74 and 75 show the *SIF vs. a* curves for the Brace B1 using IIW recommendations based on Lloyd's Register, DNV standard, and FEA, for a/c equal to 0.1 and 0.2, respectively. A good agreement can be verified between the *SIF vs. a* curves obtained based on Lloyd and FEA, for the saddle point of the Brace B1 for the tubular joint under consideration. The same conclusion can be found between the *SIF vs. a* curves obtained based on Lloyd and DNV, for the crow point. The *SIF vs. a* curve calculated using the the SCF and/or hot-spot stress values based on FEA for the crown point of the connection presents a bad results when compared with the curves based on DNV and Lloyd Register.

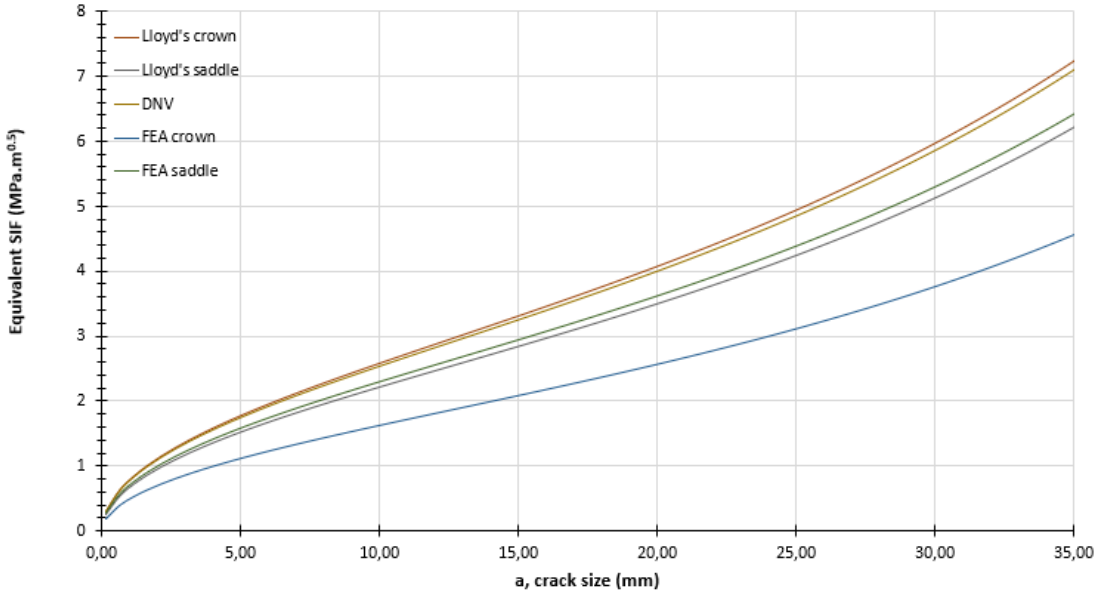


Figure 74 - *SIF vs. a* curves for the Brace B1 using IIW recommendations based on Lloyd's Register, DNV standard, and FEA: $a/c = 0.1$.

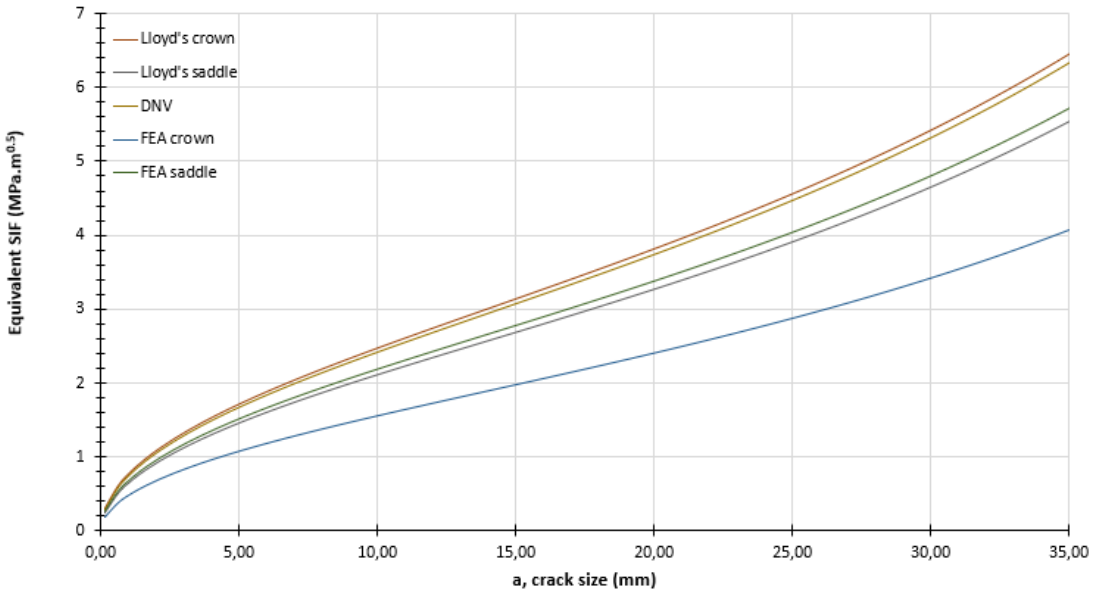


Figure 75 - *SIF vs. a* curves for the Brace B1 using IIW recommendations based on Lloyd's Register, DNV standard, and FEA: $a/c = 0.2$.

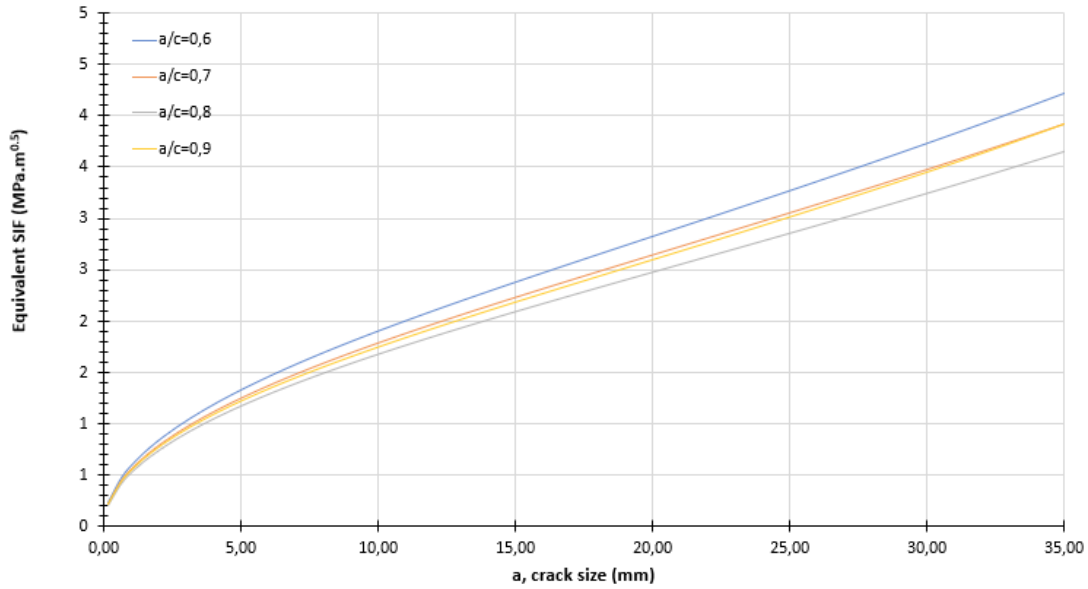


Figure 76 - *SIF vs. a* curves for the Brace B1 using IIW recommendations based on DNV standard for $\sigma_n = 12.5MPa$: $0.6 \leq a/c \leq 0.9$.

4.3.3.2 Brace B2

In Figure 77, the SIF vs. a curves for the Brace B2 using IIW recommendations based on the SCF values estimated using the Lloyd's Register, DNV standard, and FEA – a/c=0.1 – are presented. A large dispersion is found between the curves. However, a good agreement can be considered between the curves based on FEA and Lloyd Register, for the crown point. Figure 78 illustres the SIF vs. a curves for the Brace B2

using IIW recommendations based on DNV standard for $\sigma_n = 37.3MPa$, for $0.6 \leq a/c \leq 0.9$.

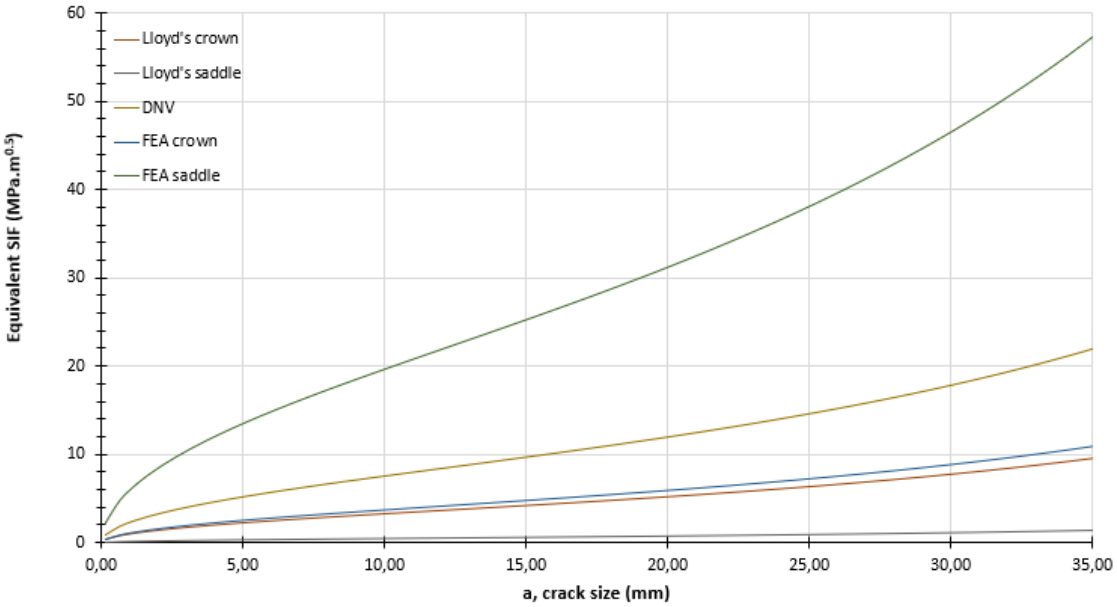


Figure 77 - *SIF vs. a* curves for the Brace B2 using IIW recommendations based on Lloyd's Register, DNV standard, and FEA: $a/c = 0.1$.

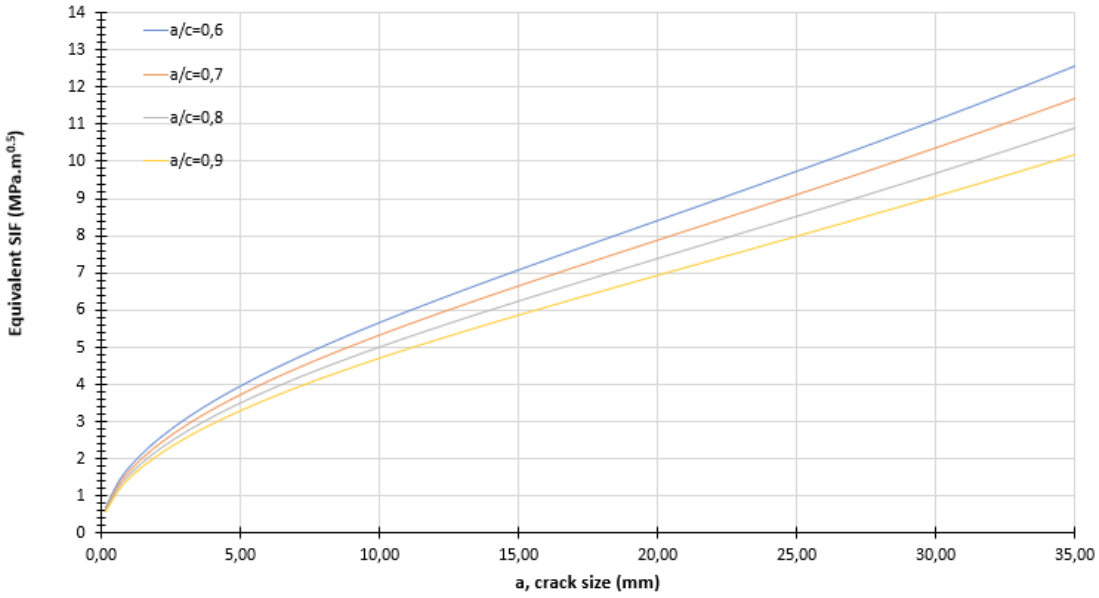


Figure 78 - *SIF vs. a* curves for the Brace B2 using IIW recommendations based on DNV standard for $\sigma_n = 37.3MPa$: $0.6 \leq a/c \leq 0.9$.

4.3.3.3 Brace B3

In Figure 79, the SIF vs. a curves for the Brace B3 using IIW recommendations based on the SCF and/or hot-spot stress values calculated using the Lloyd's Register, DNV standard, and FEA, for a/c=0.1, are presented. A good agreement can be considered between the SIF results for the crwon point, using the Lloyd Register and DNV. The same can be observed between the SIF results for the saddle point taking into account the Lloyd Register and FEA. A bad result is verified for the SIF vs. a curve based on FEA for the crown point when compared to the other curves.

Figure 80 illustrates the SIF vs. a curves for the Brace B3 using IIW recommendations based on DNV standard for $\sigma_n = 21.2MPa$: $0.6 \leq a/c \leq 0.9$.

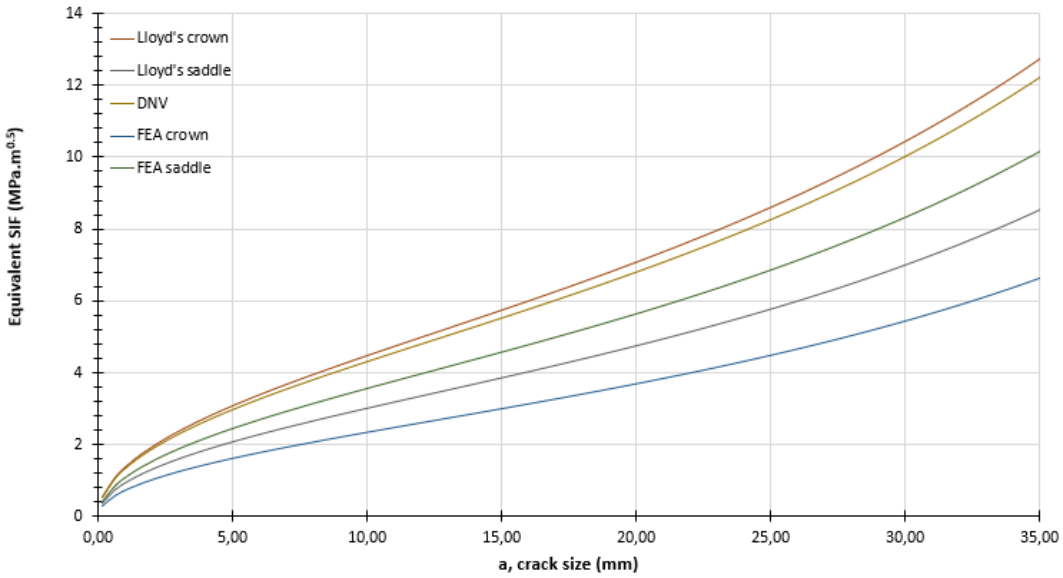


Figure 79 - *SIF vs. a* curves for the Brace B3 using IIW recommendations based on Lloyd's Register, DNV standard, and FEA: $a/c = 0.1$.

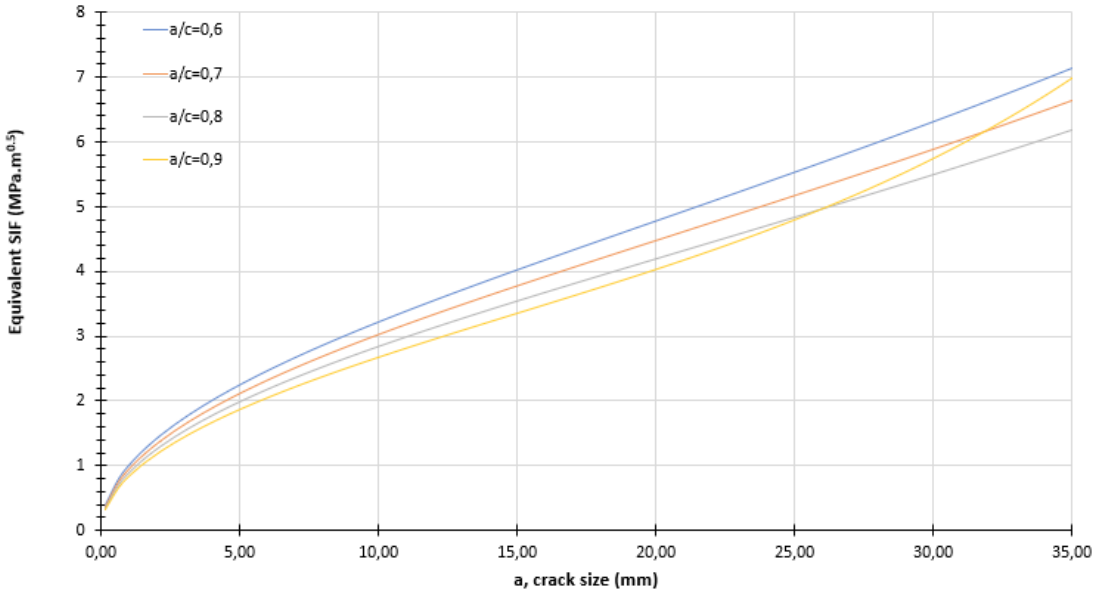
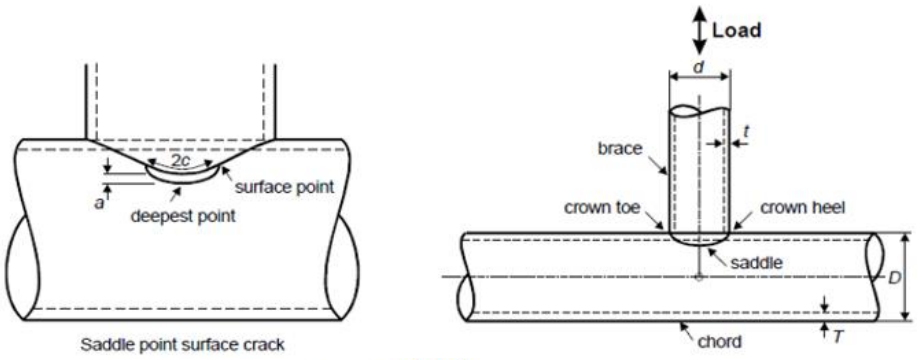


Figure 80 - *SIF vs. a* curves for the Brace B3 using IIW recommendations based on DNV standard for $\sigma_n = 21.2MPa$: $0.6 \leq a/c \leq 0.9$.

4.4 SIF evaluation on SINTAP standard

4.4.1 SINTAP standard Rules

The BRITE-EURAM project, SINTAP, aims to develop a defect assessment approach for the European Community where most of the solutions presented were collated from industry and establishments in the UK (Nuclear Electric Ltd, Magnox Electric Plc and HSE), Sweden (SAQ Kontroll AB) and Germany (Fraunhofer IWM, and GKSS). In developing this source reference, care has been taken to ensure that, wherever possible, the solutions recommended have been validated. The solutions are compared to standard solutions published elsewhere and to those in the American Petroleum Institute document API 579. It is given the recommended solutions for SIFs, guidance on calculating the limit loads and the assessment of known or assumed weld toe flaws, including fatigue cracks found in service, in brace or chord members of T, Y, K or KT joints between circular section tubes under axial and/or bending loads [36].
In order to start the calculations of the stress intensity factor, it is necessary to beware of the geometrical parameters associated. Equations (128) to (143) are used to determine the stress intensity factor of the surface point at a surface crack at the saddle point of the central brace (B2) for the balanced axial load case.



a	crack depth
$2c$	surface crack length
d	brace diameter
D	Chord diameter
L	Chord length
t	brace thickness
T	Chord thickness
α	$2L/D$
β	d/D
γ	$D/2T$
τ	t/T
σ_n	brace nominal stress

Figure 81 - T-joint description.

$$F_g = 204.08\beta^{(-0.5858-0.7492ln\beta)}\gamma^{(-2.6713-0.2884ln\beta+0.5646ln\gamma)}\tau^{(1.1491-0.2936ln\gamma-0.5043ln\tau)} \quad (128)$$

$$F_i = \beta^{0.0680A}\gamma^{(0.0473A-0.5344C-0.1218C^2)}\tau^{(-0.1299A-0.0370C)} \quad (129)$$

$$F_s = (a/T)^p(3c/d)^r \quad (130)$$

$$p = 1.0787 + 0.6397A + 0.1569A^2 + 0.0186A^3 - (0.0770 + 0.0478A + 0.0099A^2)C^2 \quad (131)$$

$$r = 0.8617 + 0.4888A + 0.1816A^2 + 0{,}0123A^3 - 0.3252C - 0.2210C^2 - 0.0275C^3 \quad (132)$$

$$A = \ln(a/T) \quad (133)$$

$$C = \ln(3c/d) \quad (134)$$

$$K_e = \sigma_n F_g F_i F_s \sqrt{\pi a} \quad (135)$$

Where the limits to the stress intensity factor solution are:

$$\alpha = 12 \quad (136)$$

$$0.4 \leq \beta \leq 0.8 \quad (137)$$

$$10 \leq y \leq 20 \quad (138)$$

$$0.3 \leq \tau \leq 1 \quad (139)$$

$$0.05 \leq \frac{a}{T} \leq 0.80 \quad (140)$$

$$0.05 \leq 3c/d \leq 1.20 \quad (141)$$

For the Axial Tension (AT) calculation, Equation (142) applies:

$$\sigma_n = \frac{4P}{\pi[d^2-(d-2t)^2]} \quad (142)$$

Where:
σ_n - nominal stress;
P - applied load in the brace.

K_e combines the contributions of the stress intensity factor components for modes I, II and III, i.e.

$$K_e = \left[\frac{{K_I}^2+{K_{II}}^2+{K_{III}}^2}{(1-\upsilon)}\right]^{1/2} \quad (143)$$

The following equations are used to determine the stress intensity factor of the surface point at a surface crack at the saddle point for the outer braces (B1) and (B3) (see Equation (144) and (145)) for the balanced axial load case. Using the Table 25 to can be estimated the constants A and B.

$$K_I = Y \cdot \sigma_n \cdot \sqrt{\pi \cdot a} \quad (144)$$

$$\frac{Y}{k_{t,hs}} = A - B \cdot \left(\frac{a}{T}\right) \quad (145)$$

Where the limits to the stress intensity factor solution are the following:

$$\theta = 60° \quad (146)$$

$$\alpha = 12 \quad (147)$$

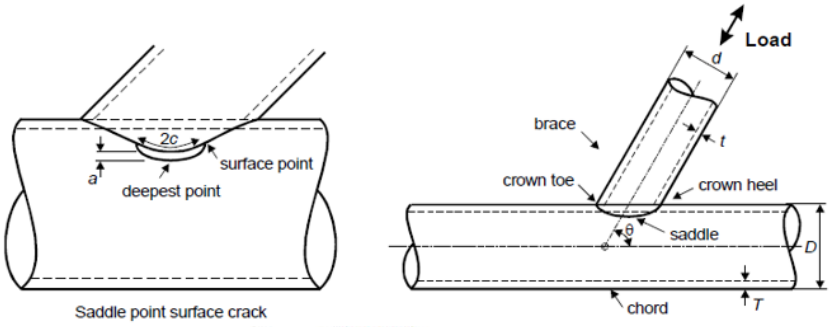
$$0.6 \leq \beta \leq 0.8 \quad (148)$$

$$10 \leq \gamma \leq 35 \quad (149)$$

$$0.2 \leq \tau \leq 1.0 \quad (150)$$

$$0.1 \leq a/T \leq 0.8 \quad (151)$$

$$0.1 \leq a/c \leq 0.4 \quad (152)$$



a	crack depth
$2c$	surface crack length
d	brace diameter
D	Chord diameter
L	Chord length
t	brace thickness
T	Chord thickness
α	$2L/D$
β	d/D
γ	$D/2T$
τ	t/T
θ	Angle between chord and brace
σ_n	brace nominal stress

Figure 82 - Y-joint description

Table 26 - constants A and B

a/c	A	B
0.1	1.22	0.69
0.2	1.07	0.84
0.3	0.96	0.83
0.4	0.87	0.81

4.4.2 Results

In this section, the $SIF\ vs\ a$ curves for the Braces B1, B2 and B3 of the KT tubular joint presented in Figure 20 (Chapter 3) based on the SINTAP standard using the SCF values calculated using the Lloyd's register, DNV standard and FEA, are shown.

4.4.2.1 Brace B1

In Figures 83 to 86 are presented the *SIF vs. a* curves for the chord side (brace B1) using SINTAP standard based on the SCF values obtained using the Lloyd's Register, DNV standard, and FEA, for several a/c values, 0.1 to 0.4, respectively. In Figures 87 to 90, the same analysis for the brace side (Brace B1) was made.

According to Figures 83-86, it can be concluded that a good agreement between the *SIF vs. a* curves obtained using SINTAP standard based on the SCF values obtained using the Lloyd's Register and DNV standard is verified. The *SIF vs. a* curves obtained using SINTAP standard based on the SCF values obtained using the FEA need need to be improved since Mendes [26] used a finite element dimension of 50mm, higher than that recommended by IIW.

According to Figures 87-90, for the *SIF vs. a* curves obtained using SINTAP standard based on the SCF values calculated using the Lloyd's Register, DNV standard, and FEA – for the brace side (Brace B3) – a good agreement is verified between Lloyd Register and DNV for the crown point of the connection. The same is verified, for the saddle point, when a comparison between Lloyd Register and FEA is made. For the FEA approach – crown point – there is no agreement when compared with other approaches.

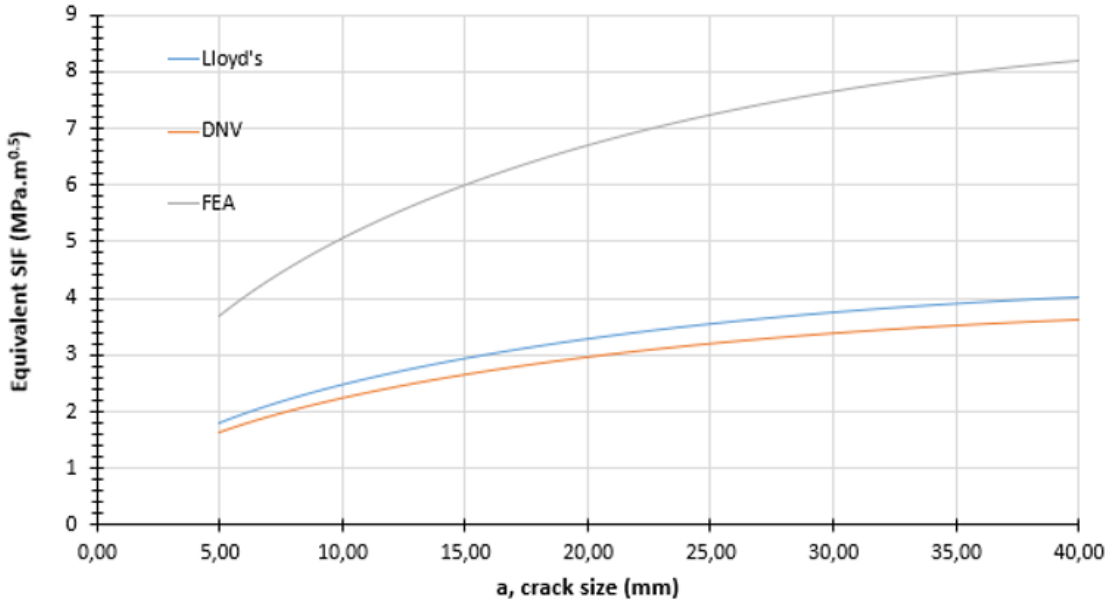


Figure 83 - *SIF vs. a* curves for the chord side (brace B1) using SINTAP standard based on the SCF values obtained using the Lloyd's Register, DNV standard, and FEA: $a/c = 0.1$.

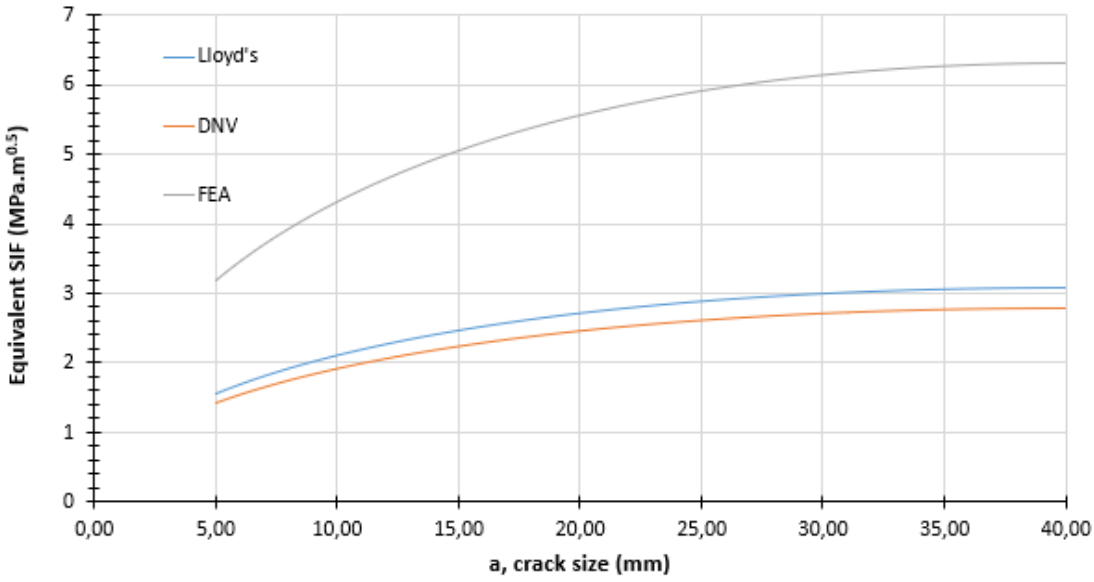


Figure 84 - *SIF vs. a* curves for the chord side (brace B1) using SINTAP standard based on the SCF values obtained using the Lloyd's Register, DNV standard, and FEA: $a/c = 0.2$.

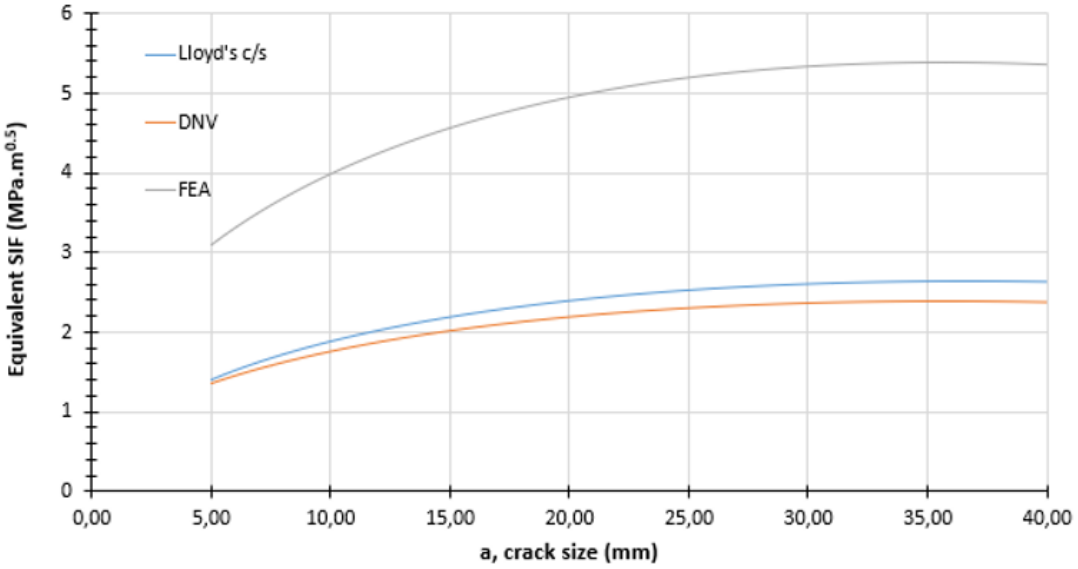


Figure 85 - *SIF vs. a* curves for the chord side (brace B1) using SINTAP standard based on the SCF values obtained using the Lloyd's Register, DNV standard, and FEA: $a/c = 0.3$.

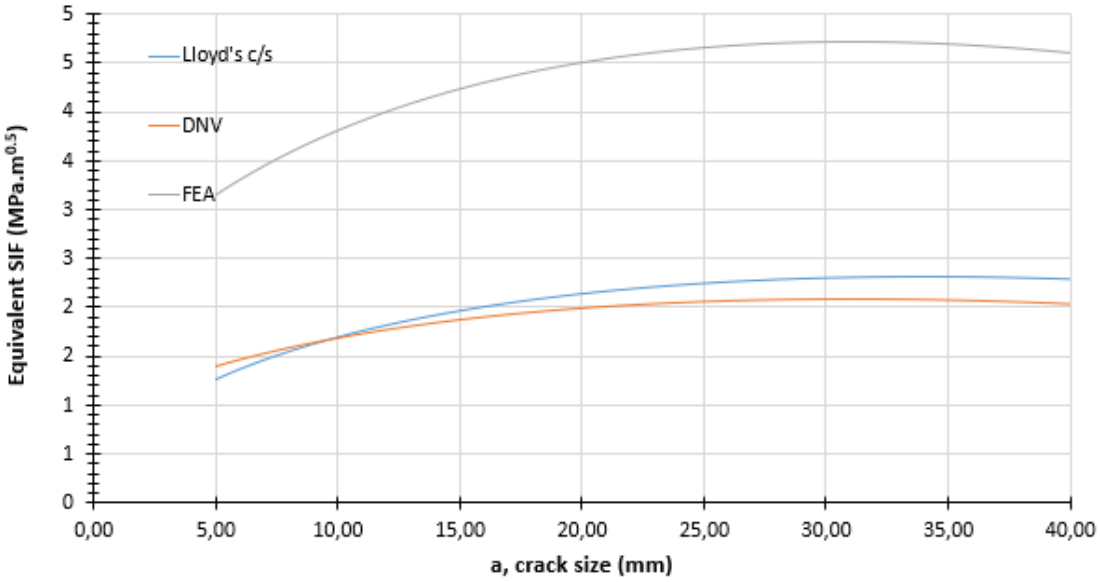


Figure 86 - *SIF vs. a* curves for the chord side (brace B1) using SINTAP standard based on the SCF values obtained using the Lloyd's Register, DNV standard, and FEA: $a/c = 0.4$.

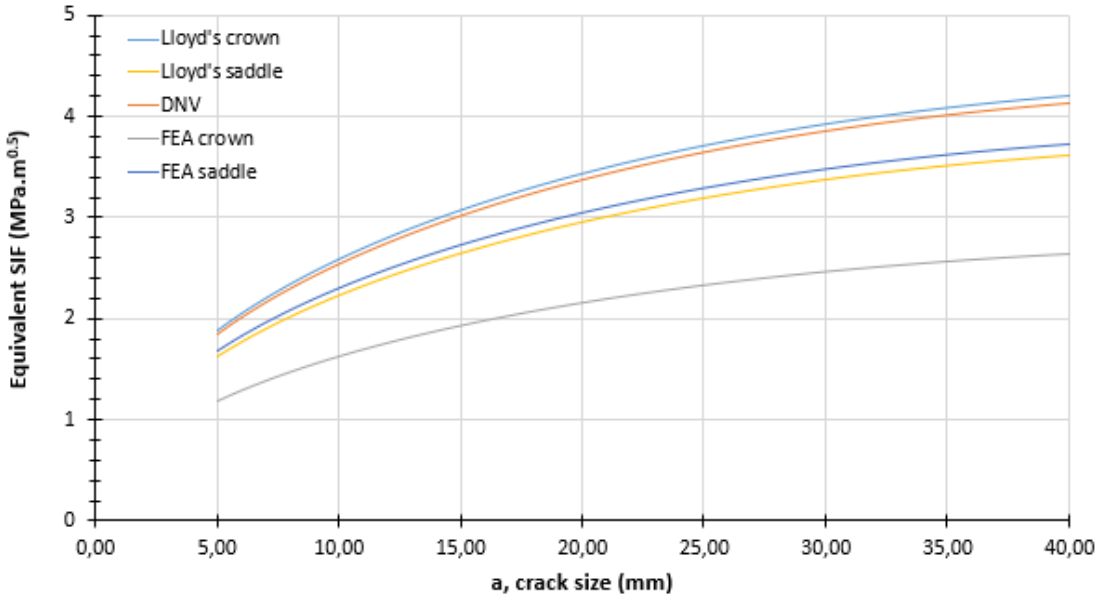


Figure 87 - *SIF vs. a* curves for the brace side (brace B1) using SINTAP standard based on the SCF values obtained using the Lloyd's Register, DNV standard, and FEA: $a/c = 0.1$.

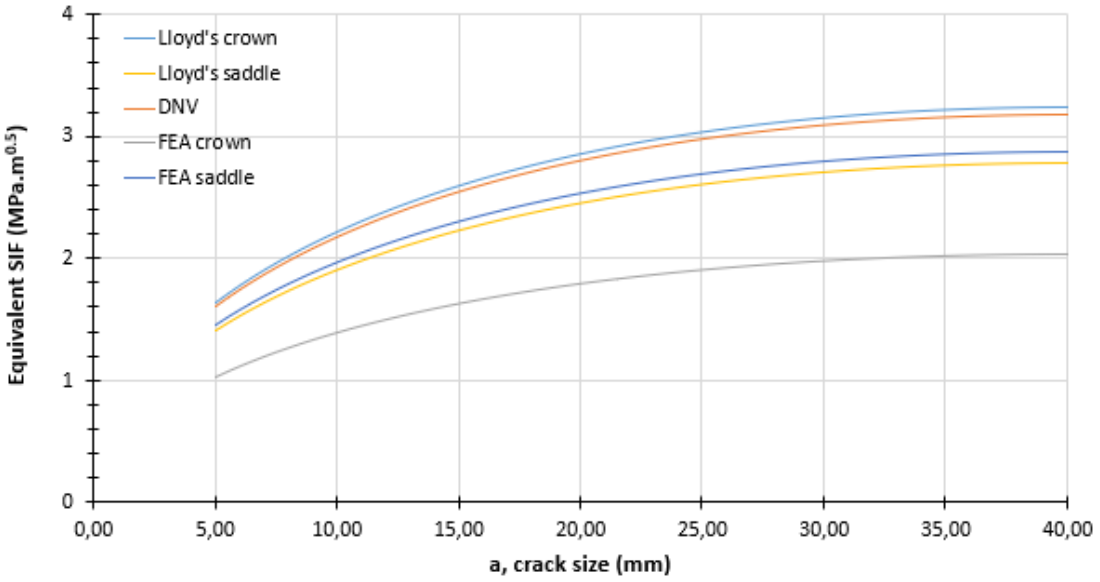


Figure 88 - *SIF vs. a* curves for the brace side (brace B1) using SINTAP standard based on the SCF values obtained using the Lloyd's Register, DNV standard, and FEA: $a/c = 0.2$.

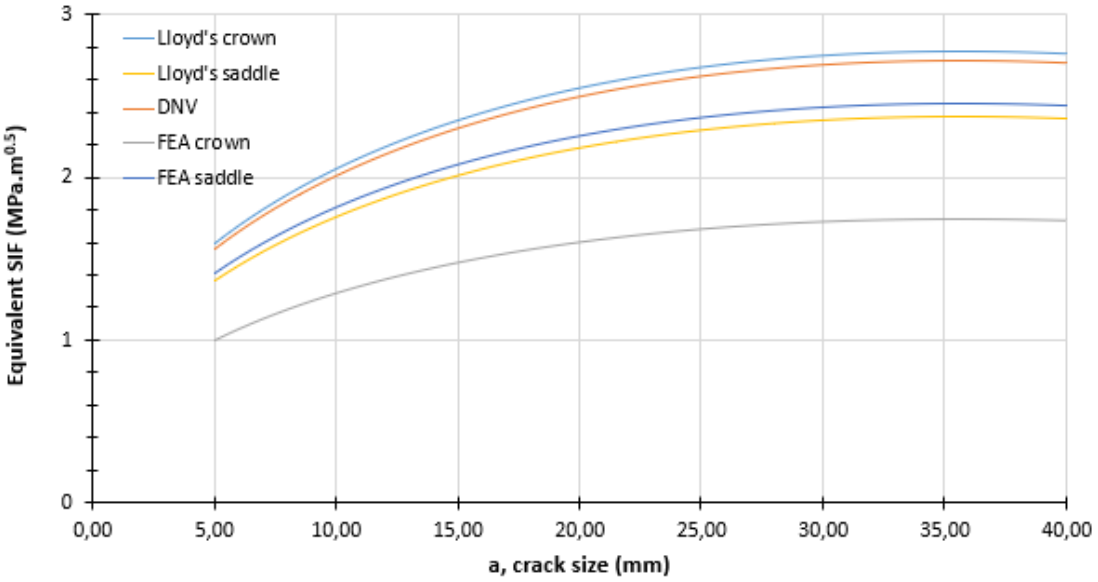


Figure 89 - *SIF vs. a* curves for the brace side (brace B1) using SINTAP standard based on the SCF values obtained using the Lloyd's Register, DNV standard, and FEA: $a/c = 0.3$.

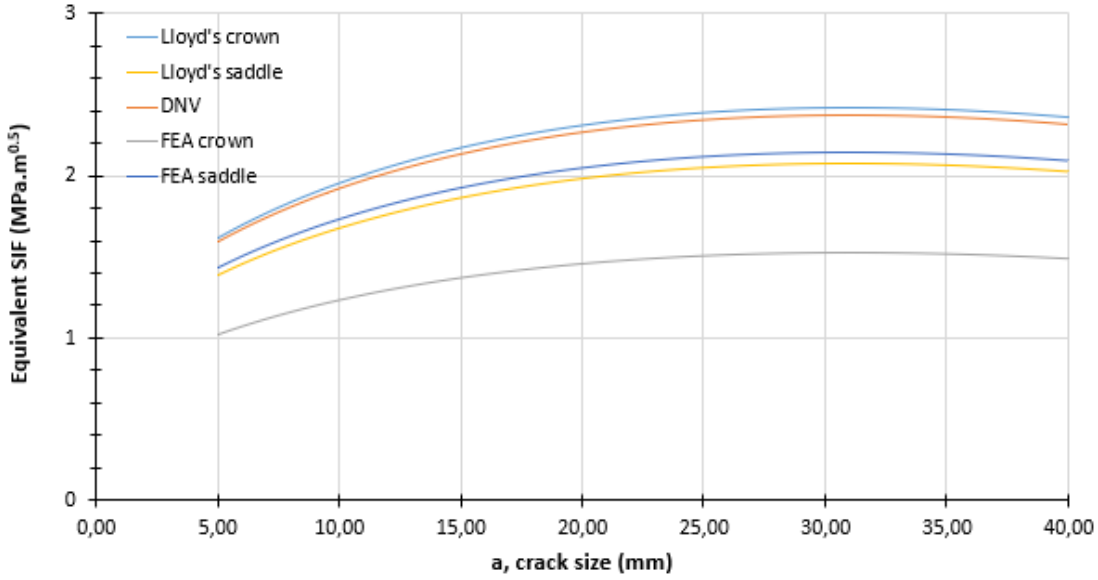


Figure 90 - *SIF vs. a* curves for the brace side (brace B1) using SINTAP standard based on the SCF values obtained using the Lloyd's Register, DNV standard, and FEA: $a/c = 0.4$.

4.4.2.2 Brace B2

Figure 91 presents the obtainded SIF vs. a curves for the Brace B2 using the SINTAP standard for $\sigma_n = 10.9MPa$, and covering $0.1 \leq a/c \leq 0.5$.

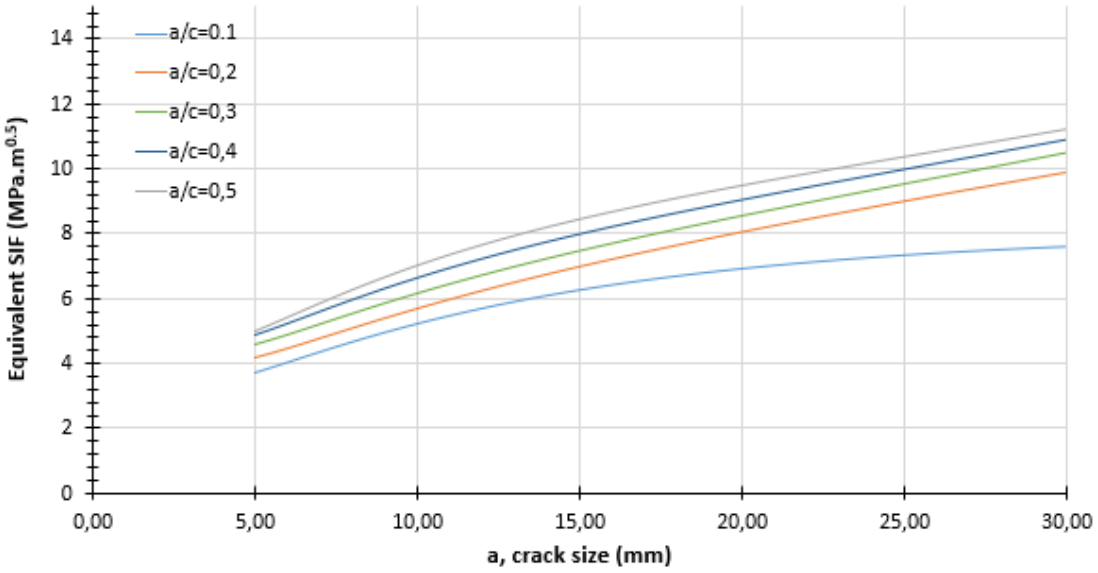


Figure 91 - Crack size and SIF values for different crack growth ratios (σ=10,9385 MPa)

4.4.2.3 Brace B3

In Figures 92 to 95 are displayed the *SIF vs. a* curves for the chord side (brace B3) using SINTAP standard based on the SCF values obtained using the Lloyd's Register, DNV standard, and FEA, for several a/c values. The same analysis for the brace side (Brace B3) was made and is illustrated in Figures 96 to 99.

The obtained results of the *SIF vs. a* curves (Figures 92 to 95) for the chord side (brace B3) using SINTAP standard based on the SCF values obtained using the Lloyd's Register, DNV standard, and FEA are compared and a bad agreement is verified between all methods used to estimate the SCF values.

For the *SIF vs. a* curves obtained using SINTAP standard based on the SCF values calculated using the Lloyd's Register, DNV standard, and FEA – for the brace side (Brace B3) – a good agreement is verified between Lloyd Register and DNV for the crown point of the connection. For the remaining approaches, there are no good results.

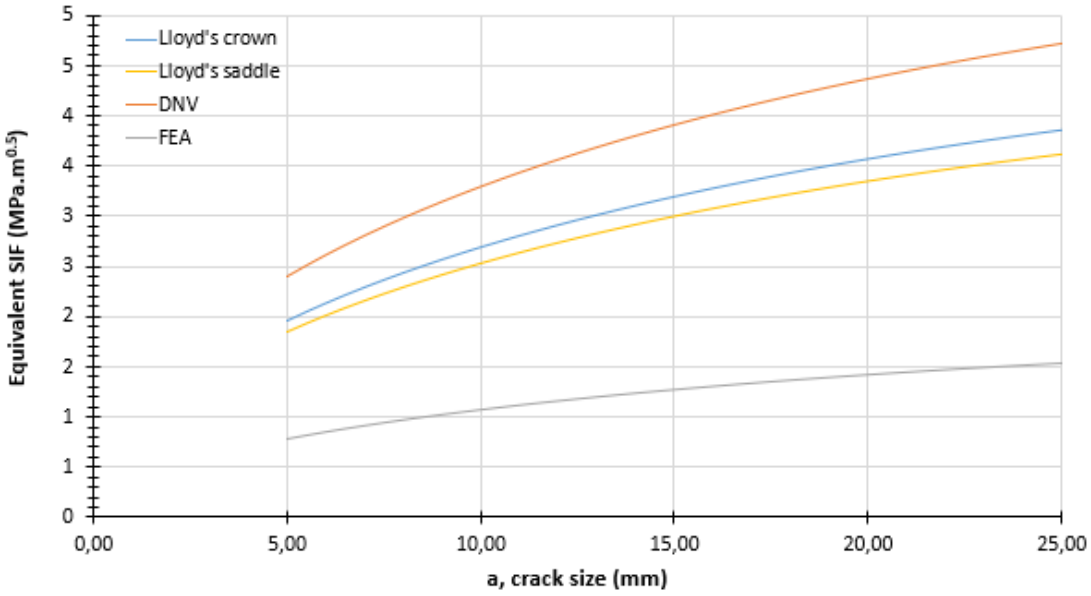


Figure 92 - *SIF vs. a* curves for the chord side (brace B3) using SINTAP standard based on the SCF values obtained using the Lloyd's Register, DNV standard, and FEA: $a/c = 0.1$.

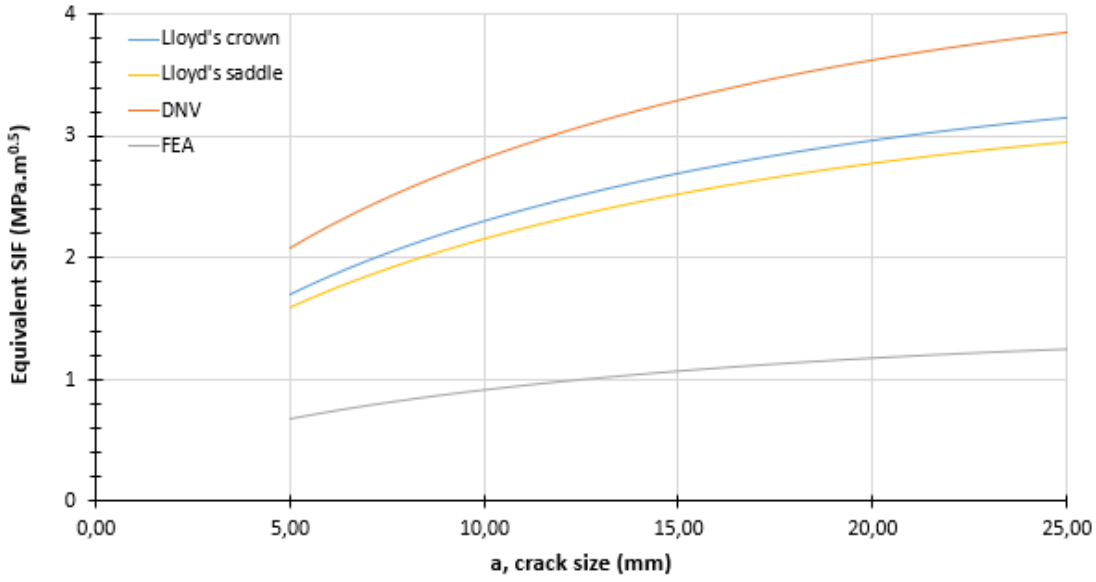


Figure 93 - *SIF vs. a* curves for the chord side (brace B3) using SINTAP standard based on the SCF values obtained using the Lloyd's Register, DNV standard, and FEA: $a/c = 0.2$.

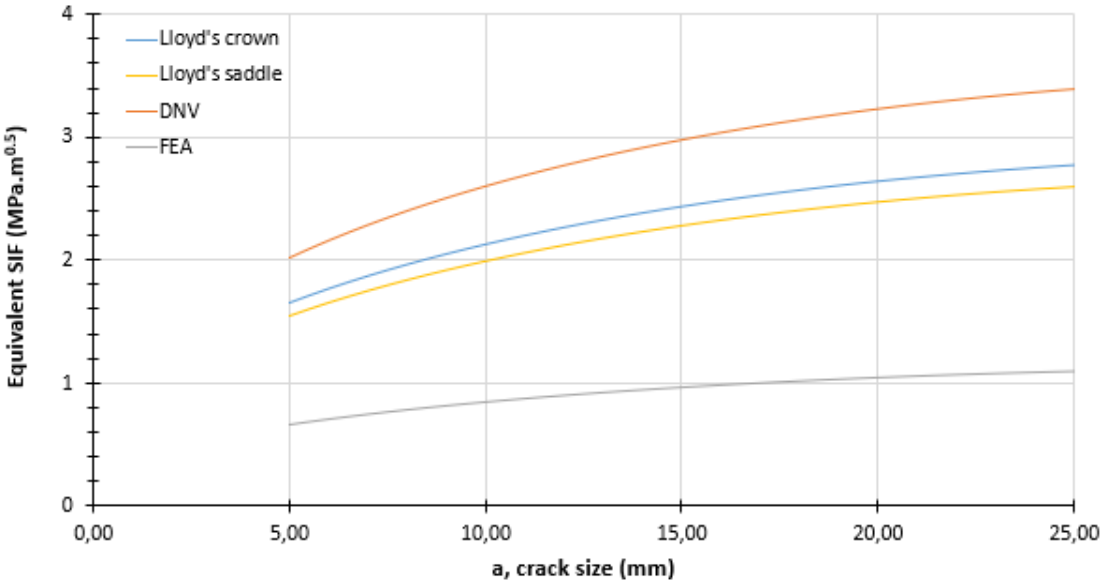


Figure 94 - *SIF vs. a* curves for the chord side (brace B3) using SINTAP standard based on the SCF values obtained using the Lloyd's Register, DNV standard, and FEA: $a/c = 0.3$.

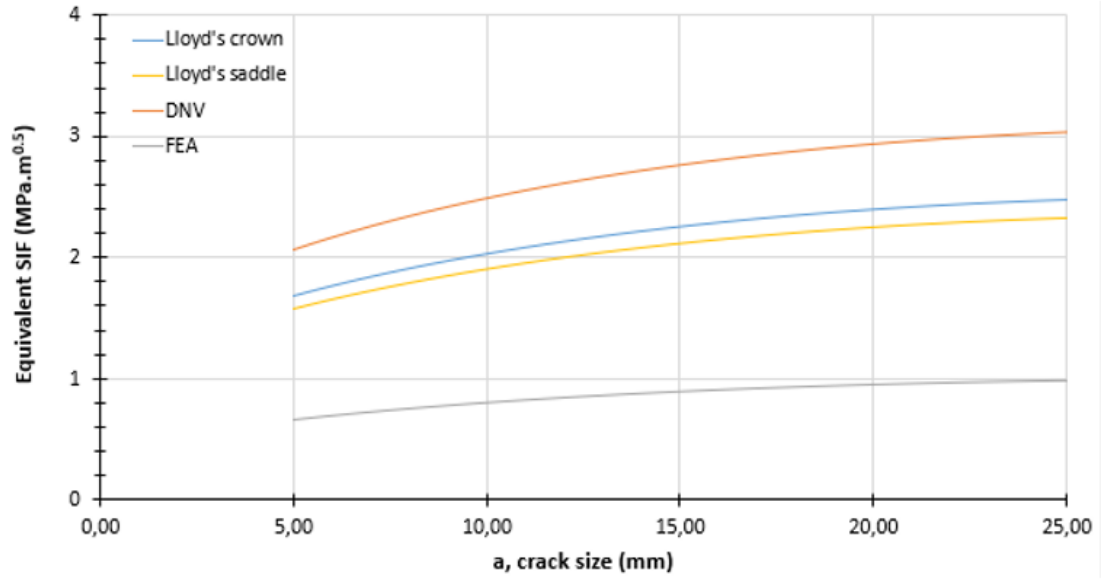


Figure 95 - *SIF vs. a* curves for the chord side (brace B3) using SINTAP standard based on the SCF values obtained using the Lloyd's Register, DNV standard, and FEA: $a/c = 0.4$.

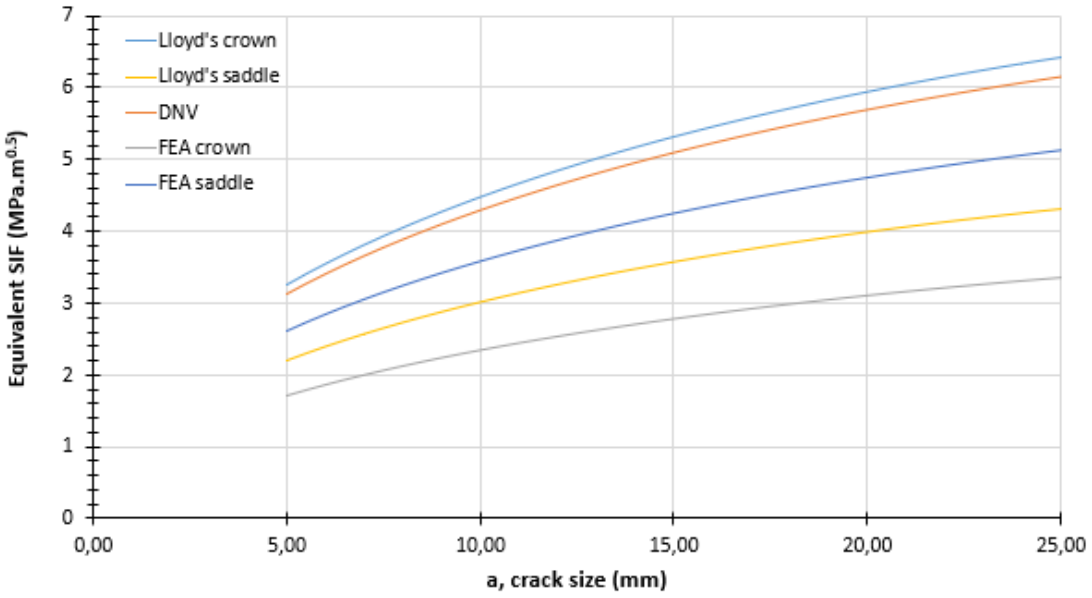


Figure 96 - *SIF vs. a* curves for the brace side (brace B3) using SINTAP standard based on the SCF values obtained using the Lloyd's Register, DNV standard, and FEA: $a/c = 0.1$.

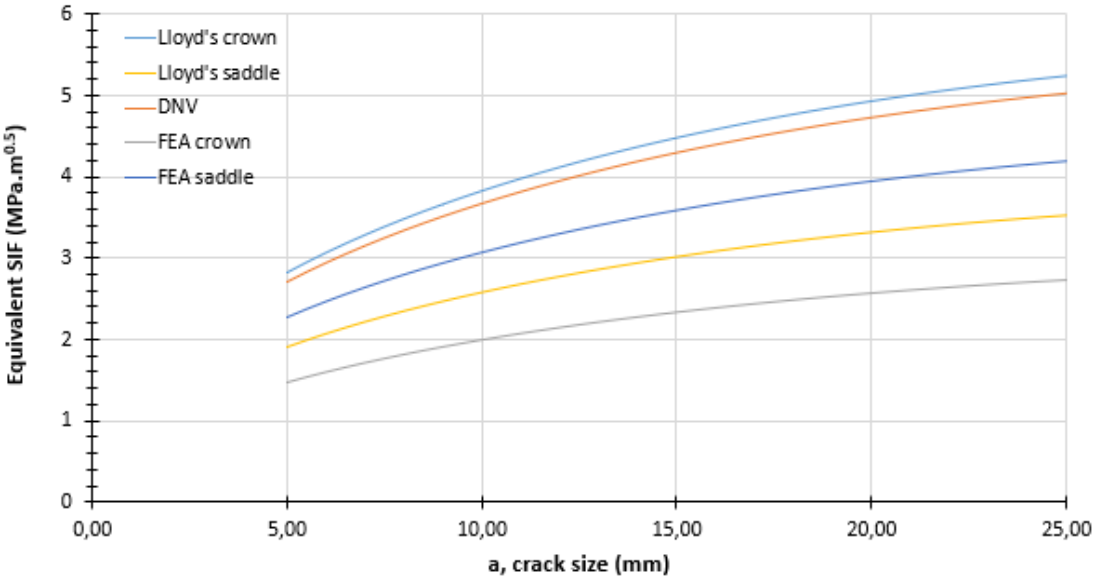


Figure 97 - *SIF vs. a* curves for the chord side (brace B3) using SINTAP standard based on the SCF values obtained using the Lloyd's Register, DNV standard, and FEA: $a/c = 0.2$.

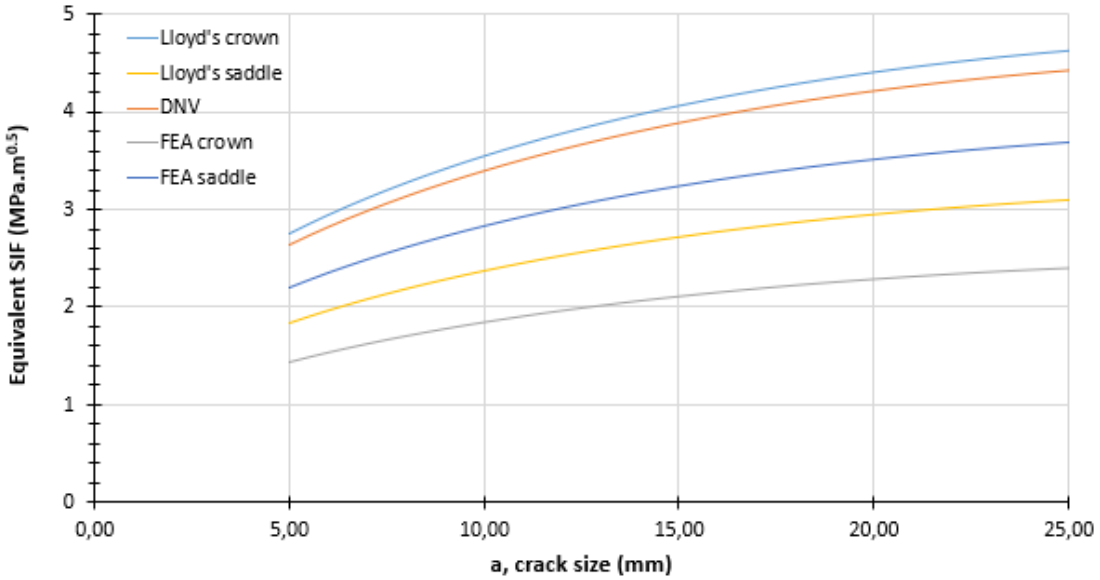


Figure 98 - *SIF vs. a* curves for the chord side (brace B3) using SINTAP standard based on the SCF values obtained using the Lloyd's Register, DNV standard, and FEA: $a/c = 0.3$.

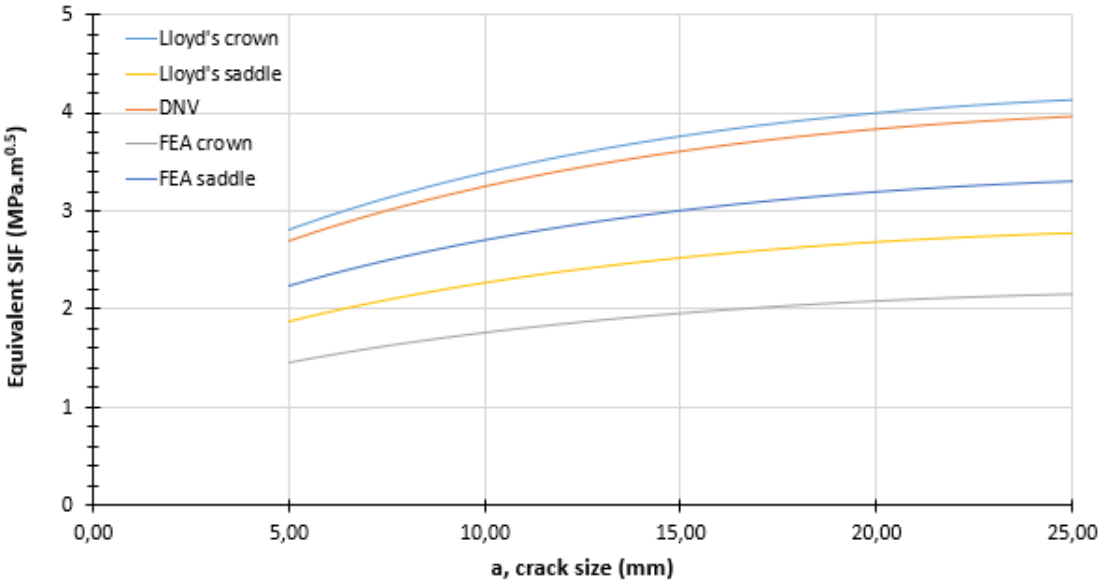


Figure 99 - *SIF vs. a* curves for the chord side (brace B3) using SINTAP standard based on the SCF values obtained using the Lloyd's Register, DNV standard, and FEA: $a/c = 0.4$.

4.5. Comparison and discussion

There is a range of values to the geometrical parameters that must be fulfilled, and these limits came from different experimental researches when trying to estimate the SIF equations for both BS7910, IIW and SINTAP standards.

Table 27 - Validity range of values according to standards

	a		c		a/c		a/B		θ		β	
	Min	Max	Min	Max	Min	Max	Min	Max	Min	Max		
BS7910	0	-	0	-	0	2	0	< 1	0	π	-	-
IIW	0	-	0	-	0	< 1	0	-	-	-	-	-
SINTAP T-joint	0,00475	0,076	0,0167	0,4	-	-	0	-	-	-	0,4	0,8
SINTAP Y-joint	0,0025	0,042	0,025	0,42	0,1	0,4	0	-	60	60	0,6	0,8

It is important to mention this range of constraints (see Table 27) because some difficulties were encountered in reconciling the same window of values for each of the available standards procedures. Specifically, the ratio a/c for the SINTAP Y-Joint case and the minimum values of crack size (a) for both SINTAP cases. Still in SINTAP calculations, an approximation was made since the angle in question in not exactly as the norm.

Table 28 - SIF comparison between BS7910, IIW and SINTAP standards

		BS7910					IIW					SINTAP					
		Lloyd		DNV	FEA		Lloyd		DNV	FEA		Lloyd		DNV	FEA		
		Crown	Saddle		Crown	Saddle	Crown	Saddle		Crown	Saddle	Crown	Saddle		Crown	Saddle	
Brace	B1	11,7708	10,0946	11,5304	7,4065	10,4299	7,2848	6,2475	7,1361	4,5838	6,4550	4,08856	3,5064	4,0051	2,5727	3,6228	
	B2	15,7001	2,3020	36,1633	17,9066	36,1633	7,9646	1,1692	18,3457	9,0827	47,6956	-	-	-	-	-	
	B3	19,5511	13,1321	18,4632	10,1905	15,6325	8,6379	5,8019	8,2897	4,5023	6,9066	7,0590	4,7414	6,7745	3,6793	5,6441	
Chord	B1	-	-	-	-	-	-	-	-	-	-	3,8952		3,5173	7,9618		
	B2	-	-	-	-	-	-	-	-	-	-	-	-	-	-		
	B3	-	-	-	-	-	-	-	-	-	-	4,2369	3,9577	5,1927	1,6841		

In Table 28, it can be seen the comparison between BS7910, IIW and SINTAP for the various SCF values obtained from Efthymiou's and Lloyd's parametric equations as well as the FE analysis. When interpreting the SIF values, they were relatively identical

between braces B1 and B3. Conclusions may not be taken about brace B2 since there is a decrease of 500% and an increase of 350% in some of its values when comparing with the other braces. However, it is not possible to assume that the calculations are incoherent but rather the values of brace B2 provided in Chapter3.

Calculations on the chord, presented in Table 28, were not possible to gather by virtue of the parametric equations which only contemplated for the brace side. Establishing a comparison between the 3 standards, it is possible to state that the SINTAP results are more conservative than BS7910 and IIW.

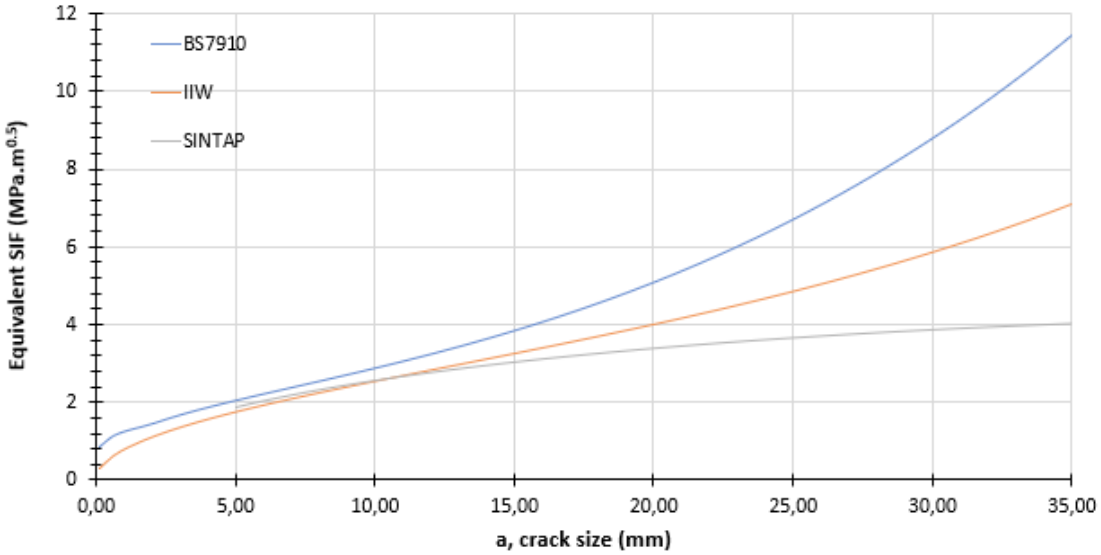


Figure 100 - *SIF vs. a* curves for the Brace B1 using BS7910, IIW and SINTAP standards based on DNV standard for $\sigma_n = 12.51MPa$: $a/c = 0.1$.

By observing Figure 100, we retain that between BS7910, IIW and SINTAP, the SIF in brace B1 is much more conservative for the SINTAP standard, while the British standard is the less conservative. There is increasing percentage of 285% bewteen both. This graphic was built, for comparative reasons, with SCF obtained from the DNV Guide values available in Chapter 3 for a a/c ratio of 0,1.

Besides SINTAP, no other standard strictly specifies the lower limit of a/c ratio. Nontheless, values lower than 0,1 should not be taken into consideration as the curves are little realistic and conservative when compared with higher ratios.

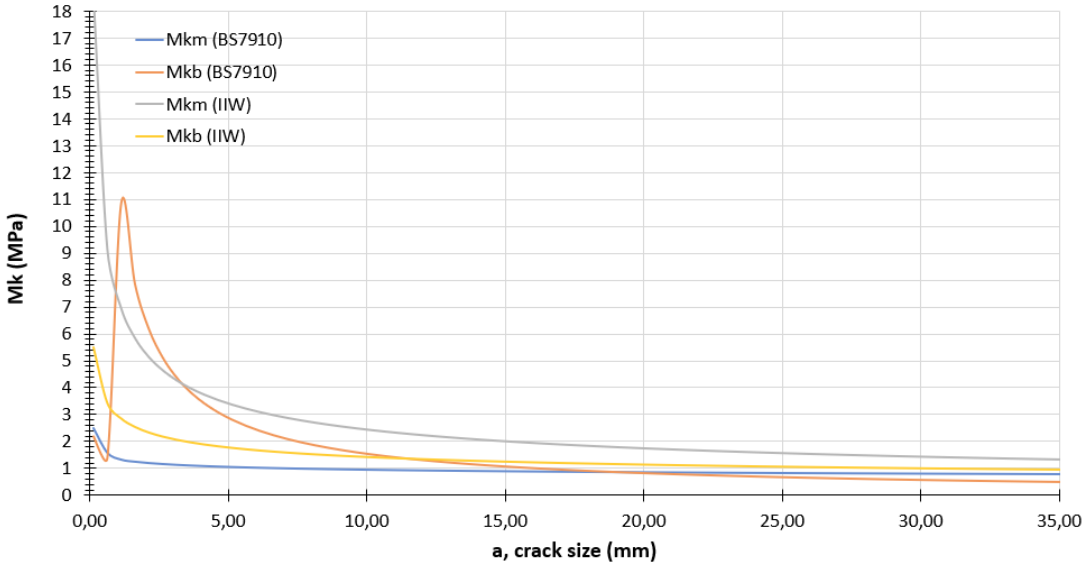


Figure 101 – M_k vs. a curves for the Brace B1 using BS7910 and IIW to compare M_{km} and M_{kb} values: a/c = 0.1.

Figure 101 shows SIF vs. a curves for the Brace B1 using BS7910 and IIW to compare M_{km} and M_{kb} values with a a/c = 0.1 ratio. there is a big difference between M_{km} of both standards, having around an increasing percentage of 900% at the beginning. The trend is to aproximate values, but only for larger-scale cracks. M_{kb} owes its unusual aspect to the change of equation when in calculations because of the range of the geometrical parameters. To conclude, IIW is more conservative than BS7910 standard.

5. Conclusions and future works

5.1 Conclusions

In this section, conclusions on stress intensity factor between the analytical parametric equations of BS7910, IIW and SINTAP standards. In order to do so, SCF values obtained previously from Lloyd and Efthymiou parametric equations and FEM analysis were used. It was verified that the values of SCF used, in general, are more conservative for the analytical parametric equations than the finite element analysis. For this reason, and because of discrepancies observed, specially in brace B2, little comparison on this element was made. Typically, a finite element analysis leads to better results for the SCF calculations, however, it is mandatory to establish the most accurate type of mesh element and mesh refinement around the intersections of brace and chord. When it isn't accomplished, non-accurate results are obtained, and the most appropriate way for the stress concentration factor calculation to estimate the fatigue life of offshore tubular joints is compromised. For the study of SIF results, it is possible to conclude that the analytical results are more conservative for the SINTAP standards when compared to others, as well as the M_k values. For a a/c ratio lower than 0,1, it is possible to state that the graphic curves do not behave precisely as the others showing a much steep growth. At last, a finite element analysis on the stress intensity factor would be relevant to create a reinforced opinion on how adequate and precise each analytical standard is and to add real value information.

5.2 Future works

Regarding possible future works, the refinement of the mesh is one of the first possible procedures so that a better and accurate observation and understanding of the influence of the finite element size towards the evaluation of the SCF and consequently SIF values is obtained. The addition of the welding fillet in all joints to create a more realistic numerical study to be possible to investigate more precisely its influence and to better estimate the elements' fatigue life due to the better results. The inclusion of the in plane bending case and out of plane bending in the analytical calculations would also be worth studying. Moreover, the construction of a numerical model able to correctly calculate the stress intensity factor values so it would be possible to compare with the analytical results gathered in this study as well as considering the other different loading cases.

Bibliographic References

[1] Maheswaran, J. (2014). Fatigue life estimation of tubular joints in offshore jacket according to the SCFs in DNV-RP-C203, with comparison of the SCFs in ABAQUS/CAE. *Master Dissertation in University of Stavanger.*

[2] Chakrabarti, S. K. (2005). *Handbook of offshore engineering*. Elsevier.

[3] El-Reedy, M. A. (2012). Introduction to Offshore Structures. *Offshore Structures: Design, Construction and Maintenance.,* 1-21. doi:10.1016/b978-0-12-385475-9.00001-8

[4] McLendon, R. (2019, July 31). Types of offshore oil rigs. Retrieved from https://www.mnn.com/earth-matters/energy/stories/types-of-offshore-oil-rigs

[5] Narayanan, R. and T.M. Roberts, 1991. Structures practice. Subjected to Repeated Loading: Stability and strength. London: Elsevier Applied Science

[6] Ahmadi, H., & Zavvar, E. (2015, 06). Stress concentration factors induced by out-of-plane bending loads in ring-stiffened tubular KT-joints of jacket structures. Thin-Walled Structures, 91, 82-95. doi:10.1016/j.tws.2015.02.011

[7] Khedmati, M. R., Rigo, P., Amrane, A., & Nazari, M. (2013, 06). Assessment of Fatigue Reliability for Jacket-Type Offshore Platforms Considering Dynamic Behavior. *Volume 2B: Structures, Safety and Reliability*. doi:10.1115/omae2013-11568

[8] Saini, D. S., Karmakar, D., & Ray-Chaudhuri, S. (2016, 09). A review of stress concentration factors in tubular and non-tubular joints for design of offshore installations. *Journal of Ocean Engineering and Science, 1*(3), 186-202. doi:10.1016/j.joes.2016.06.006

[9] Ahmadi, H., & Mayeli, V. (2018, 12). Probabilistic analysis of the local joint flexibility in two-planar tubular DK-joints of offshore jacket structures under in-plane bending loads. *Applied Ocean Research, 81*, 126-140. doi:10.1016/j.apor.2018.10.011

[10] Det Norske Veritas, *DNV-RP-C203: Fatigue Design of Offshore Structures*, Norway, 2016

[11] Liu, Y., & Mahadevan, S. (2010). Probabilistic fatigue life prediction of composite materials. *Fatigue Life Prediction of Composites and Composite Structures,* 220-248. doi:10.1533/9781845699796.2.220

[12] Radaj, D., Sonsino, C., & Fricke, W. (2006). Nominal stress approach for welded joints. Fatigue Assessment of Welded Joints by Local Approaches, 13-32 doi:10.1533/9781845691882.13

[13] Djavit, Djan Eirik, Strande, Erik, *Master's Thesis: Fatigue failure analysis of fillet welded joints used in offshore structures*, 2013

[14] Department of Energy (1984) Offshore Installations: Guidance on Design and Construction. Her Majesty's Stationery Office, London.

[15] Minguez, E. L. (2015). Fatigue & Fracture Mechanics of Offshore Wind Turbine Support Structures. *Doctorate Thesis in Cranfield University.*

[16] Radaj, Dieter, *Design and Analysis of Fatigue Resistant Welded Structures*, 1990

[17] Hobbacher, A. (2018). *Recommendations for fatigue design of welded joints and components*. SPRINGER.

[18] American Petroleum Institute (API) , API RP 2A-WSD Recommended Practice for Planning, Designing and Constructing Fixed Offshore Plat- forms: Working Stress Design, American Petroleum Institute, Washing- ton, D.C, 2005 .

[19] X.L. Zhao , S. Herion , J.A. Packer , R. Puthli , G. Sedlacek , J. Wardenier , K. Weynand , A. van Wingerde , N. Yeomans , Design Guide for Circular and Rectangular Hollow Section Joints Under Fatigue Loading, Verlag TÜV Rheinland, K¨oln, Germany, 2000 .

[20] Kuang, J.G.; Potvin, A.B. and Leick, R.D., Stress concentration in tubular joints, Offshore Technology Conference, OTC 2205, 1975

[21] Li H, Chen SJ (1983) Foundation of fracture theory. Sichuan People's Publishing House, Cheng du

[22] Jie, Z., Li, Y., & Wei, X. (2016, 07). Analysis of the stress intensity factor of welded joints under prior corrosion and complex stress fields. *Journal of Modern Transportation, 24*(4), 270-276. doi:10.1007/s40534-016-0114-6

[23] BUDDEN, P.J. and M.R. JONES, 1989. *Mixed mode fracture*. CEGB Report RD/B/6159/R89. Berkeley, Glos.: BNL — Central Electricity Generating Board.

[24] Lotsberg, I., Fjeldstad, A., & Ronold, K. O. (2016, 06). Background for Revision of DNVGL-RP-C203 Fatigue Design of Offshore Steel Structures in 2016. *Volume 4: Materials Technology*. doi:10.1115/omae2016-54939

[25] Efthymiou, M., Development of SCF formulae and generalized influence functions for use in fatigue analysis, Surrey, 1988

[26] Mendes, P.J.S.C. (2018). STRESS CONCENTRATION FACTOR EVALUATION IN OFFSHORE TUBULAR KT-JOINT FOR FATIGUE DESIGN. Master Dissertation in Faculdade de Engenharia da Universidade do Porto.

[27] *Guide to methods for assessing the acceptability of flaws in metallic structures: British standard BS 7910:2005*. (2005). BSI, British Standards Institution.

[28] Correia, J.A. (2018). Fatigue. Fracture mechanics - theoretical background. CIE5126, Part 1, Lecture 9 in INEGI/Faculty of Engineering, University of Porto.

[29] https://www.nafems.org/training/courses/introduction-to-fea/] , Agosto 2019

[30] *Stress concentration factors for simple tubular joints: Assessment of existing and development of new parametric formulae*. (1997). HSE Books.

[31] Ahmadi, H., Mohammadi, A. H., & Yeganeh, A. (2015, 09). Probability density functions of SCFs in internally ring-stiffened tubular KT-joints of offshore structures subjected to axial loading. Thin-Walled Structures, 94, 485-499. doi:10.1016/j.tws.2015.05.012

[32] https://www.steelconstruction.info/Material_selection_and_product_specification, Junho 2018

[33] Bowness, D., & Lee, M. M. (2002). Fracture mechanics assessment of fatigue cracks in offshore tubular structures. HSE Books.

[34] Irwin C.R.: Analysis of stresses and strains near the end of a crack transversing a plate. *J. Appl. Mech*. 1957, **24**, 361–364.

[35] H. Tada, P. C. Paris and G. Irwin, The Stress Analysis of Cracks Handbook, Del Research Corporation (1985).

[36] Laham S. Al. (1999, 04). Stress Intensity Factor and Limit Load Handbook. Group Head, Assessment Technology Group